EXPERIMENTAL STUDY OF STRAIN WAVE PROPAGATION IN QUARTER-HARD ELECTROLYTIC COPPER BARS

by

CLIFFORD JOHN ANDERSON

B.A.Sc., University of British Columbia, 1963.

A THESIS SUBMITTED IN PARTIAL FULFILMENT OF THE REQUIREMENTS FOR THE DEGREE OF

MASTER OF APPLIED SCIENCE

in the Department

of

Mechanical Engineering

We accept this thesis as conforming to the required standard

THE UNIVERSITY OF BRITISH COLUMBIA

MARCH, 1965

In presenting this thesis in partial fulfilment of the requirements for an advanced degree at the University of British Columbia, I agree that the Library shall make it freely available for reference and study. I further agree that permission for extensive copying of this thesis for scholarly purposes may be granted by the Head of my Department or by his representatives. It is understood that copying or publication of this thesis for financial gain shall not be allowed without my written permission.

Department of **Mechanical Engineering**

The University of British Columbia,
Vancouver 8, Canada.

Date **March 19, 1965**

ABSTRACT

Specimens of quarter-hard electrolytic copper, twenty feet in length and one-quarter inch in diameter, were statically prestressed and subjected to impact loading. Dynamic strain vs time traces, for both loading and unloading waves, were obtained using resistance-type strain gages mounted at various positions along the specimens. Permanent strain increments resulting from each impact were determined. Prestress levels ranged from values well below the yield point of the material to values exceeding the yield point. Impact velocities and impact durations were also varied.

The experimental strain wave shape and propagation velocity in bars prestressed well below the yield point were found to compare favorably with the theoretical elastic wave shape and velocity. The unloading waves propagated in bars prestressed above the yield point were found to be similar in shape to the elastic waves observed and to propagate at the elastic velocity without diminution of amplitude.

For loading waves propagated in material prestressed above the yield point the incipient portion of plastic strain waves was found to propagate at the elastic velocity. The lower strain increments of the plastic strain waves were found to propagate at higher velocities and the highest strain increments were found to propagate at lower velocities than would be predicted from a strain-rate-independent theory. For the loading waves, a method was developed

to approximate the dynamic loading curves (stress-strain relation followed during impact loading). From the dynamic loading curves, the peak stress levels of the plastic strain pulses were found to be significantly higher than the stresses at equivalent strains on the static stress-strain curve.

The results tended, at least qualitatively, to support a strain-rate-dependent wave propagation theory rather than a strain-rate-independent one.

ACKNOWLEDGEMENT

The author wishes to express gratitude to Dr. H. Ramsey whose constant advice and encouragement were responsible for the success of this research. The author also wishes to express appreciation to Mr. P. Hurren and Mr. J. Hoar, technicians, whose dedicated assistance on technical matters greatly accelerated the research program.

Thanks must be expressed to the Mechanical and Metallurgical Engineering Departments for the use of their facilities, and to the Architecture Department and Electrical Engineering Department for the loan of electronic equipment.

Financial assistance for the research was provided by the National Research Council of Canada, Grant A 1685. Specimens were donated by Noranda Copper Mills Limited.

TABLE OF CONTENTS

LIST OF FIGURES

List of Figures cont.

List of Figures cont.

TABLE OF NOMENCLATURE

c = Wave propagation velocity

c_n = Propagation velocity of n th increment of plastic wave

c_o = Elastic wave propagation velocity

E = Young's Modulus

e = Coefficient of restitution

t = Time from initiation of impact

u = Displacement in x direction

V = Impact velocity

V_h = Hammer velocity

V_p = Platform velocity

W_h = Hammer weight

W_p = Platform weight

x = Distance from impact point

$\epsilon = \frac{du}{dx}$ = Strain

ϵ_1 = Constant plastic strain

ϵ_{dy} = Dynamic strain

ϵ_n = Strain increment corresponding to c_n

ϵ_p = Plastic strain

ϵ_{pe} = Permanent strain

ϵ_y = Strain at elastic limit of material

σ = Stress

σ_d = Dynamic stress

σ_{pr} = Prestress

$\psi = \frac{d\sigma}{d\epsilon}$ = Tangent modulus to static stress-strain curve

Table of Nomenclature cont.

ψ_n = Tangent Modulus to dynamic loading curve corresponding to c_n

ρ = Mass density of material

m.sec. = Milli-seconds

μ in./in. = Micro-inches per inch strain

$\langle y \rangle$ = Value in brackets described by y, $y>0$ and by 0, $y<0$.

I INTRODUCTION

Up to the time that a theory for the propagation of plastic deformations was developed, two methods were used to evaluate the impact behaviour of materials. The methods were: the breaking of a notched bar and the failure in tension or compression of a short cylinder. These tests showed that for moderate impact velocity, the energy absorbed in an impact test was greater than the energy absorbed in a static test. It was also found that as the impact velocities increased beyond a certain point, this tendency was reversed. No theory was available to explain the mechanism of plastic wave propagation which occurs in such tests, hence the observations stated above were accepted as physical facts without theoretical qualification.

During the Second World War, a number of investigators became interested in the impact behaviour of materials in connection with the ability of structures to withstand shock loading due to bombing and armour penetration by projectiles. From these preliminary investigations arose an interest in the theoretical aspects of impact loading of materials to stress levels well in excess of the yield point. This interest resulted in a formulation of a concept of plastic wave propagation. With the first theoretical and experimental work in this field the idea of a critical impact velocity arose. It was theorized that subjection of a material to impact velocities in excess of this critical velocity would result in premature rupture of the material with very little energy being absorbed.

A large amount of experimental and theoretical work in the field of plastic wave propagation has been carried out in the past

few years and has resulted in both strain-rate-dependent and strain-rate-independent theories being developed. Experimental results tend to indicate that both theories have some merit.

The overall field of plastic wave theory is now being investigated in relation to problems in projectile impact and high speed machining as well as in relation to impact behaviour of structures.

II STATEMENT OF PROBLEM

The preliminary phase of the problem was to design and construct apparatus capable of prestressing suitably sized specimens into the plastic state and of subjecting the specimens to short duration, small amplitude impact loads in a manner which permitted the loading and unloading strain waves to be studied simultaneously. Instrumentation was also required in order to permanently record the strain vs time plots and permanent strain magnitudes at a number of positions on the specimens.

The main phase of the problem was to determine the elastic and the plastic strain wave propagation velocities and to correlate these with the prestress positions on the static stress-strain curve for the material. The problem also entailed checking the elastic and plastic strain wave shapes against the theoretical wave shapes and determining whether the material was acting in a strain-rate-dependent manner or in a strain-rate-independent manner.

III REVIEW OF PAST WORK

The laws governing the propagation of elastic waves in bars have been known since 1807 when the problem was analysed by Thomas Young, (after whom the elastic modulus was named). Young showed that the elastic propagation process was governed by the one dimensional wave equation, the solution of which describes two waves travelling, unchanged in shape, in opposite directions at a velocity $c_0 = \sqrt{E/\rho}$.

The development of equations and determination of the influence of parameters governing the behaviour of materials subjected to rapid deformations in the plastic region of the stress-strain curve poses many problems. Consequently, conflicting theories have arisen in the past two decades.

The simplest development of a plastic wave propagation theory was proposed by T. von Kármán [8] * in 1941. The theory is based on the assumption that the dynamic response of the material follows the static stress-strain curve.

The complete solution is expressed in three parts:

for $x > c_0 t$, $\epsilon = 0$ where $c_0 = (E/\rho)^{\frac{1}{2}}$

for $c_1 t < x < c_0 t$, $\epsilon_y < \epsilon < \epsilon_1$ where $c = (\Psi/\rho)^{\frac{1}{2}}$

for $x < c_1 t$, $\epsilon = \epsilon_1$ (const.) where $c_1 = \left(\frac{\Psi(\epsilon=\epsilon_1)}{\rho}\right)^{\frac{1}{2}}$.

The solution describes an elastic wave front propagating at a velocity c_0, a plastic wave front propagating at a velocity c_1, and strain increments between propagating at velocities depending

---

*Numbers in square brackets refer to numbered references in the Bibliography.

upon ψ (the tangent modulus to the static stress-strain curve) thus implying that the wave continually changes shape as it propagates. This analysis also gives an interpretation of the critical impact velocity. When $\psi=0$, the propagation velocity $c_1 = 0$, hence any further strain increments of the wave do not propagate, and premature rupture occurs.

von Kármán and Duwez [8] attempted to correlate experimental results with the foregoing plastic theory by means of an experiment in which measurements were taken after transients had died out. This was done by measuring the permanent strain distribution after impact. Results were obtained for annealed copper using impact velocities of 23.1 fps to 171 fps and varying impact durations.

The results indicated that a region of constant plastic strain did exist for some distance from the impact point, the distance depending upon the impact duration. It was shown that the plastic strain agreed closely with the theoretical strain ϵ_1, calculated from the impact velocity V. The shape of the experimental permanent strain distribution curve was found to vary considerably from the theoretical shape, suggesting the possibility that the simple strain-rate independent plastic theory required revision to take into account a strain-rate effect.

M.P. White and Le Van Griffis [10] presented a method of predicting the final strain distribution in a long ductile rod using the simple strain-rate-independent plastic theory based upon the assumption that dynamic loading followed the static stress-strain curve.

They assumed $c = \left(\frac{\psi}{\rho}\right)^{\frac{1}{2}}$ for any increment of the strain pulse and worked with short duration, large magnitude pulses.

The incremental velocity assumption when using short duration pulses results in an unloading wave travelling at the elastic velocity c_o which, after a finite time, gives rise to a secondary wave front travelling at a velocity c_o and moving in a direction opposite to the primary wave front. The analysis gives permanent strain distribution consisting of a constant strain level for a certain distance from the impact point followed by a decreasing strain level approaching zero at some finite distance from the impact point.

The only real difference between the White - Le Van Griffis analysis and the von Kármán - Duwez analysis is the consideration of the secondary wave front in the former.

Duwez and Clark [19] performed an experiment similar to that of von Kármán and Duwez in which they subjected copper specimens to high velocity impacts. By measuring the permanent strain in successive elements, they found that a region of constant plastic strain existed at the impact end of the specimen. This again tended to support the simple strain-rate-independent plastic theory.

It has been suggested that anomalies between experimental results and the simple plastic theory were due, at least in part, to strain-rate effects. A general development of strain-rate-dependent theory was formulated by L.E. Malvern [11], who has worked out numerical solutions assuming that the plastic creep rate is proportional to the imposed stress minus the static stress at the same strain.

Malvern's solutions showed that the strain-rate effect causes small strains to be propagated more rapidly than would be predicted from the simple plastic analysis. The reverse effect is indicated in the case of large magnitude strains with the strain-rate effect giving lower propagation velocities than would be predicted using the simple theory. Also the solution considering the strain-rate effect gave a much higher stress near the impact point since the dynamic loading was considered to be elastic, even above the static yield point.

The strain-rate-dependent theory fails to predict a constant strain region near the impact point, consequently it does fall into considerable disagreement with many of the observed results.

Alter and Curtis [13] in an experiment to correlate the theory of Malvern, observed the propagation of plastic strain pulses along a lead bar. In an attempt to determine decisively the importance of the strain-rate effect, they superimposed two strain pulses separated by a short time interval. The results of the experiment showed:

(a) The head of the pulse travels at a velocity c_o.

(b) Following the head is a large increment of strain which separates rapidly from the elastic head as the pulse propagates along the specimen.

(c) With the superimposed strain pulses, the heads of both pulses travel at velocity c_o but the plastic parts of the pulses tend to join together.

Alter and Curtis thus showed that the strain-rate effect is important in explaining the behaviour of strain pulses propagating in lead.

Sternglass and Stuart [9] experimented with the propagation of strain pulses in prestressed materials in order to validate either the simple plastic theory or the strain-rate-dependent theory. Their experimental procedure was to prestress copper specimens in a tension testing machine, then to apply short duration (< 1 m.sec.), small amplitude ($< 10^3$ μin./in.) strain pulses. The shape of the propagating wave was studied at various points along the specimen in order to determine the parameters governing the pulse amplitude, pulse width, propagation velocity, and change in shape of the pulse.

The preliminary tests of Sternglass and Stuart in the elastic region agreed satisfactorily with theory. Results relating to propagation in the plastic region, however, seemed to point to inadequacies in the simple strain-rate-independent theory. The results showed:

(a) Velocity of wave front (regardless of prestress) was c_0.

(b) $c_n \gg \left(\frac{\psi}{\rho}\right)^{\frac{1}{2}}$.

(c) Dispersion of pulses propagating in the plastic region occurred and appeared to increase with increasing pulse width.

(d) The percent broadening of the pulse did not depend upon the initial amplitude.

(e) The amplitude of the plastic pulse appeared to decay exponentially from the impact point.

(f) $V \neq \int_{\epsilon_1}^{\epsilon_2} \left(\frac{\psi}{\rho}\right)^{\frac{1}{2}} d\epsilon$.

(g) The width of the pulse increased linearly with the hammer mass.

In general, the results of Sternglass and Stuart showed that the von Kármán theory was not satisfactory to describe the transient phenomena of impact.

Clark and Wood [14] investigated the dynamic response of materials by rapidly loading specimens (at a rate of 5×10^6 psi/sec) and simultaneously measuring the stress and strain in the material. They found that for mild steel, which is characterized by a well defined yield point, a finite time interval was required to initiate plastic flow. The time interval ranged from a few milliseconds at 51,000 psi to a few seconds at 37,000 psi. This implies that in impact testing of mild steel where deformation pulses of short duration and of plastic amplitude are to be propagated, the measured pulse amplitude (strain) would be that of the elastic case. No experimentation was done, however, for the case of a material prestressed plastically before impact loading.

For materials with no well defined yield point, Clark and Wood found that no time lag occurred before initiation of plastic flow. They also showed that for materials such as 24 S-T aluminum alloy and 75 S-T aluminum alloy, the rapid loading stress-strain relations fell very close to the static stress-strain curves. This result implies that dynamic loading follows closely the static stress-strain curve at least for these two materials. It must be realized,

however, that rapid loading in this case is much slower than the loading rate in impact testing.

J.F. Bell and A. Stein [18] discuss a trigger-mechanism in the incremental finite loading wave theory in relation to impact tests on annealed aluminum. In the Bell and Stein tests, incremental compression loading waves were propagated following the application of a dynamic prestress. They found that only the incipient portion of the loading wave propagated at the elastic velocity, the rest of the strain wave propagating at velocities predicted from the quasi-static stress-strain curve. This result was observed even when the strain wave amplitude was greater than the original elastic limit of the material. The results quoted tended to support a strain-rate-independent theory with a small elastic strain triggering the plastic flow. The strain-rate-independent interpretation is further upheld by the fact that the incipient strain increment of the wave was found to propagate at c_o only after the prestress had reached a quasi-static condition.

Bell states that the strain-rate-dependent theory (Malvern [11]) is inconsistent with results obtained from annealed aluminum, annealed copper, and lead, and that the rate-independent finite amplitude trigger-mechanism theory is in closer agreement with the results obtained from the aforementioned materials.

The net result to date of the theoretical and experimental work done in the field of longitudinal strain-wave propagation in rods is that although the strain-rate-independent theory of von Kármán does not describe adequately the propagation process, the

same rate-independent theory with the trigger-mechanism modification of Bell gives reasonable agreement with much of the experimental work. The strain-rate-dependent theory of Malvern, on the other hand, also gives close agreement with some of the experimental work. Consequently, the validity of the strain-rate-dependent and strain-rate-independent theories is still in question.

IV THEORY

In order that the results obtained from experimental research be meaningful, consideration must be given to the theoretical aspects of the problem being investigated. The theory developed in the following paragraphs gives a mathematical explanation of the stress wave propagation process, showing the effect of various parameters when the propagation is occurring in materials in the elastic or in the plastic state.

The one-dimensional wave equation for longitudinal waves in elastic bars is;

$$\frac{\partial^2 u}{\partial t^2} = c_o^2 \frac{\partial^2 u}{\partial x^2} \tag{1}$$

where

$$c_o = \left(\frac{E}{\rho}\right)^{\frac{1}{2}} \tag{2}$$

The propagation velocity c_o of deformation is governed by the parameters, density and Young's modulus.

When a body travelling at a velocity V strikes the end of a semi-infinite elastic bar, the compressive stress σ at the struck end of the bar varies according to

$$\sigma = V\sqrt{E\rho}\ \exp\left[-t\sqrt{E\rho}/m\right], \tag{3}$$

where m is the mass of the impacting body per unit cross-sectional area of the bar [1]. The maximum stress, which becomes the maximum amplitude of the stress pulse propagated into the bar at velocity c_o, depends linearly on the velocity of the striking body. The rate of decrease of the stress depends upon the mass of the striking body.

In the case of an impact where momentum is transferred from a hammer to a platform and then to a rod, and where only the hammer velocity is known, the hammer-platform impact must be considered in order to determine the impact velocity acting on the specimen. Two extreme cases of hammer-platform impact may be considered; elastic and perfectly inelastic (the difference being only in the choice of value for the coefficient of restitution, e).

The initial platform velocity $(V_p)_i = 0$ and the final platform velocity $(V_p)_f = V$ where V is the velocity imparted to the specimen from the hammer-platform impact.

Now $$e = \frac{(V_h)_f - (V_p)_f}{(V_h)_i}$$

and from conservation of linear momentum

$$(M_h V_h)_i = (M_h V_h)_f - (M_p V_p)_f$$

where M_h and M_p are the hammer and platform masses and where the subscripts i and f refer to the initial and final conditions. Solving for $(V_p)_f$, we find

$$(V_p)_f = \frac{(1+e)}{\left(1+\frac{M_p}{M_h}\right)} (V_h)_i \quad . \tag{4a}$$

For a perfectly elastic impact, $e = 1$ and

$$V_1 = 2 \left(\frac{M_h}{M_h + M_p}\right) (V_h)_i$$

where V_1 is the velocity imparted to the specimen for a perfectly elastic hammer-platform impact.

For a perfectly inelastic impact where $e = 0$, we find

$$V_0 = \frac{M_h}{M_p + M_h} (V_h)_i \tag{4b}$$

where V_o is the impact velocity acting on the specimen for a perfectly inelastic hammer-platform impact.

These equations show that depending upon the nature of the hammer-platform impact, the peak amplitude of the elastic strain pulse should be in the range

$$\frac{V_o}{c_o} < \epsilon_e < \frac{V_1}{c_o}$$

This implies that if e = constant for a range of V_h values, the elastic strain amplitude ϵ_e should be linearly dependent upon V_h.

In linear elastic materials, the wave propagation process is easily described. The stress wave shape can be calculated theoretically and the wave is shown to travel in the material unchanged in shape with all deformation being reversible. When stress waves are propagated in plastic materials, however, the wave propagation process is not easily described, due to the non-linearity and irreversibility of the stress-strain relationship.

The set of three first-order differential equations governing the propagation of longitudinal stress waves in rods is:

$$\frac{\partial \epsilon}{\partial t} = F(\sigma,\epsilon)\frac{\partial \sigma}{\partial t} + q(\sigma,\epsilon) \qquad \text{(constitutive equation)} \quad (5a)$$

$$\frac{\partial \sigma}{\partial x} = \rho \frac{\partial v}{\partial t} \qquad \text{(equation of motion)} \quad (5b)$$

$$\frac{\partial v}{\partial x} = \frac{\partial \epsilon}{\partial t} \qquad \text{(equation of continuity)} \quad (5c)$$

The constitutive equation (5a)* is in the general form used by J. Lubliner [17]. It can be shown that if $q(\sigma,\epsilon)=0$ and $F(\sigma,\epsilon)=\frac{1}{E}$,

---

* Numbers in curved brackets refer to equation numbers

then the situation is that of the elastic case, and the solution is identical to that given earlier.

The general form of the constitutive equation contains a dynamic loading term and a creep term.

The static stress-strain curve is described by:

$$g(\sigma, \epsilon) = 0$$

or $$\sigma = f(\epsilon) \quad .$$

For constant stress,

$$\frac{\partial \sigma}{\partial t} = 0$$

and

$$\frac{\partial \epsilon}{\partial t} = g(\sigma, \epsilon) \quad \text{(creep term).} \tag{6a}$$

For an imposed stress less than the stress described by the corresponding strain position on the static stress-strain curve,

$$\sigma < f(\epsilon)$$

then $$g(\sigma, \epsilon) \equiv 0$$

Hence, (6a) becomes

$$\frac{\partial \epsilon}{\partial t} = \langle g(\sigma, \epsilon) \rangle \quad . \tag{6b}$$

When the stress rate is very large, then the constitutive equation reduces to:

$$\frac{d\epsilon}{d\sigma} = F(\sigma, \epsilon)$$

where $F(\sigma, \epsilon)$ is a function derived from the dynamic loading curve.

The dynamic loading curve

$$\sigma = f(\epsilon, \epsilon_p) \tag{7a}$$

is a plot of σ vs. ϵ for very large (theoretically infinite) loading rates. The parameter ϵ_p describes the initial state of the material, consequently (7a) represents a family of dynamic loading curves, each curve corresponding to an initial strain condition described by ϵ_p. The function $F(\sigma,\epsilon)$ in the constitutive equation (5a) is related to a specific dynamic loading curve by

$$\frac{d\sigma}{d\epsilon} = \frac{1}{F(\sigma,\epsilon)} \tag{7b}$$

Since the dynamic loading curve is assumed to vary for different values of ϵ_p, the function $F(\sigma,\epsilon)$ as used in (5a) will also be different for different values of ϵ_p.

Unloading is generally assumed to occur elastically, therefore the complete constitutive equation becomes:

$$\frac{\partial \epsilon}{\partial t} = \langle g(\sigma,\epsilon)\rangle + \begin{cases} F(\sigma,\epsilon)\,\dfrac{\partial \sigma}{\partial t}\,, & \dfrac{\partial \sigma}{\partial t} \geq 0 \\ \left(\dfrac{1}{E}\right)\dfrac{\partial \sigma}{\partial t}\,, & \dfrac{\partial \sigma}{\partial t} < 0 \end{cases} \tag{8}$$

By the suitable choice of terms in the general constitutive equation (5a), the strain-rate-independent theory of von Kármán [8] or the strain-rate-dependent theory of Malvern [11] can be derived as can the simple elastic theory.

The von Kármán theory assumes that during impact the loading curve follows the static stress-strain curve for the material. With this assumption the constitutive equation becomes:

$$\frac{\partial \epsilon}{\partial t} = \frac{1}{\psi}\frac{\partial \sigma}{\partial t}\,. \tag{9}$$

In deriving (9), the following relations were used:

$$g(\sigma, \epsilon) = 0$$
$$F(\sigma, \epsilon) = \frac{1}{\psi} \quad .$$

The Malvern theory assumes that a strain-rate effect is present and that dynamic loading occurs along the elastic line of slope E. Malvern used the relations

$$g(\sigma, \epsilon) = K[\sigma - f(\epsilon)] \ ,$$

where $f(\epsilon)$ is a function describing the static stress-strain relation, and

$$F(\sigma, \epsilon) = \frac{1}{E}$$

to derive the complete constitutive equation

$$\frac{\partial \epsilon}{\partial t} = \frac{1}{E} \frac{\partial \sigma}{\partial t} + K[\sigma - f(\epsilon)] \quad . \tag{10}$$

The elastic theory is derived using the relations

$$g(\sigma, \epsilon) = 0$$

and

$$F(\sigma, \epsilon) = \frac{1}{E} \quad .$$

These relations form the constitutive equation

$$\frac{d\epsilon}{d\sigma} = \frac{1}{E}$$

which, when solved with (5b) and (5c) gives rise to the simple elastic result (2).

In the case of the strain-rate-independent theory, the strain wave propagation process is described by three equations, the constitutive equation being of the form of (9):

$$\frac{\partial \epsilon}{\partial t} = \frac{1}{\psi} \frac{\partial \sigma}{\partial t} \qquad \text{(constitutive equation)}$$

$$\frac{\partial \sigma}{\partial x} = \rho \frac{\partial v}{\partial t} \qquad \text{(equation of motion)}$$

$$\frac{\partial v}{\partial x} = \frac{\partial \epsilon}{\partial t} \quad . \qquad \text{(equation of continuity)}$$

From this set of partial differential equations, the one-dimensional wave equation can be derived for longitudinal waves in plastic bars:

$$\frac{\partial^2 u}{\partial t^2} = \frac{\psi}{\rho} \frac{\partial^2 u}{\partial x^2} \quad . \tag{11}$$

Considering a cross-section of material at a distance x from the origin in a semi-infinite rod (diameter small compared to the length of wave being propagated) stretching from the origin to minus infinity, we find that the boundary conditions are [8]:

$$u = Vt \qquad \text{at} \qquad x = 0$$

$$u = 0 \qquad \text{at} \qquad x = -\infty$$

A solution satisfying the boundary condition at $x=0$ is:

$$u = V\left[t + \frac{x}{c_1}\right]$$

and

$$\epsilon = \frac{\partial u}{\partial x} = \frac{V}{c_1} \quad . \tag{12}$$

Another solution is found by setting $\frac{\psi}{\rho} = \frac{x^2}{t^2} = \lambda^2$ (13)

Then $\epsilon = f(\lambda)$

and $$u = \int_{-\infty}^{x} \epsilon \, dx = \int_{-\infty}^{x} f(\lambda) \, dx = t \int_{-\infty}^{\lambda} f(\lambda) \, d\lambda \quad .$$

Differentiating with respect to x and t, we find

$$\frac{\partial^2 u}{\partial t^2} = \frac{\lambda^2}{t} f'(\lambda) \tag{14a}$$

and

$$\frac{\partial^2 u}{\partial x^2} = \frac{1}{t} f'(\lambda) \quad . \tag{14b}$$

Substituting (14a) and (14b) into (11), we find that:

$f'(\lambda) = 0$ leading to (12)

or $\rho\lambda^2 = \psi$ leading to (13) .

The complete solution for the strain-rate-independent theory is expressed in three parts:

for $x > c_0 t$, $\epsilon = 0$ where $c_0 = \left(\frac{E}{\rho}\right)^{\frac{1}{2}}$

for $c_1 t < x < c_0 t$, $\epsilon_Y < \epsilon < \epsilon_1$ and $c = \left(\frac{\psi}{\rho}\right)^{\frac{1}{2}}$

for $x < c_1 t$, $\epsilon_1 = \frac{V}{c_1}$ where $c_1 = \left(\frac{\psi(\epsilon=\epsilon_1)}{\rho}\right)^{\frac{1}{2}}$.

The solution describes an elastic wave front of amplitude ϵ_Y propagating at c_0, a plastic wave front of amplitude ϵ_1, propagating at c_1 and intermediate strain increments propagating at velocities $c = \left(\frac{\psi}{\rho}\right)^{\frac{1}{2}}$.

A plot of constant strain values in the x-t plane results in a series of straight lines of varying slopes. The solution also gives an interpretation of critical impact velocity; when $\psi = 0$, the propagation velocity $c_1 = 0$, hence any strain increments above those corresponding to $\psi = 0$ do not propagate. This results in premature rupture of the rod with little energy being absorbed.

It can be shown that the plastic strain ϵ_1 as a function of the impact velocity V is described by the following equation:

$$V = \int_0^{\epsilon_1} \left(\frac{\psi}{\rho}\right)^{\frac{1}{2}} d\epsilon \quad .$$

Solution of the special case when $\psi = E$ reduces to the familiar form:

$$\epsilon = \frac{V}{c_0} \quad .$$

In the case of the strain-rate-dependent theory, a constitutive equation of the form of (10) can be used. The strain wave propagation process can then be described by the following three

equations:

$$\frac{\partial \epsilon}{\partial t} = \frac{1}{E}\frac{\partial \sigma}{\partial t} + K[\sigma - f(\epsilon)] \qquad \text{(constitutive equation)}$$

$$\frac{\partial \sigma}{\partial x} = \rho \frac{\partial v}{\partial t} \qquad \text{(equation of motion)}$$

$$\frac{\partial v}{\partial x} = \frac{\partial \epsilon}{\partial t} \qquad \text{(equation of continuity)}$$

The solution of the above equations has been carried out by Malvern [11] using numerical techniques after assuming a suitable function for the quasi-static stress-strain relation.

The significance of Malvern's strain rate solution is most apparent in the x-t plane. It is found that when strain-rate dependency is assumed, the constant strain lines appear in the x-t plane as concave-upward curves. The low magnitude strain increments propagate at higher velocity than would be predicted from the strain-rate-independent theory, and the high magnitude strains propagate at a lower velocity than the rate-independent theory would predict.

V EXPERIMENTAL APPARATUS

In general, the experimental apparatus is designed to load a specimen to a pre-determined stress level, initiate a strain pulse, measure the stress level, read out the shape of the strain pulse at specific positions on the specimen, and to read out the static strain at specific points on the specimen.

Because of these requirements, three distinct systems are needed: a mechanical system to load the specimen and to initiate the stress waves; an electronic system to measure the specimen pre-stress, to read out the static strain at specific positions on the specimen, and to read out the dynamic strain at specific positions on the specimen after impact; and a recording system to preserve the strain vs time plots of a number of positions on the specimen.

5.1 MECHANICAL SYSTEM

The mechanical system, although composed of many different components, can be described as being made up of two sub-systems, the load applying system and the impact producing system.

The load applying system, Fig. 1. applies load directly to a suspended specimen through a lever. This method of loading does not allow the specimen to creep to a lower stress level during testing. The pin-connected grip arrangements at the upper and lower ends of the specimen provides for self-alignment of the specimen, and the vertical guide at one end of the loading beam provides lateral stability. Coarse and fine adjustments for the loading beam position are provided.

The impact producing system, Fig. 2., consists of a hammer, falling a variable distance under the influence of gravity, striking a light platform fixed to the specimen at some position between the upper and lower grips. Unloading waves are propagated below the platform and loading waves, above. The hammer weight is variable by the addition of weights, and the impact velocity can be varied by changing the drop height of the hammer above the platform. The position of the hammer pivot point is adjustable as is the position of the impact receiving screws.

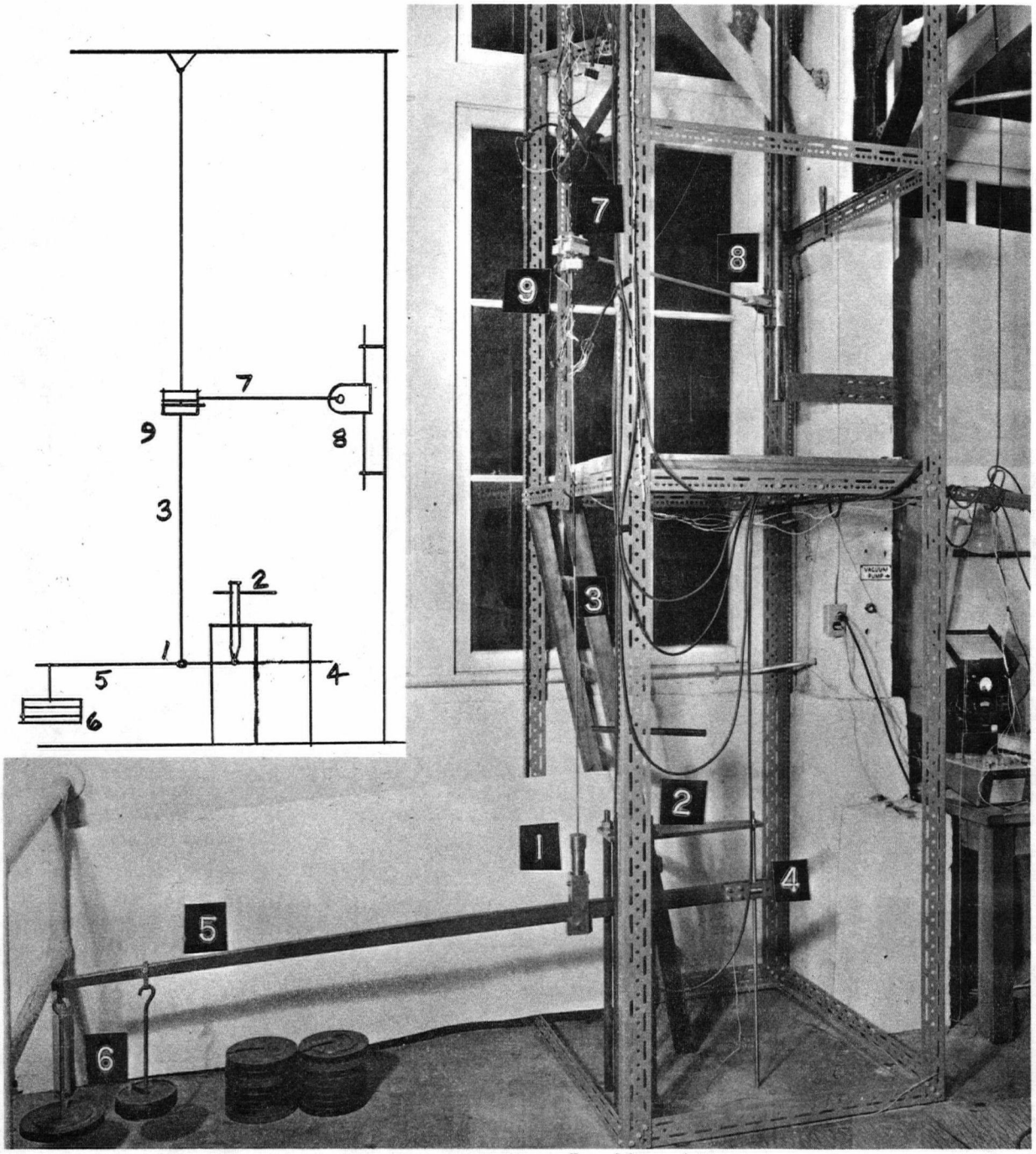

1. Lower grip
2. Fine adjustment
3. Specimen
4. Lateral guide
5. Loading beam
6. Weights
7. Hammer
8. Hammer adjustments
9. Platform

Fig. 1. Mechanical Apparatus Photograph

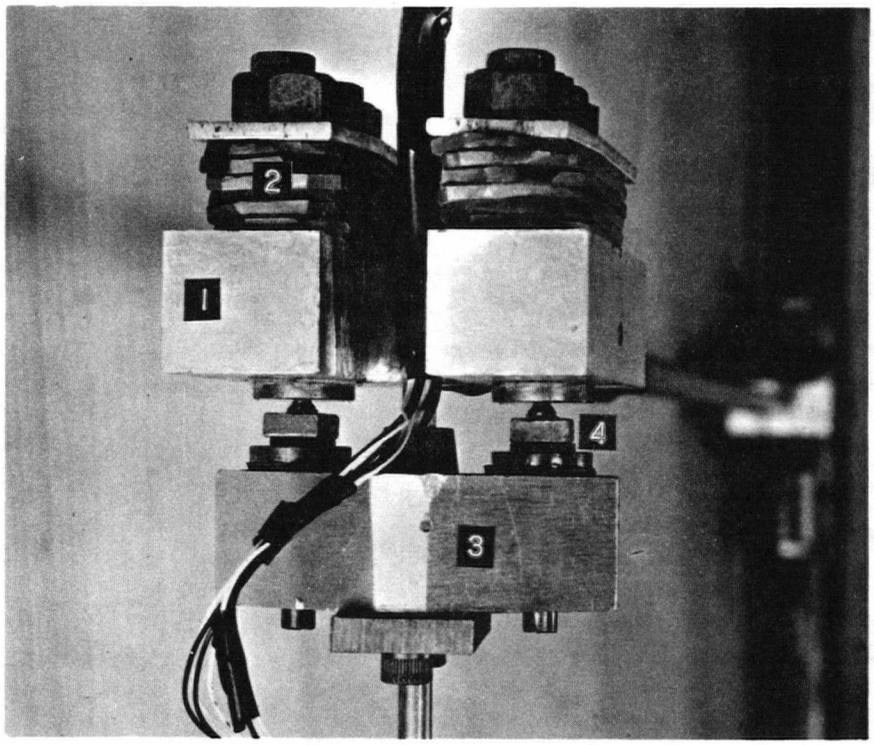

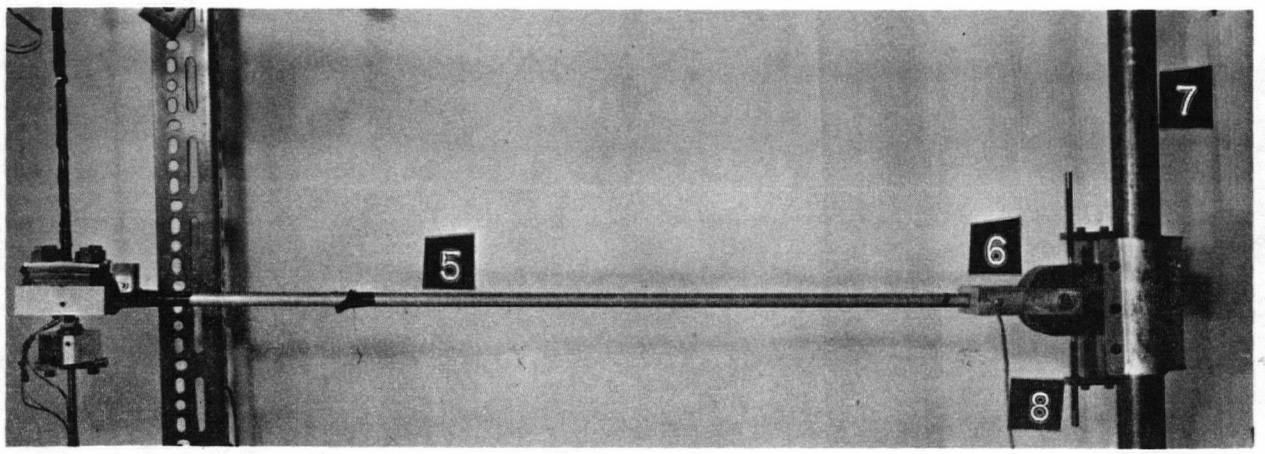

1. Hammer head
2. Lead weights
3. Platform
4. Impact receiving screws
5. Hammer arm
6. Hammer pivot
7. Coarse adjustment
8. Fine adjustment

Fig. 2. Hammer and Platform Photographs

5.2 ELECTRONIC SYSTEM

The electronic system is designed to do three things: to determine the prestress level of the specimen; to drop the hammer positively, triggering the oscilloscopes at the instant of impact and recording on the oscilloscopes the strain vs time plots of specific points on the specimen; and to allow the accurate measurement of static strain at specific points of the specimen. These functions are accomplished by five separate sub-systems integrated by a central control unit, Figs. 3. and 4.

The five sub-systems are:

(i) Load measuring circuit

(ii) Electromagnetic hammer release circuit

(iii) Cathode-ray oscilloscope (C.R.O.) triggering circuit

(iv) Dynamic strain readout circuit

(v) Static strain readout circuit

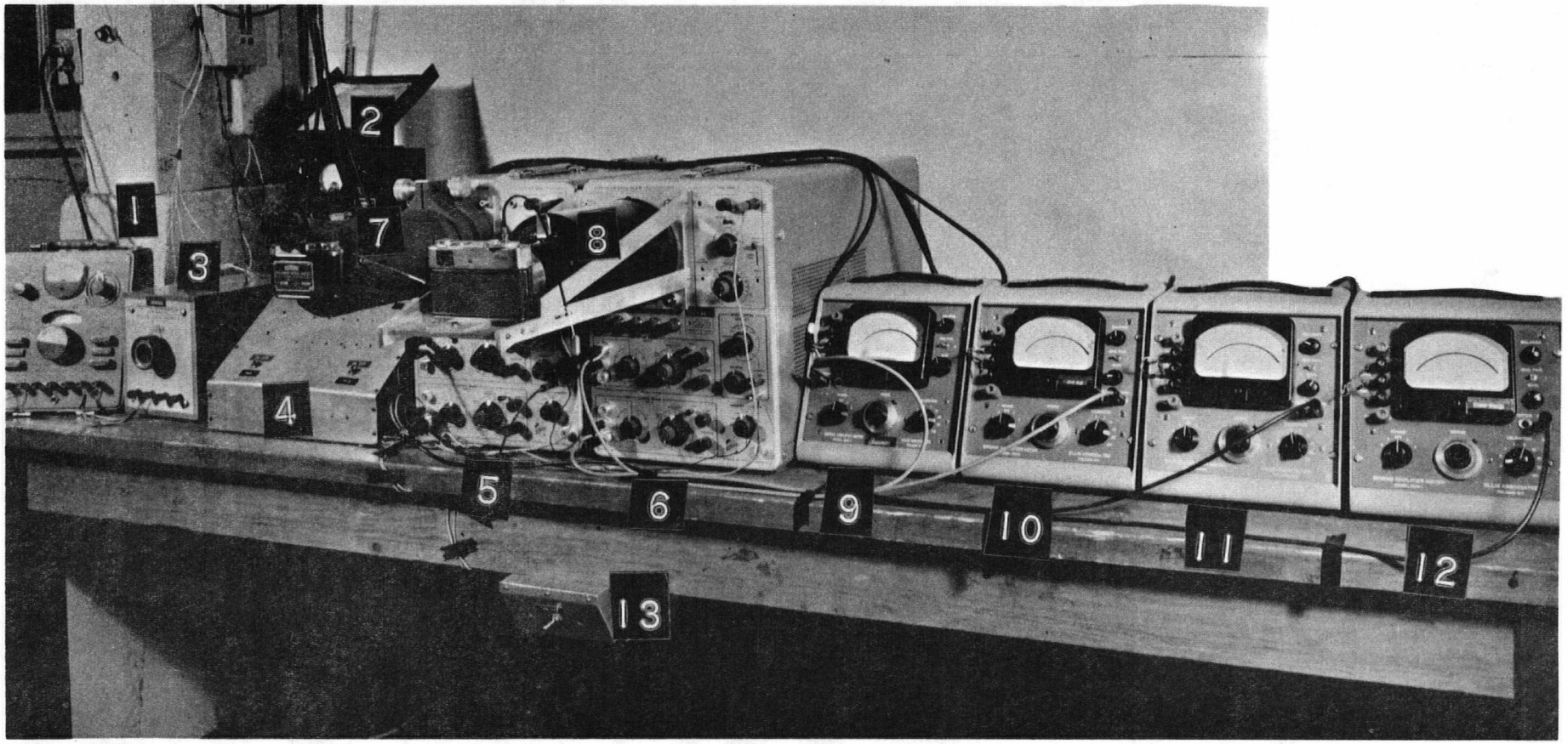

1. Baldwin SR-4 strain indicator for permanent strain readout
2. Baldwin SR-4 strain indicator for load cell readout
3. Polyphase switch
4. Control box
5. & 6. Tektronix 502-A oscilloscopes
7. Dumont 35 mm oscilloscope camera
8. Yashica 35 mm camera and oscilloscope adapter
9.-12. Ellis BAM-1 units
13. Knee operated on-off switch for electromagnet

Fig. 3. Instrumentation

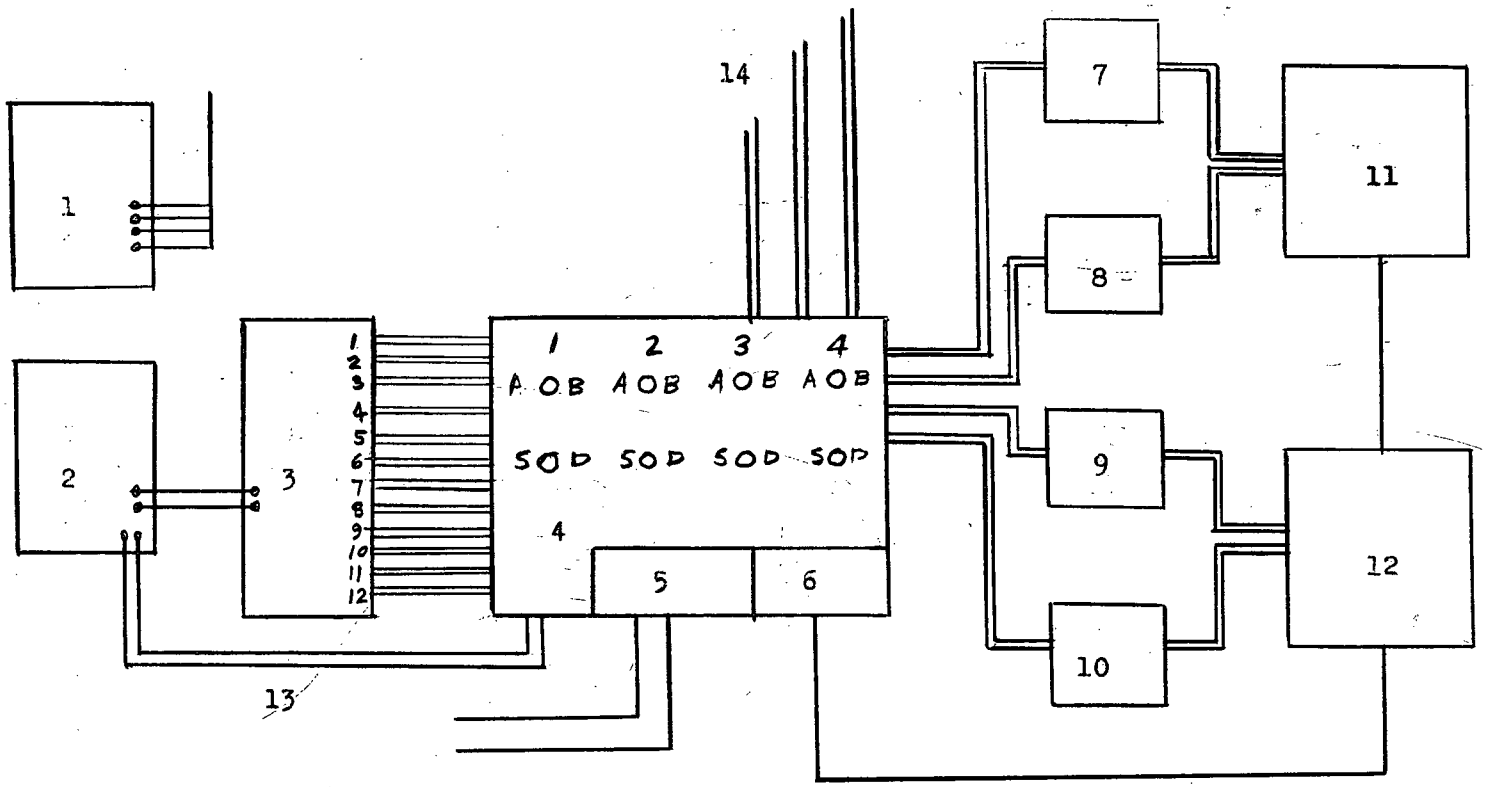

1. SR-4 readout for load cell.
2. SR-4 static strain readout.
3. Polyphase switch.
4. Central control and switching unit.
5. Electromagnet circuit.
6. Triggering circuit.
7.-10. Ellis BAM-1 units.
11.-12. Tektronix 502-A oscilloscopes.
13. Static compensating gage leads.
14. Active strain gage input leads.

Fig. 4. Block Diagram of Electronic Circuit

5.3 RECORDING SYSTEM

The recording system consists of two 35 mm cameras suitably adapted for oscilloscope work. High speed black-and-white film is used with time exposure and large lens opening.

Details of the experimental apparatus, calibration of equipment, and test procedure can be found in Appendix A.

VI RESULTS AND DISCUSSION

6.1 PRELIMINARY RESEARCH

The first phase of the research was carried out using cold-drawn and hot-rolled mild steel specimens. The prime purpose of testing in this phase was to check the equipment operation, gage mounting techniques and recording methods, and to become familiar with all facets of equipment operation. The small set of data obtained from this preliminary research served to show that pulse amplitudes could be predicted with reasonable accuracy and that the shape of the pulses could be reproduced provided that the parameters governing impact and the prestress were held constant.

Certain problems associated with the testing of the cold-drawn and hot-rolled mild steel rods prevented the gathering of any amount of significant data from these tests. The cold-drawn material was found to deform plastically only at the upper grip (on reflection of the strain wave) when the prestress was very high. No sign of plastic wave propagation was observed on the oscilloscope traces in the loading or unloading regions. The hot-rolled material, on the other hand, was decidedly inconsistent in cross-section so that the state of stress at any given point on the specimen was indeterminable. Although no meaningful results were obtained from the hot-rolled or cold-drawn steel specimens, the tests did serve to give some indication of the problems in experimentation that would be encountered with specimens prestressed into the plastic region.

6.2 STUDY OF LOADING AND UNLOADING WAVES

The second phase of the research program consisted of impact testing quarter-hard electrolytic copper specimens. Loading and unloading waves were studied by mounting strain gages above and below the impact point. In the series of tests, various hammer velocities and hammer masses were employed to initiate impacts at a number of specific prestress values, the prestress values being both in the elastic and plastic regions of the quasi-static stress-strain curve.

Results in the Elastic Region

In the elastic region, the loading and unloading waves were identical and did not appear to decay or disperse as they propagated. The amplitude of the strain waves was found to be linearly dependent on hammer velocity at impact, Fig. 26.* and the calculated theoretical wave shapes compared favorably with the recorded shapes of the loading and unloading waves, Fig. 5. (Sample calculations can be found in Appendix B.) The propagation velocities of the waves were identical and were within the calculated elastic propagation velocity of 12,420 fps $\pm$ 4%.

Results in the Plastic Region

In the plastic region, the unloading strain wave remained almost identical in shape to its appearance in the elastic region. The loading strain wave, however, started out after impact as a very

---

*Figs. 26. to 41. inclusive are found in Appendix C.

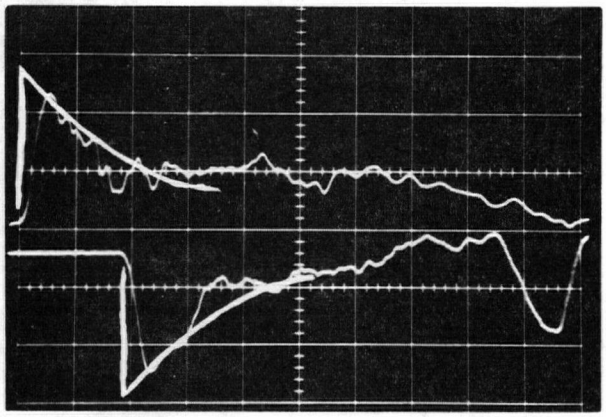

Top trace is 1" from impact
Bottom trace is 57" from impact

Note reflected loading wave in lower trace occurring after about 1.7 m.sec.

Reflected unloading wave appears in traces after about 0.9 m.sec.

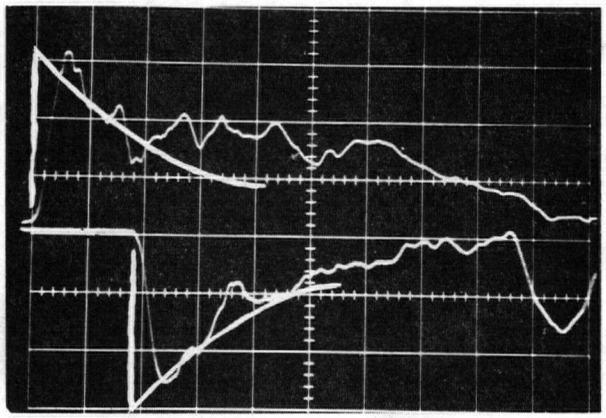

The wide superimposed curve is the theoretical exponential wave shape.

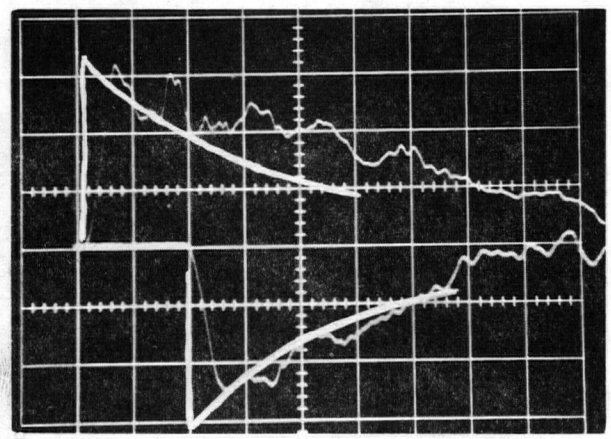

W_h = 1.265 lb.
1.977 lb.
2.857 lb.

σ_{pr} = 8,750 psi

V_h = 11.66 psi

W_p = 0.765 lb.

Horizontal = 0.2 m.sec/cm.

Vertical = 250 μin./in. per cm.

Fig. 5. Comparison of Theoretical and Experimental Shape of Elastic Strain Waves

high amplitude wave, decaying rapidly as it propagated. The complete shape of the loading wave is not discernable because of the occurrence of reflected waves. The unloading tail on the plastic loading wave does, however, appear to be quite different from the tail on the elastic loading wave, being much flatter in nature.

It appears that there is no difference (within $\pm$ 2%) between the propagation velocities of the first increments of the plastic loading and unloading waves and the elastic waves, all velocities being 12,420 fps. It is also apparent that strain increments above a certain strain level in the loading wave are propagated at sub-elastic velocities. This accounts for the bending or flattening of the wave front as propagation of the wave progresses, Fig. 6.

The fact that initial increments of strain initiated at plastic prestress propagated at the elastic velocity while successively higher increments of strain propagated at successively lower velocities sparked an interest in establishing the complete shape of the dynamic decay curves (plots of maximum strain wave amplitude vs distance from impact) and permanent strain distribution curves at various levels of prestress. This interest motivated the third phase of the research program.

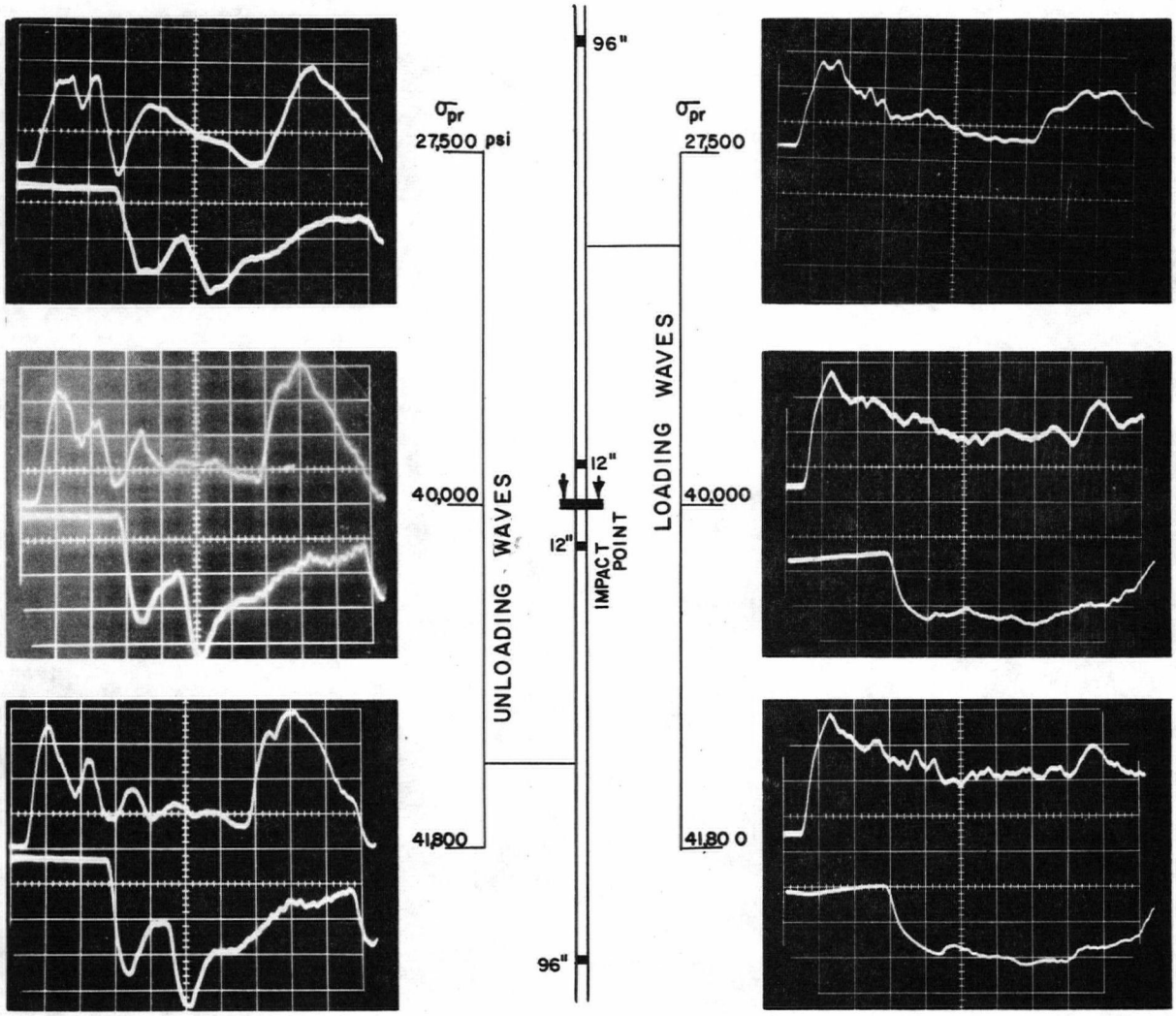

Note that the reflected unloading strain waves in the unloading region are very similar in shape in all three photographs. In the loading region, the reflected loading waves are lost at the higher prestresses. The strain waves in the loading region change shape considerably between the two gages at the higher prestress while the strain waves in the unloading region propagate with little change in shape.

V_h = 9.55 fps.

W_p = 0.765 lb.

W_h = 2.417 lb.

Horizontal = 0.2 m.sec/cm.

Vertical = 200 μ in./in. per cm.

The upper trace in each photograph is from the position closest to the impact point, the lower traces being from the more distant position.

Fig. 6. Comparison of Loading and Unloading Strain Waves.

6.3 DETAILED STUDY OF LOADING WAVES

The third phase of research was carried out with the impact receiving platform being placed about one-third of the way from the bottom of the specimen and with all strain gages except one being mounted above the impact point. This arrangement was adopted to give a more complete picture of the decay and dispersion characteristics of the propagating plastic pulse. In each test series of the set, the prestress was increased to predetermined levels. In different series, the hammer velocity and hammer weight were varied independently at each prestress level. This, of course, gave a series of dynamic decay curves for different hammer velocities and a series of curves for different hammer weights at each prestress. For each series of dynamic decay curves, there was also a series of permanent strain distribution curves obtained.

Results in the Elastic Region

In the elastic region, it was again found that the propagation velocity of the strain waves was 12,420 fps ($\pm$ 2%). The elastic pulses were found to attentuate negligibly, even over distances of from 8 to 10 feet, Figs. 7. and 8. It was observed, however, that the pulse recorded very near the impact point was, in all cases, erratic and of slightly higher amplitude than the pulses recorded at successively more distant stations. No noticeable permanent deformation was observed at the low elastic prestress levels. The recorded wave shapes were found to agree satisfactorily

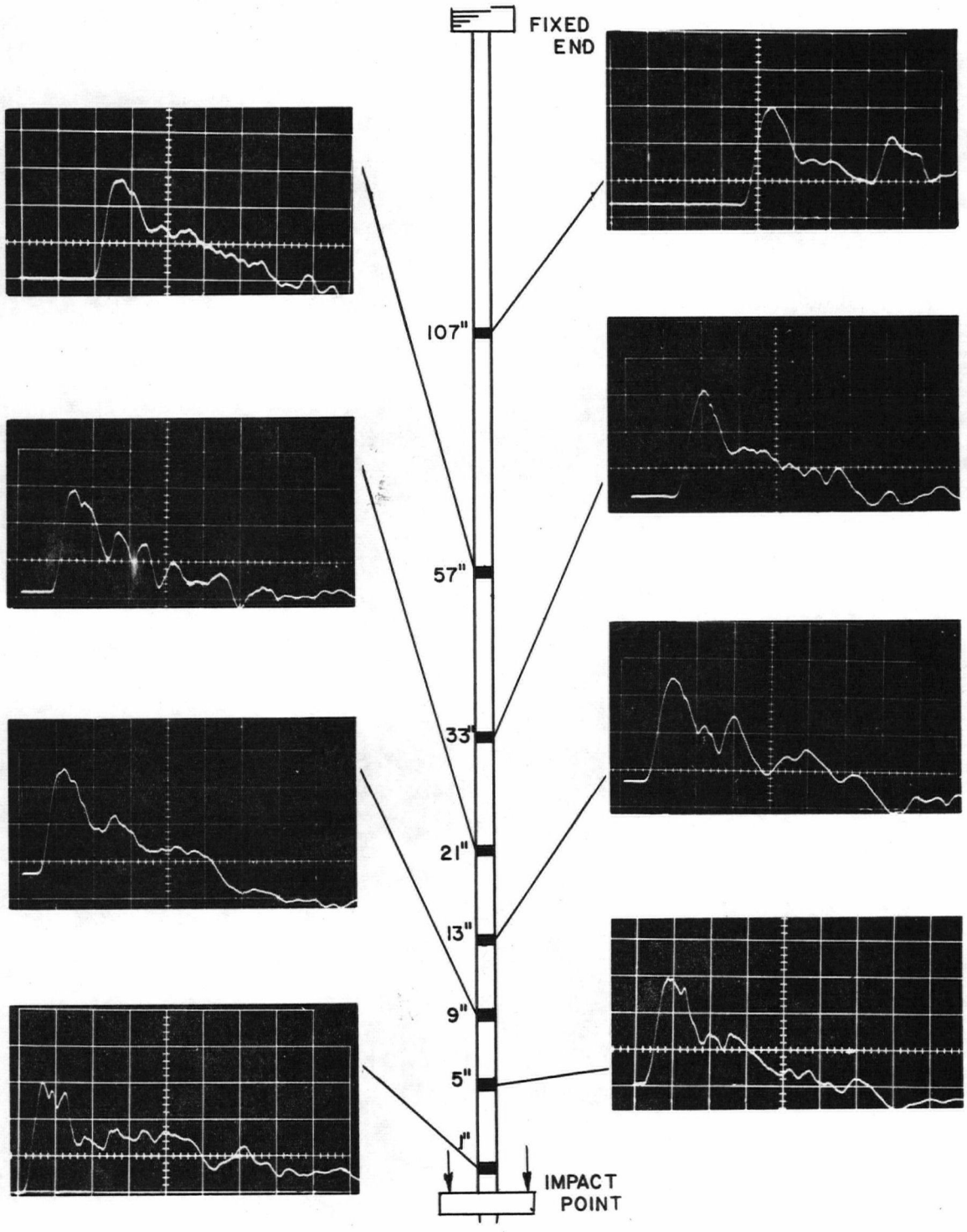

σ_{pr} = 19,550 psi

V_h = 11.66 fps

W_h = 1.977 lb.

W_p = 0.765 lb.

Horizontal = 0.2 m.sec/cm.

Vertical = 250 μ in./in. per cm.

Fig. 7. Elastic Strain Wave at Eight Positions in Loading Region

Cu specimen #2

σ_{pr} = 8,750 psi

W_h = 2,867 lb.

W_p = 0.765 lb.

V_h = 11.66 fps

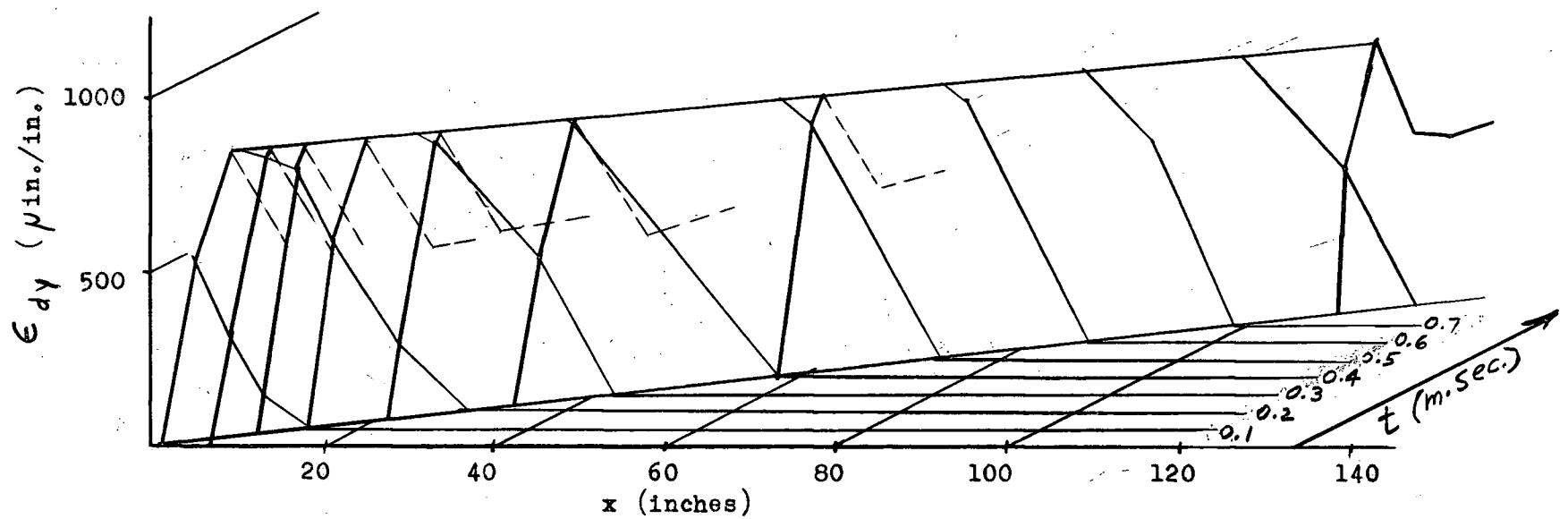

Fig. 8. Dynamic Strain vs Distance From Impact vs Time for Elastic Strain Wave

with the calculated theoretical wave shapes except in the case of the recorded wave nearest the impact point.

Results in the Plastic Region in the ϵ-x Plane

In the plastic region, the pulses were found to change shape quite drastically from the impact point to successively further recording positions, Figs. 9. and 10. The decay curves appeared to be exponential in shape, becoming much steeper and decaying to lower values when the prestress level was raised, Fig. 28. It is also apparent that all pulses propagated at a given prestress level did not decay to a common strain level within the eight feet over which readings were taken. Pulses of large initial amplitude were found to decay to higher strain levels than were pulses of low initial amplitude, Figs. 29. and 30. In all cases, the pulses began with amplitudes larger than the elastic amplitudes and decayed to amplitudes below the elastic amplitudes, where the elastic amplitude is the amplitude of an equivalent pulse propagated in the elastic region of the quasi-static stress-strain curve.

The permanent strain distribution curves show that most of the impact energy was expended deforming the sections of the specimen very close to the impact point and close to the upper grip. Very little deformation occurred in the central section of the loading end of the specimen or below the impact point in the unloading section of the specimen. It is also apparent from the plots of permanent strain readings after successive impacts that the permanent strain increments for each impact at a given set of conditions were approximately the same, Fig. 11. However, a change in the prestress

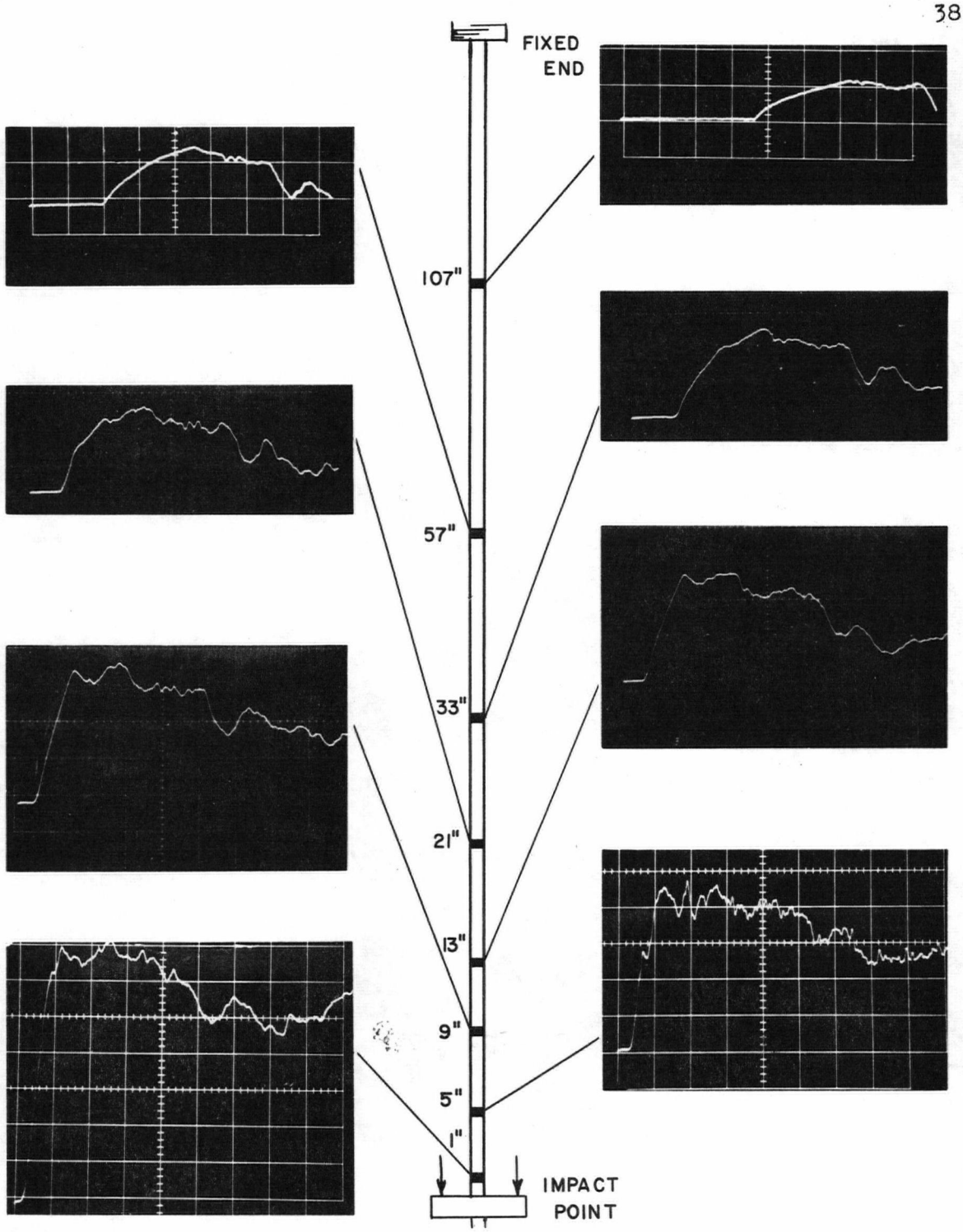

σ_{pr} = 45,700 psi

V_h = 11.66 fps

W_h = 1.977 lb.

W_p = 0.765 lb.

Horizontal = 0.2 m.sec/cm.

Vertical = 250 μ in./in/ per cm.

Fig. 9. Plastic Strain Wave at Eight Positions in Loading Region

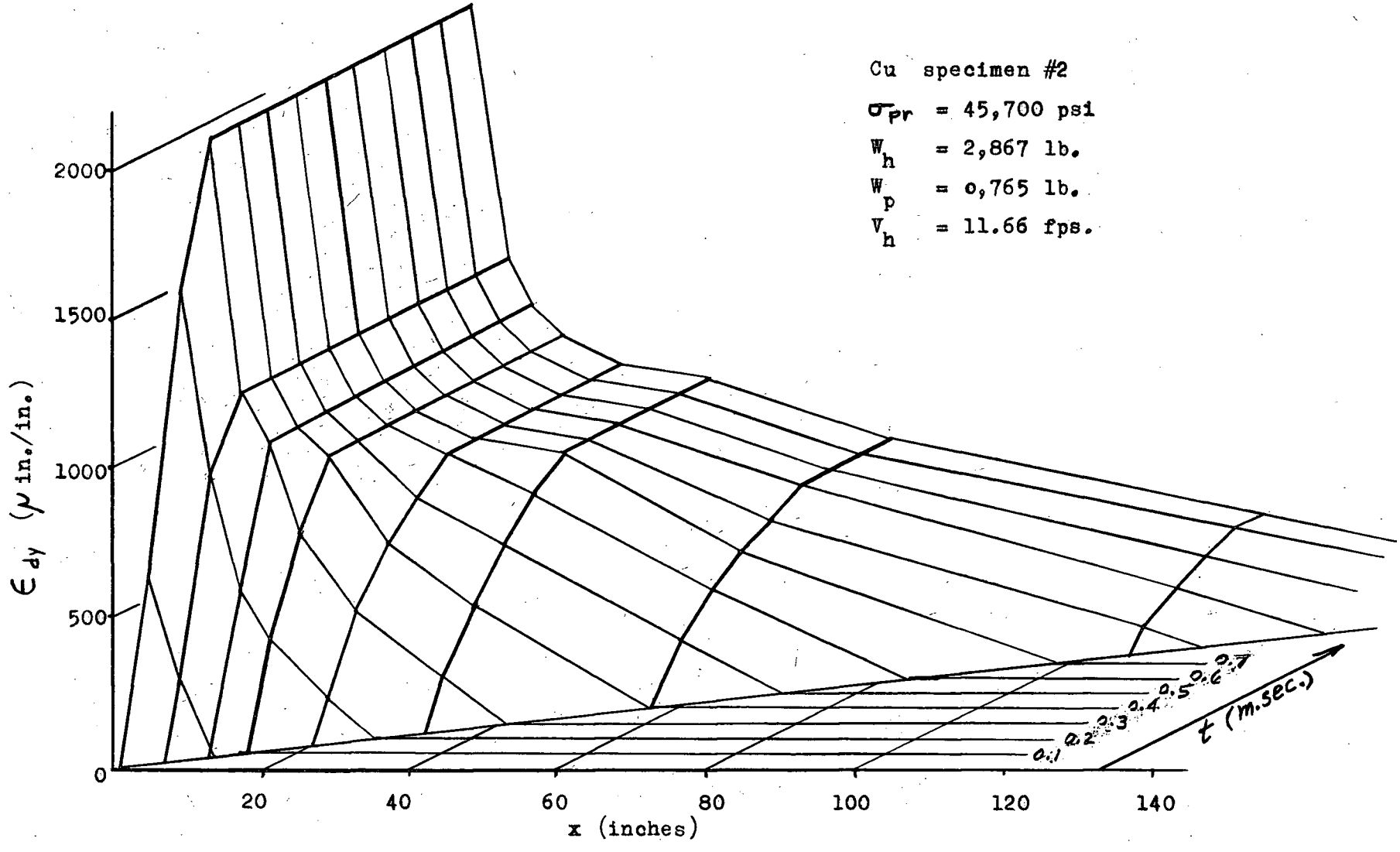

Fig. 10. Dynamic Strain vs Distance from Impact vs Time for Plastic Strain Wave

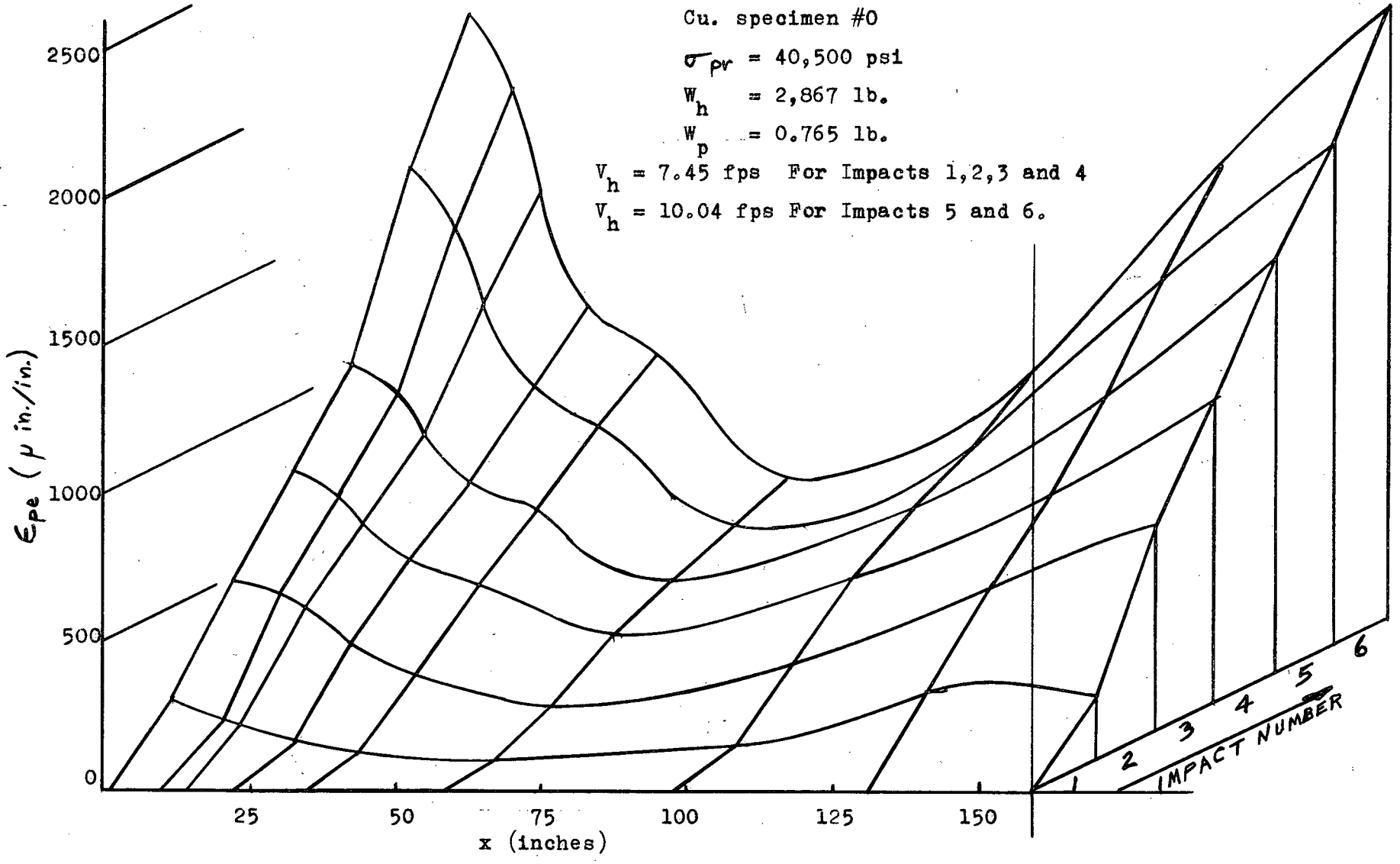

Fig. 11. Permanent Strain vs Distance from Impact for Six Impacts

level, hammer velocity or hammer weight greatly alters the shape of the permanent strain distribution curve, Figs. 31. 32. and 33.

Results in the Plastic Region in the x-t Plane

The propagation velocity of the first increment of the plastic strain waves was invariably found to be the elastic propagation velocity c_o = 12,420 fps $\pm$ 2%. This velocity persisted regardless of the level of prestress to which the specimen had been loaded. Successive increments of strain (after the initial elastic increment) were found to propagate at velocities successively lower than c_o (which is evident as a flattening of the wave front as propagation progresses Fig. 12.), the propagation velocity of a given increment being dependent upon the prestress condition of the specimen. This fact can be seen by observing that as the prestress level is raised, the wave front decreases in slope at a given position above the impact point, Figs. 13. and 14. The loading wave at the highest prestresses appears to have a plateau of constant strain following the wavefront. This plateau is interrupted by the reflection of the unloading wave from the lower grip which occurs after a pulse length of about 0.8 milliseconds, Fig. 27.

The plotting of constant strain levels in the x-t plane is accomplished by laying off the times t elapsed from initiation of impact until the strain rises to a given level ϵ at a distance x from the impact point. Plotting the constant strain levels in the x-t plane gives a family of important curves. The plot of elastic wavefronts in the x-t plane would appear as a family of parallel lines of slope $1/c_o$. The plot of constant strain curves for plastic

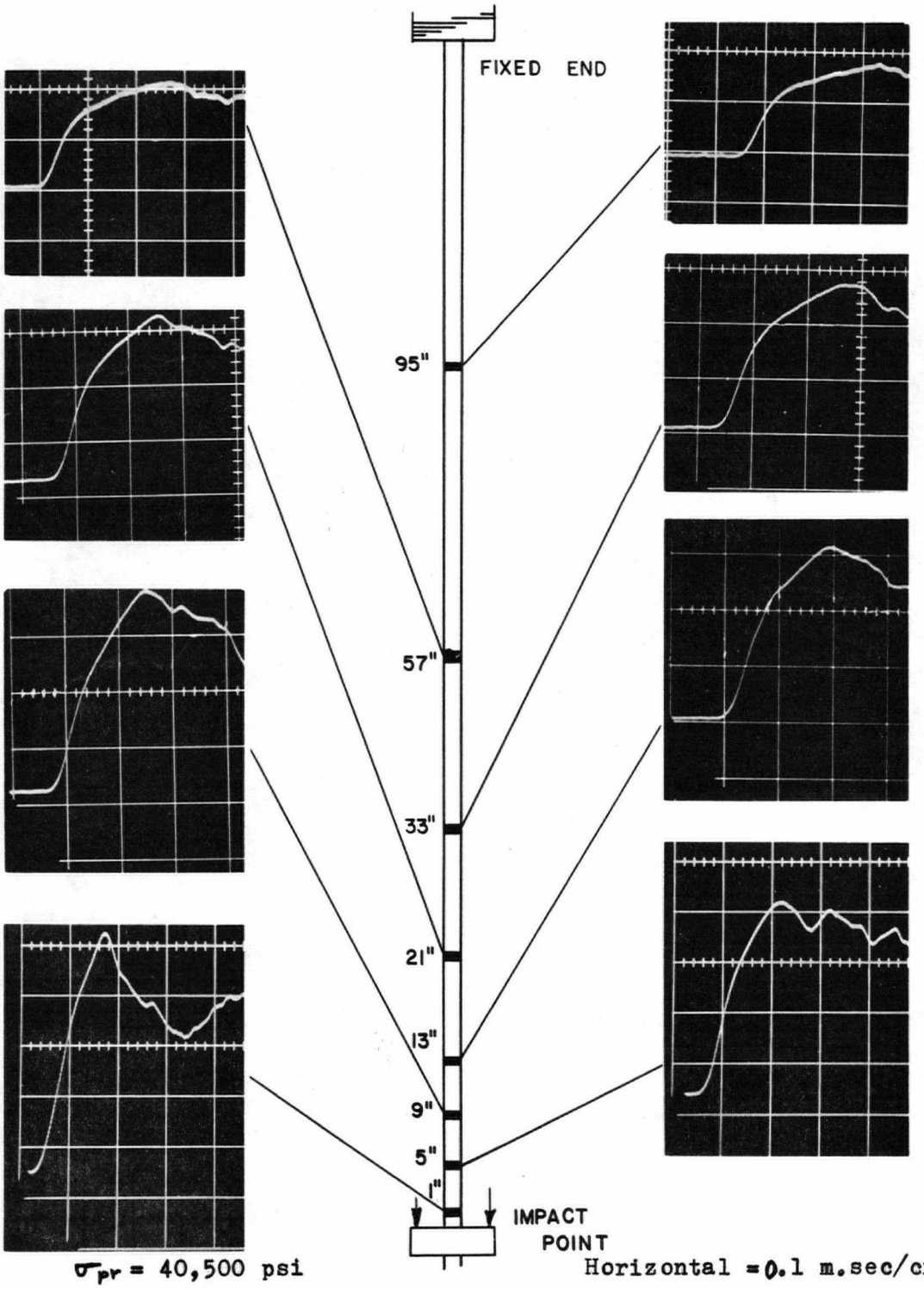

σ_{pr} = 40,500 psi

V_h = 11.66 fps

W_h = 2.857 lb.

W_p = 0.765 lb.

Horizontal = 0.1 m.sec/cm.

Vertical = 250 in./in. per cm.

Fig. 12. Strain Wave Front at Eight Positions in Loading Region

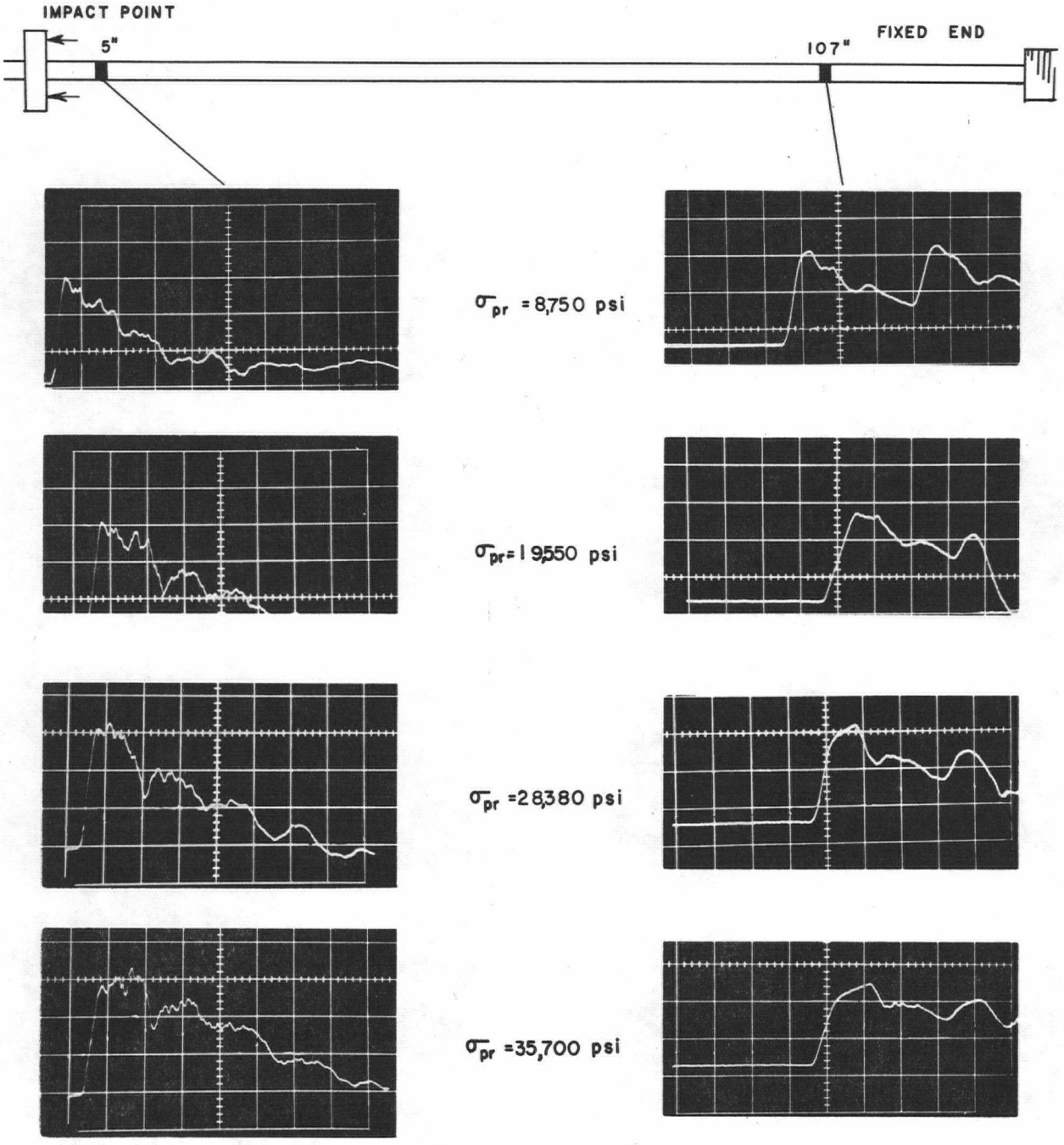

V_h = 11.66 fps

W_h = 2.857 lb.

W_p = 0.765 lb.

Horizontal = 0.2 m.sec/cm.

Vertical = 250 in./in. per cm.

Fig. 13. Shape of Strain Wave at Two Positions In Loading Region for σ_{pr} = 8,750, 19,550, 28,360, 35,700 psi.

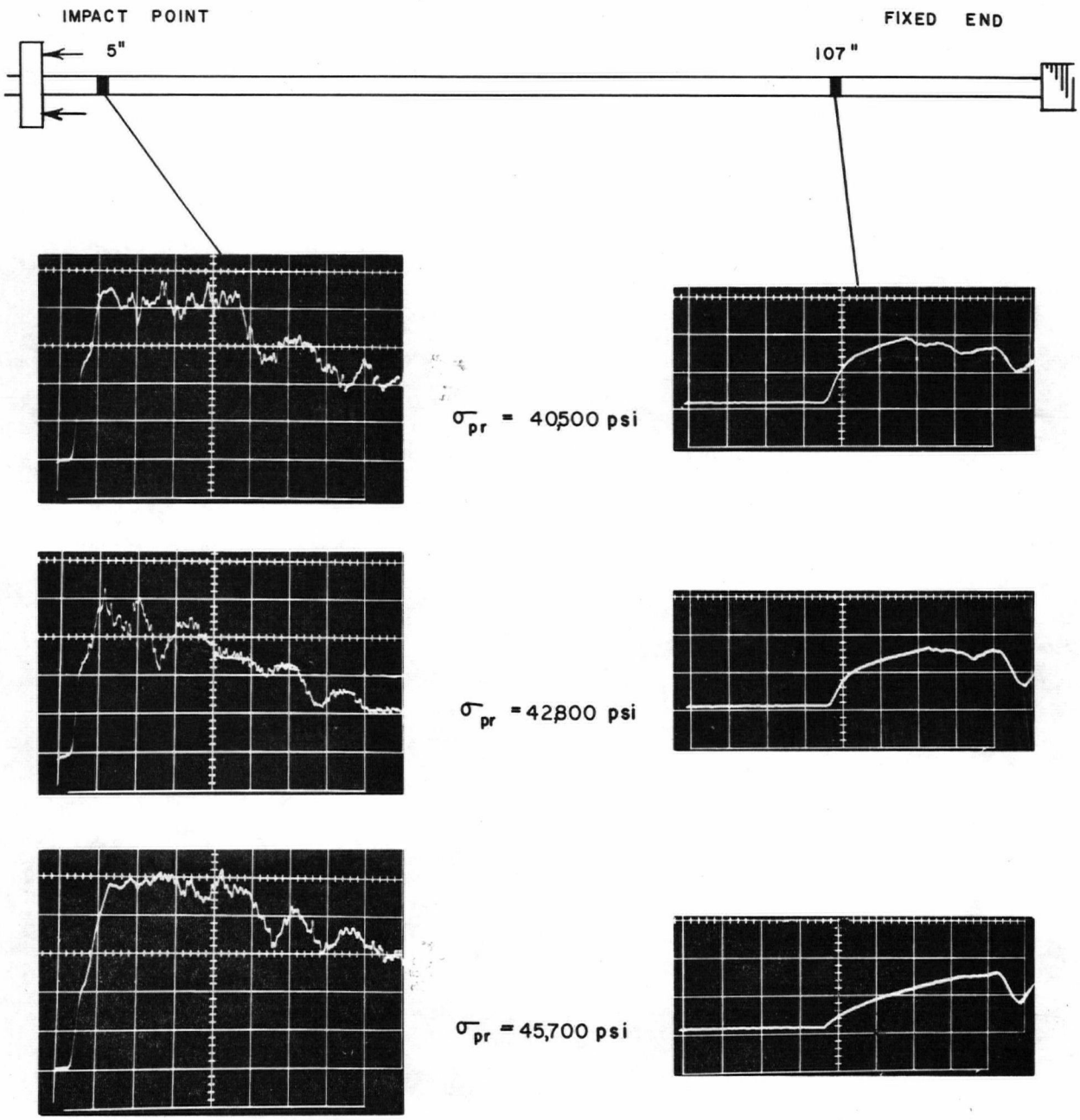

V_h = 11.66 fps
W_h = 2.857 lb.
W_p = 0.765 lb.

Horizontal = 0.2 m.sec/cm.
Vertical = 250 in./in. per cm.

Fig. 14. Shape of Strain Wave at Two Positions In Loading Region For σ_{pr} = 40,500, 42,800, 45,700 psi

wave fronts, on the other hand, appears as a family of non-parallel curves. The first curve (corresponding to the first infinitesimal increment of strain) plots as a straight line of slope $1/c_o$. The curves for succeeding strain increments can be approximated by straight lines of slopes $1/c_n$, Fig. 15. Knowing the respective c_n for the n strain increments, the effective deformation moduli ψ_n can be calculated. It is then possible to plot the dynamic loading (stress-strain) curve, Fig. 16. (See Appendix B for sample calculation).

The determination of the quasi-static stress-strain relation in itself proved to be a challenging problem. Test specimens with machined portions of reduced cross-section were found to give inconsistent diagrams. Consequently the stress-strain diagrams used in the results were obtained by pulling in tension 1/4 inch diameter test specimens that had previously been prestressed to 42,500 psi, Fig. 25. Appendix A. The load value was read from an Instron testing machine, and strain was read directly from a resistance strain gage (Budd Metalfilm C9-121) mounted on the specimen. An interesting feature of the stress-strain diagram is that at a strain rate of .005 in/in/min. the ultimate limit appears to be 50,500 psi, the curve being level at this stress up to about 3% strain. When the strain-rate is suddenly increased by a factor of 100 during the test, the ultimate limit appears to jump to about 52,500 psi from the previously established level of 50,500 psi.

It is interesting to note that the dynamic loading curves in all cases begin with greater slope and end with lesser slope than

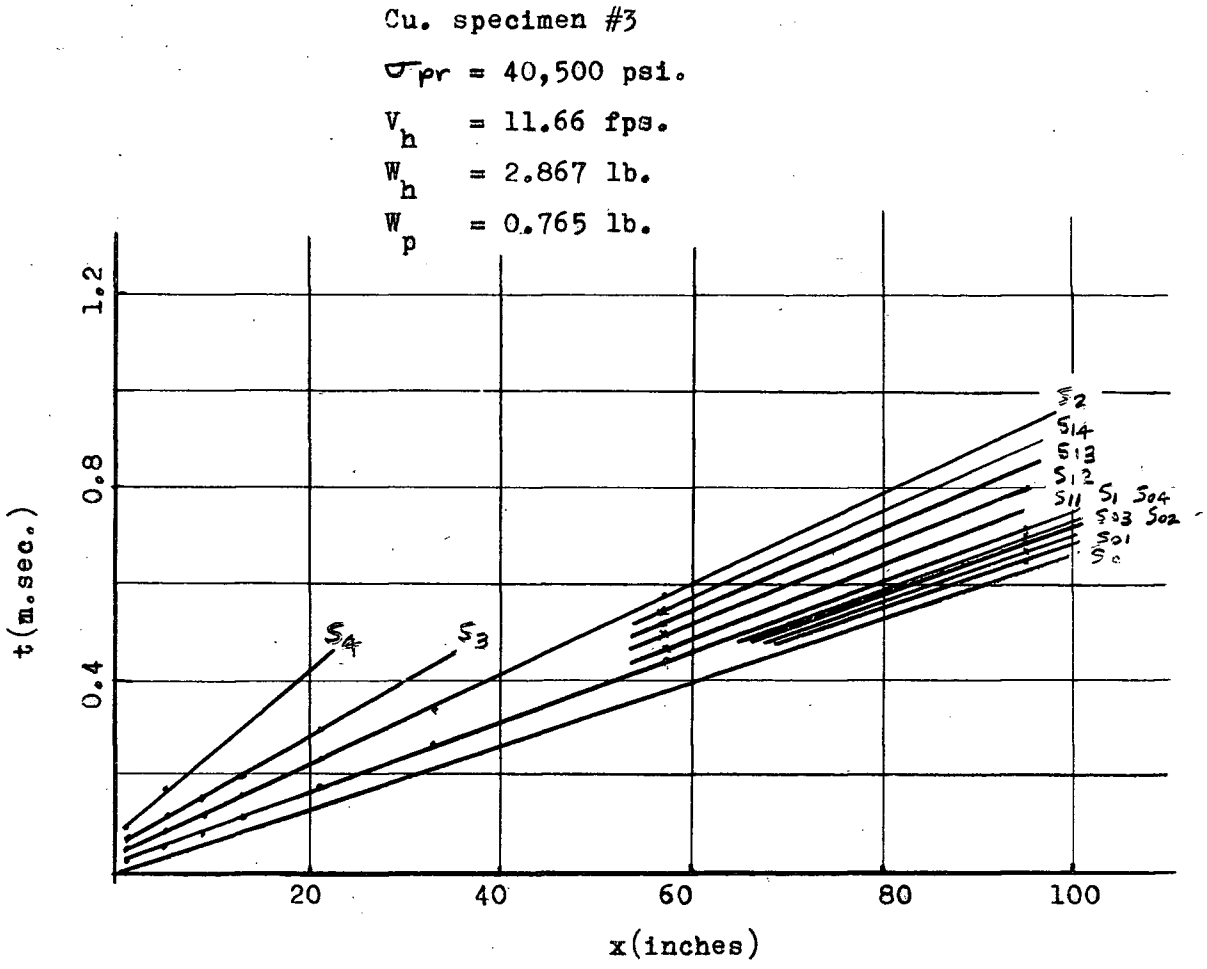

SLOPES	Δε (μ in./in.)
S_0 = .33	
S_{01} = .334	50
S_{02} = .338	50
S_{03} = .342	50
S_{04} = .346	50
S_1 = .35	50
S_{11} = .368	50
S_{12} = .386	50
S_{13} = .404	50
S_{14} = .422	50
S_2 = .44	250
S_3 = .675	125
S_4 = .95	

Fig. 15. Constant Strain Curves in x-t Plane for Cu. Specimen #3.

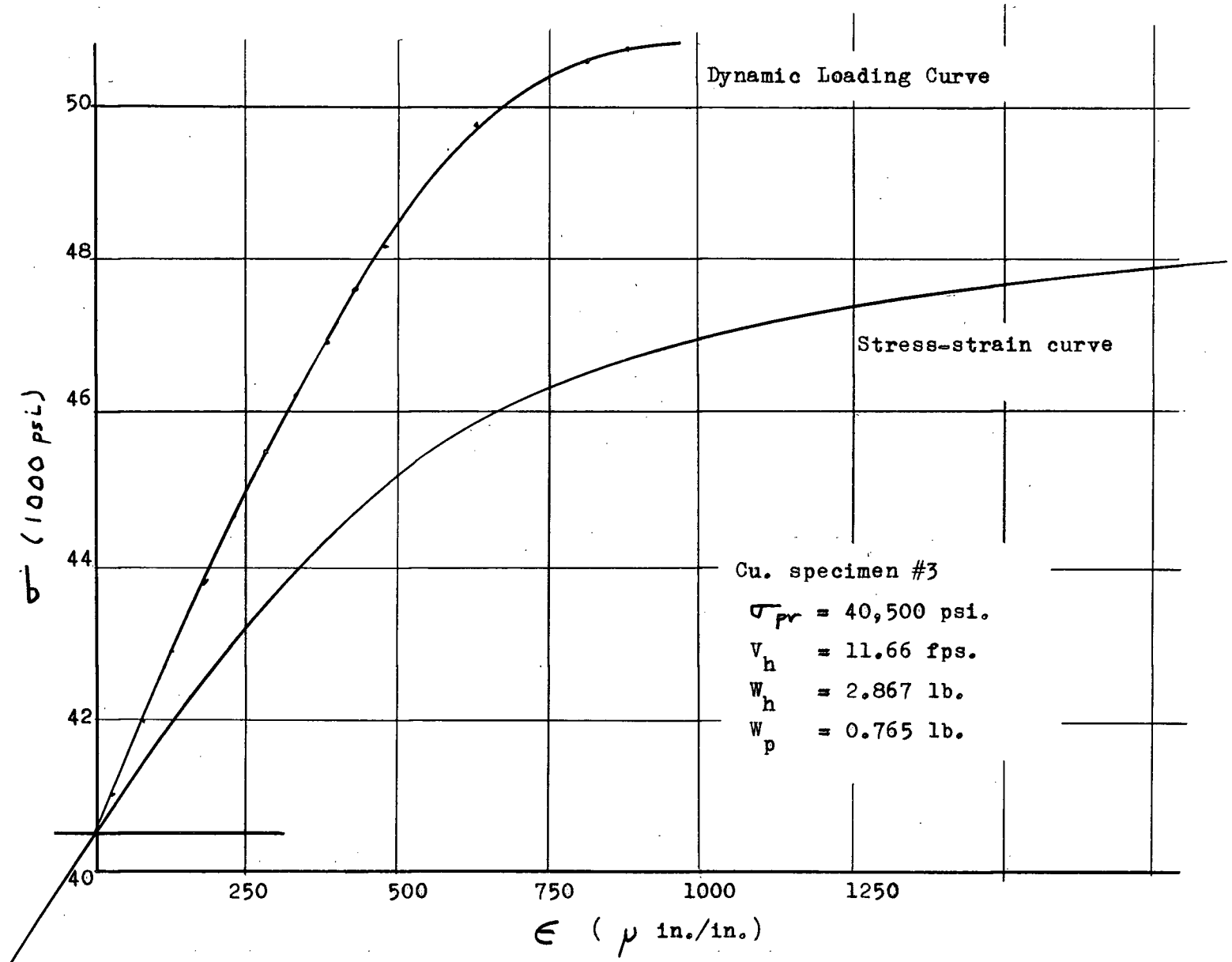

Fig. 16. Dynamic Loading Curve on Quasi-Static Stress-Strain Curve for Cu. Specimen #3.

the equivalent portion of the quasi-static stress-strain curve, Figs. 16. 37. and 41. This implies that initial increments of strain are propagated at higher velocities than would be predicted by the von Kármán theory. Conversely, the highest increments of strain are propagated at lower velocities than the von Kármán theory predicts. It is also notable that the peak stress to which the strain waves rise is in excess of the stress at the same strain position on the quasi-static stress-strain curve. The results, in fact, tend to qualitatively support the Malvern strain-rate-dependent theory. Furthermore, although the constant strain curves in the x-t plane have been approximated by straight lines, it is conceivable that concave-upward curves could be fitted to the plots near the impact position, Figs. 34. to 36. and 38. to 40. This would further strengthen support of the strain-rate-dependent theory. Whether or not this curvature actually exists could only be determined by more extensive testing.

The deformations initiated at low impact velocities were found to have wave fronts of lower amplitude and slightly different slope than those of the high impact velocity deformations. The only apparent difference due to the aforementioned observation is that for the low velocity impacts, the highest strain increments propagated at lower velocities than did the equivalent strain increments in the high velocity impact. This effect appears in the σ vs. ϵ plot with the lower velocity impacts giving rise to dynamic loading curves which are located between the high velocity dynamic loading curve and the quasi-static stress-strain curve, Fig. 37. This implies that the

highest strain increments of the low impact velocity pulses are initiated at a lower strain-rate than are the equivalent strain increments in the high impact velocity pulse. Again, more extensive experimentation would be required to support this result, since the variation could be due to a statistical scatter.

The particle velocity, at a position five inches from the impact point, as calculated by performing a numerical integration of the equation $V = \int_0^{\epsilon} \left(\frac{\psi_n}{\rho}\right)^{\frac{1}{2}} d\epsilon$, is found to compare reasonably well with the actual impact velocity. The particle velocity should agree exactly with the actual impact velocity only at the point of impact since the upper strain increments are cut off and the strain energy absorbed into the material in the form of permanent deformation as the deformation wave propagates, thus causing a decrease in the particle velocity as the distance from impact increases.

Results from Work-hardening Test

In the final part of the experimental work, a deliberately work-hardened copper specimen prestressed into the plastic region (plastic region in the virgin quarter-hard material) was impact tested. In the work-hardened material, it was found that the strain wave amplitude was lower just above the impact point and did not decay as rapidly or to as low a strain level as did the identical pulse in the virgin material. It was also noted that for the work-hardened material, less permanent deformation occurred than did for the virgin material, especially near the impact point. At the upper grip, the permanent deformation after impact was greater in the work-hardened material than in the virgin material, Fig. 17. This effect

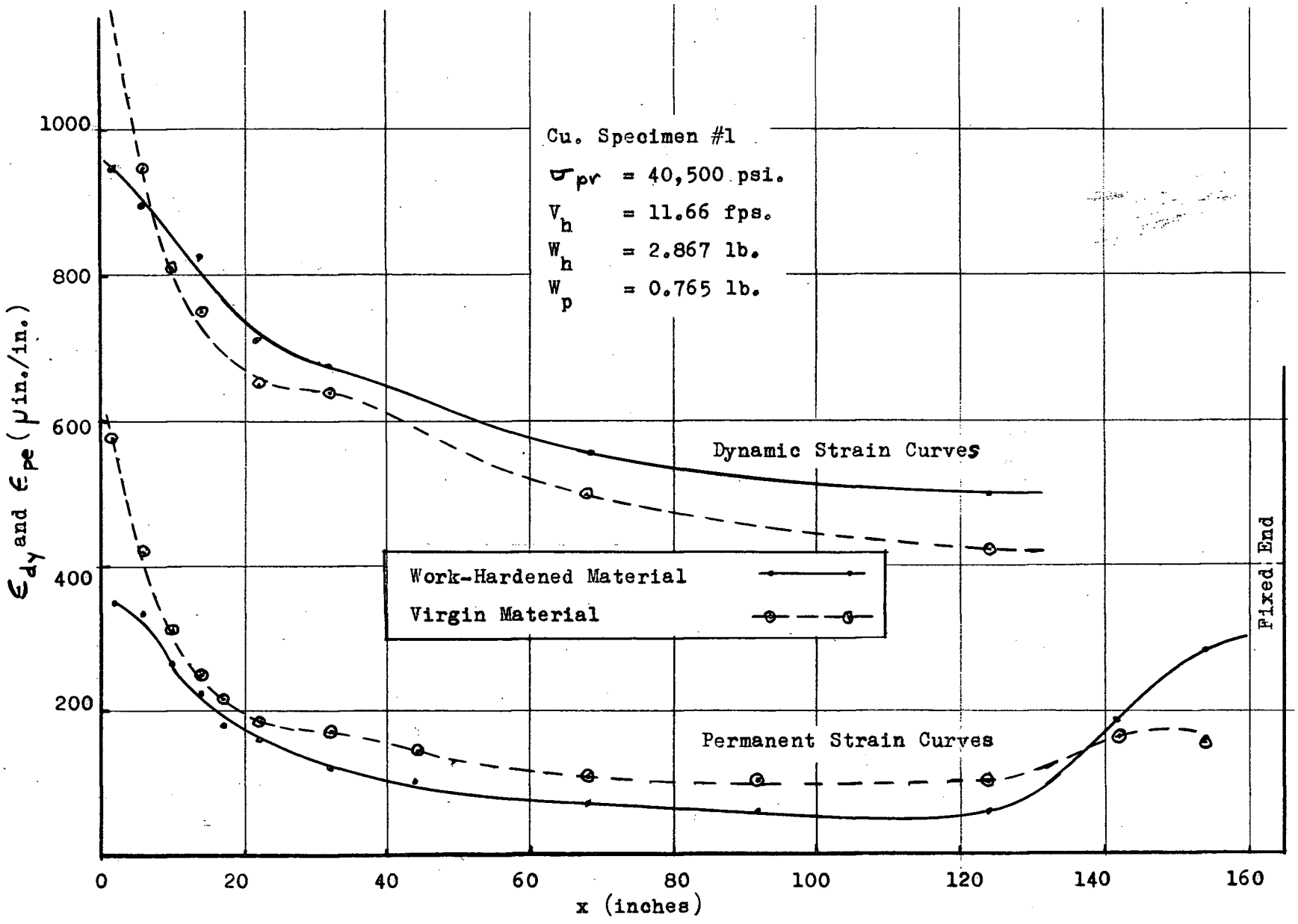

Fig. 17. Comparison of Dynamic and Permanent Strain Curves in Work-Hardened and Virgin Material

is due to the work-hardened material behaving in a more elastic manner than the virgin material, which causes less energy to be absorbed as permanent deformation along the specimen. The resulting high energy wave effectively doubles in amplitude upon reflection from the upper grip creating a region of large permanent deformation in the vicinity of the grip.

VII CONCLUSIONS AND REMARKS

It has been found that the equipment developed for this project provides an excellent method to study the strain wave propagation process. The direct method of applying prestress to a specimen is advantageous since it prevents possible change in prestress during testing due to creep.

The amplitude of the elastic strain waves is found to be linearly dependent upon the hammer velocity of impact for a given hammer to platform mass ratio. The actual elastic strain wave shape is described satisfactorily by the equation

$$\epsilon = \epsilon_0 \exp\left[-2t\sqrt{E\rho}/m\right]$$

provided a coefficient of restitution of 0.1 is assumed in calculating the effective impact velocity of the hammer and platform. It is also found that the pulse shape is satisfactorily reproducible from impact to impact provided the prestress and parameters governing pulse-shape are held constant.

The erratic elastic wave shape in the neighborhood of four to eight diameters from the impact position is attributable to an inhomogeneous stress condition through the cross-section of the specimen. By St. Venant's principle, this effect disappears as propagation of the stress wave proceeds. Except for the first few diameters from the impact point, the elastic wave propagates at the elastic velocity, 12,420 fps, with the occurrence of negligible decay or dispersion.

The incipient strain increment of the loading and unloading waves propagates at the elastic velocity, c_0, regardless of the prestress condition of the specimen.

The unloading wave is invariably elastic in shape and propagates with no noticeable shape change. The plastic strain wave amplitude, however, reduces rapidly as the wave propagates and becomes asymptotic to a constant strain level at infinity (the strain level depending upon the prestress condition of the specimen).

The permanent strain distribution curves are similar in shape to the dynamic decay curves, the difference being generally attributable to the elastic recovery of the strain waves. The large amount of permanent strain observed near the upper grip is caused by the increase of the strain pulse amplitude in the region of the upper grip resulting from the reflection of the pulse from the fixed upper end of the specimen.

The initial increments of strain in the propagating wave travel at greater velocities than those predicted by the von Kármán theory $\left(c_i > \left(\frac{\psi_i}{\rho}\right)^{\frac{1}{2}}\right)$ and the highest increments of strain in the propagating wave travel at lower velocities than those predicted by the von Kármán theory $\left(c_f < \left(\frac{\psi_f}{\rho}\right)^{\frac{1}{2}}\right)$, showing that the strain-rate-dependent theory is, at least qualitatively, supported for the case of strain wave propagation in quarter-hard electrolytic copper.

SUGGESTIONS FOR FURTHER RESEARCH

It is believed that when further plastic stress wave research is carried out on the type of equipment used in this research project, the adoption of the following suggestions would allow the analysis of the problem to proceed in a more exact and meaningful way:

(a) Annealed specimens should be used in order to give a lower yield point and easier reproducibility in future tests.

(b) The specimens should be taken directly from the elastic condition to the plastic prestress at which the test is to proceed. A different specimen should be used for each plastic prestress level at which the material is to be tested.

(c) A known, simple shape of impulse such as a square or triangular wave should be propagated. This could be accomplished by using a cam or by stopping a heavy hammer and light platform against an anvil.

(d) A readout of platform velocity from the time it begins moving until it comes to rest should be available.

(e) As fast an oscilloscope sweep as possible should be used in order to study the wave fronts in greater detail.

(f) The oscilloscope traces should be cleaned up by refining the shielding of leads and gages and by using gold-plated switches throughout the switching control. The use of a faster film would also contribute to finer traces by allowing lower beam intensity to be used.

For further research, it would also be of considerable interest to study materials such as annealed mild steel (with its heterogeneous yielding) and materials with a concave-upward stress-strain relationship.

VIII APPENDICES

APPENDIX A

DETAILS OF EXPERIMENTAL APPARATUS, CALIBRATION, AND TEST PROCEDURE

DETAILS OF EXPERIMENTAL APPARATUS

Load Applying System

The general criteria adopted in the loading system design was that all components should withstand a specimen loading of up to 5,000 pounds. This permits a maximum stress of about 100,000 psi to be imposed on 1/4 inch diameter specimen. The system was designed to be adaptable to specimen lengths of 17 feet to 20 feet and specimen diameters of 3/16 inch to 5/16 inch, with specimens of any material being acceptable.

Because of the fact that the specimens were to be plastically prestressed, the method of gripping the specimen ends presented a difficult and important design problem. It was assumed that threaded ends, vise grips or any of the conventional gripping methods would not suffice to hold the specimens at the highest prestresses. The result was that an inexpensive self-tightening grip was designed. In the grip, a circular tapered section, made of Keewatin tool steel hardened and tempered to Rockwell C50 hardness, is drawn into a mating tapered section as the load is applied, Fig. 18. This action increases the normal force between the hardened tapered section and the specimen as the load is increased. In its final form, the taper is split into three segments and threaded internally to provide a good gripping surface. The mating tapers are clamped together in the main grip body.

The grips were tested on a tension testing machine up to 5,000 pounds load and were found to work very well.

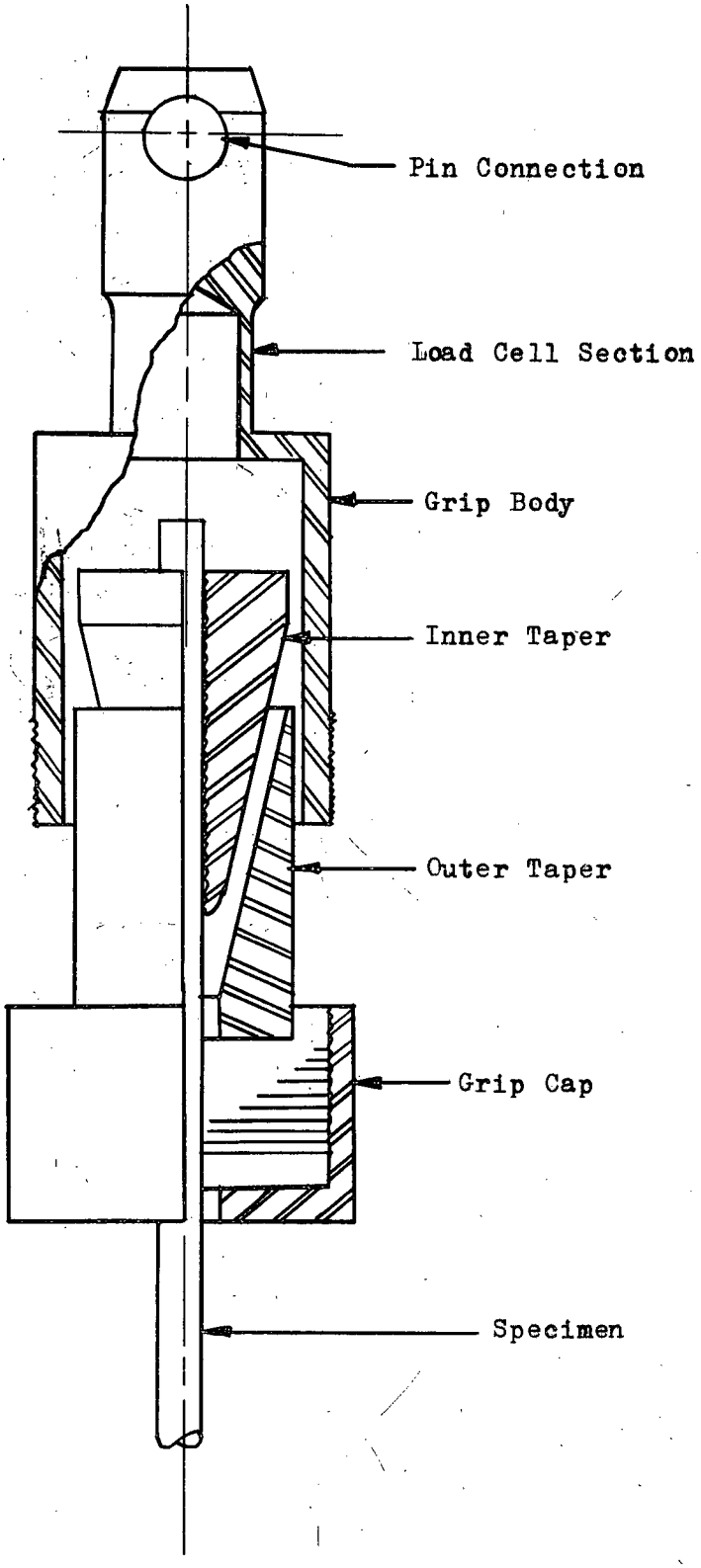

Fig. 18. Grip Detail

One grip was designed with a section of reduced cross-section on its shank upon which strain gages (Budd Metalfilm C6-121) were mounted. When calibrated, this provides an effective load measuring device.

The upper grip is pin-connected to a bracket which, in turn, is pin-connected to one end of a section of tubing. The two pins, being at right angles to each other, provide automatic longitudinal alignment of the specimen when a load is applied. The tube is provided with holes every four inches of its three foot length. A pin fastener through any one of the holes pins the tube-bracket-grip arrangement to a plate which in turn, is supported by a pair of 3 x 9 inch wooden beams. This mechanism serves as a coarse adjustment allowing any specimen length from 17 to 20 feet in length to be accommodated in the apparatus.

The lower grip is pin-connected to a bracket which attaches to the loading beam by means of a shaft riding in a phosphor bronze bearing. The pin and shaft are at right angles to each other to provide self-alignment of the specimen.

The loading beam has been designed to give a 10 to 1 mechanical advantage thus requiring 500 pounds of weights to impose the maximum stress for which the system is designed. The fulcrum of the beam is connected to a bracket by means of a shaft riding in a phosphor bronze bearing. The bracket, in turn, rides in a bearing in the lower end of the male portion of a screw jack. The female portion of the jack is rigidly fastened to a frame which is anchored to the concrete floor. The beam overhangs the pivot point where it

is guided, by means of rollers, along a vertical member, thus providing lateral stability for the loading beam, Fig. 19.

The screw-jack adjusting mechanism is, of course, necessary for fine adjustments since small strains in the specimen are magnified ten times at the loading end of the beam. Adjustment of up to eleven inches is provided.

Although the simple beam loading mechanism (as used here) does not appear to be an elegant method of imposing uniaxial tensile stress on a specimen, this device was deemed necessary due to the extreme length of specimens being used. This type of loading does, however, offer an advantage over strain imposing machines such as the Instron testing machine. The advantage is that direct loading does not allow the specimen to relax or to creep to a lower stress level during testing.

Impact Producing and Transmitting System

In general, the impact producing and transmitting mechanism consists of a hammer falling under the influence of gravity striking a platform mounted on the specimen.

The platform was required to be light and to transmit the impact to the specimen without slipping. This function was fulfilled by fabricating the platform of aluminum, with hardened high-carbon steel impact-receiving inserts. The aluminum platform was equipped with a tapered hole at its central position, which mates with three sections of a hardened and tempered Keewatin steel taper. The threaded interior surfaces of the taper with the

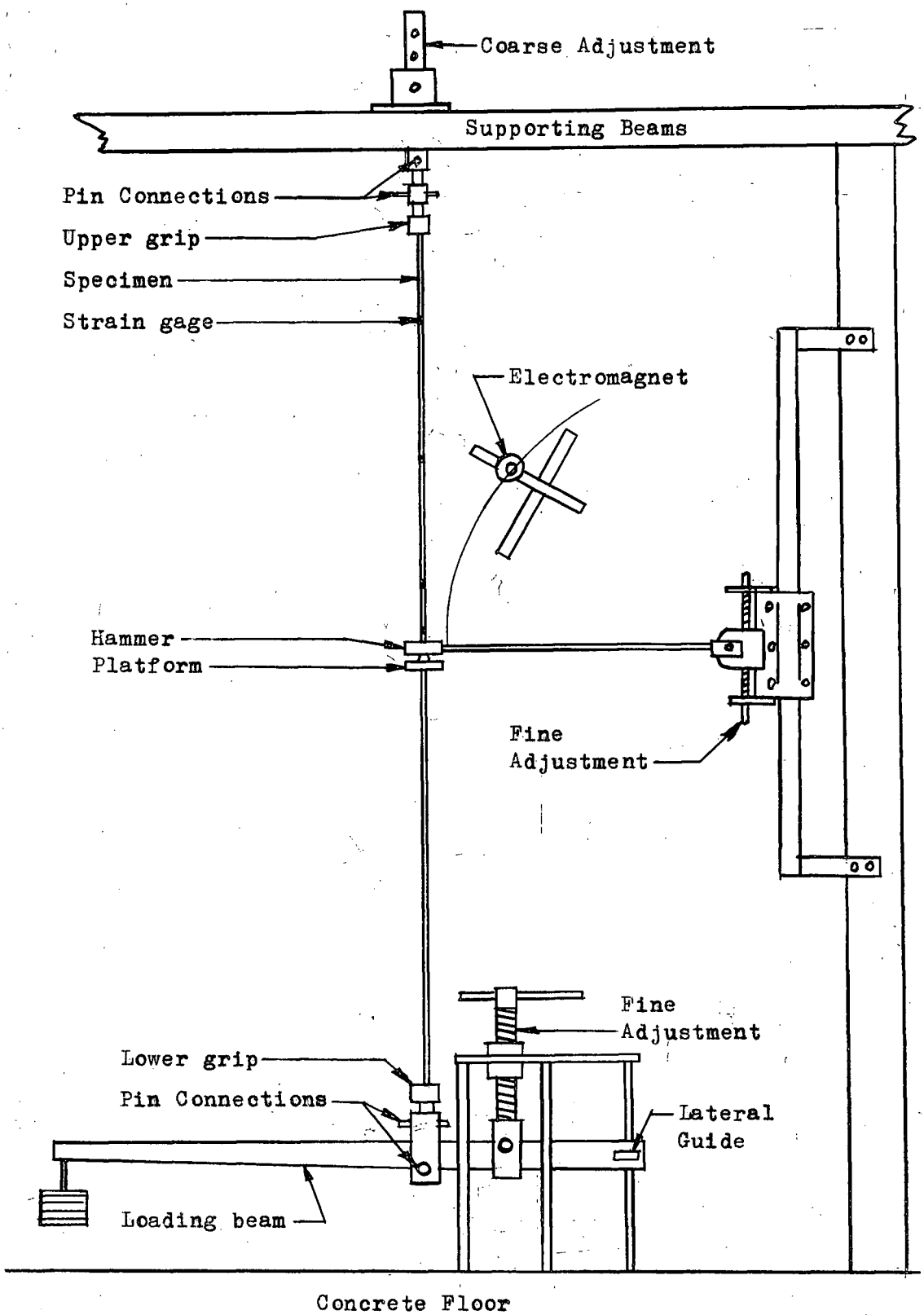

Fig. 19. Mechanical System

self-tightening principle has proved to be adequate to transmit impulses of large magnitude with no measurable slippage of the platform. The impact receiving inserts are equipped with screw adjustments to provide for even transmission of the impact, thereby insuring that bending is not induced in the specimen, Fig. 20.

The striking hammer, consisting of an aluminum head and a light tubular aluminum arm, is pivoted on a roller bearing. The hammer head is equipped with hardened, high-carbon steel impact-transmitting pads, located 36 inches from the pivot point, and is designed for the addition of up to three pounds of lead weights. The hammer pivot point is equipped with a coarse adjustment allowing seven feet of vertical movement, and a fine screw adjustment allowing the hammer to be accurately positioned and levelled before each impact.

An electro-magnetic positioning and positive release mechanism is also included in the striking hammer system. The electro-magnet position is adjustable in two directions thus allowing the hammer to be accurately positioned at any drop height from 0 to 25 inches above the platform. This allows for impact velocities of 0 to 12 fps to be produced in the specimen by the hammer-platform impact.

Load Measuring Circuit

The upper grip is designed to serve as a load cell. Four Budd Metalfilm strain gages (C6-121 series) are mounted on the section of reduced cross-sectional area on the shank of the grip; two

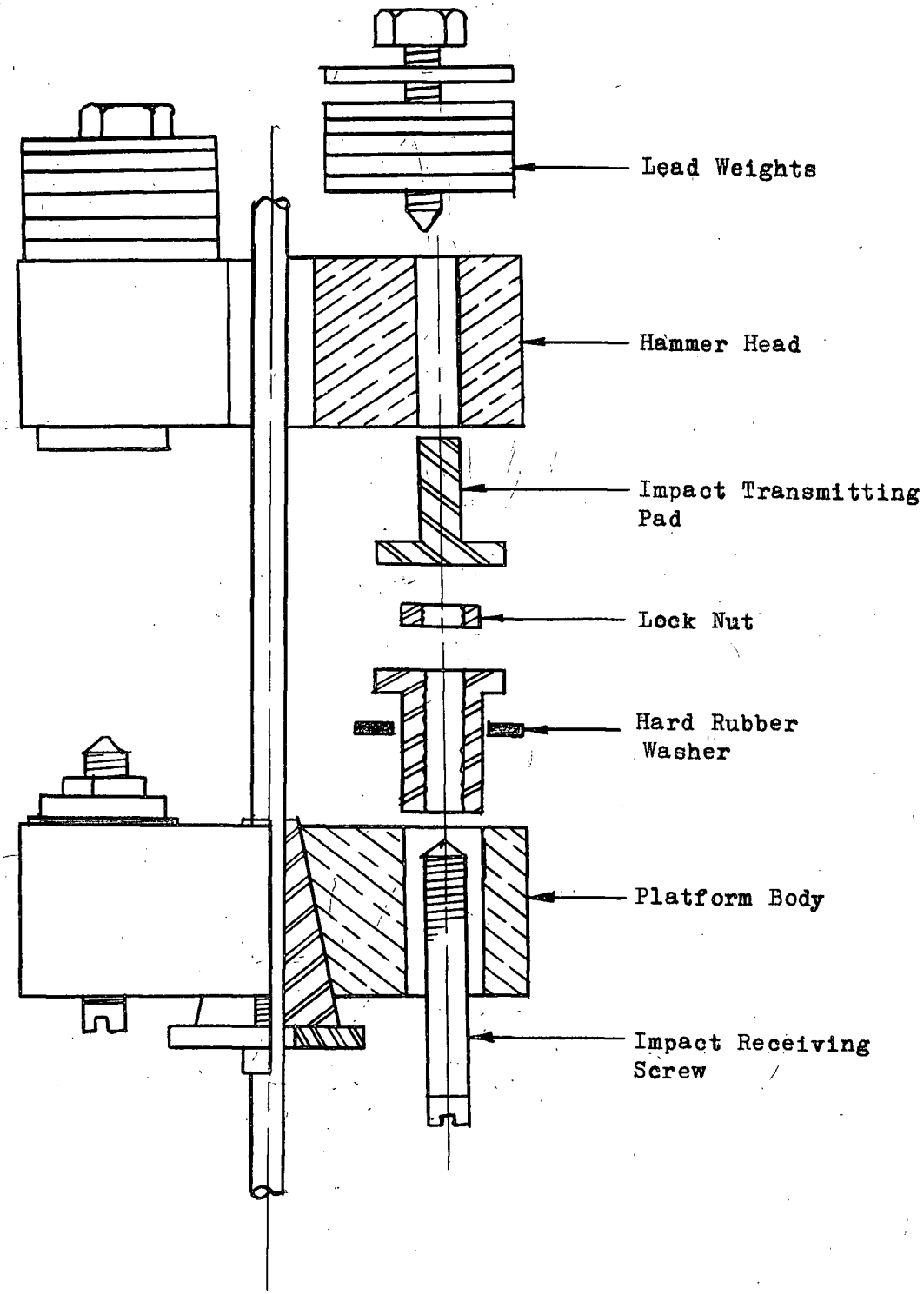

Fig. 20. Hammer-Platform Detail

diametrically opposed gages mounted longitudinally and two diametrically opposed gages mounted circumferentially. The gages are wired into a four-arm wheatstone bridge; the longitudinal gages being in two opposing arms and the circumferential gages in the other two arms, Fig. 21. The bridge is read out on a Baldwin SR-4 strain indicator. Due to the features of a four-arm bridge, the strain reading is about 2.6 times the reading that would be given by a single tension strain gage thus allowing precise load measurements to be made. A further feature of the four-arm bridge is that is offers complete temperature compensation.

Electromagnetic Hammer Release Circuit

The electromagnetic hammer release circuit is designed to hold a maximum hammer weight of six pounds, the hammer being released when the electromagnet is de-energized. The electromagnet is an eight ohm coil of light insulated copper wire wound on a mild steel core. Energization is provided by a 9 volt D.C. potential supplied by six conventional D-cell batteries.

In order to prevent C.R.O. triggering with the collapse of the magnetic field when the magnet is de-energized, a 0.1 μf. capacitor is connected in parallel with the coil. A power on-off switch is provided in the main control unit and a knee-operated remote on-off switch is used to energize and de-energize the magnet, thus retaining and dropping the hammer when required, Fig. 22.

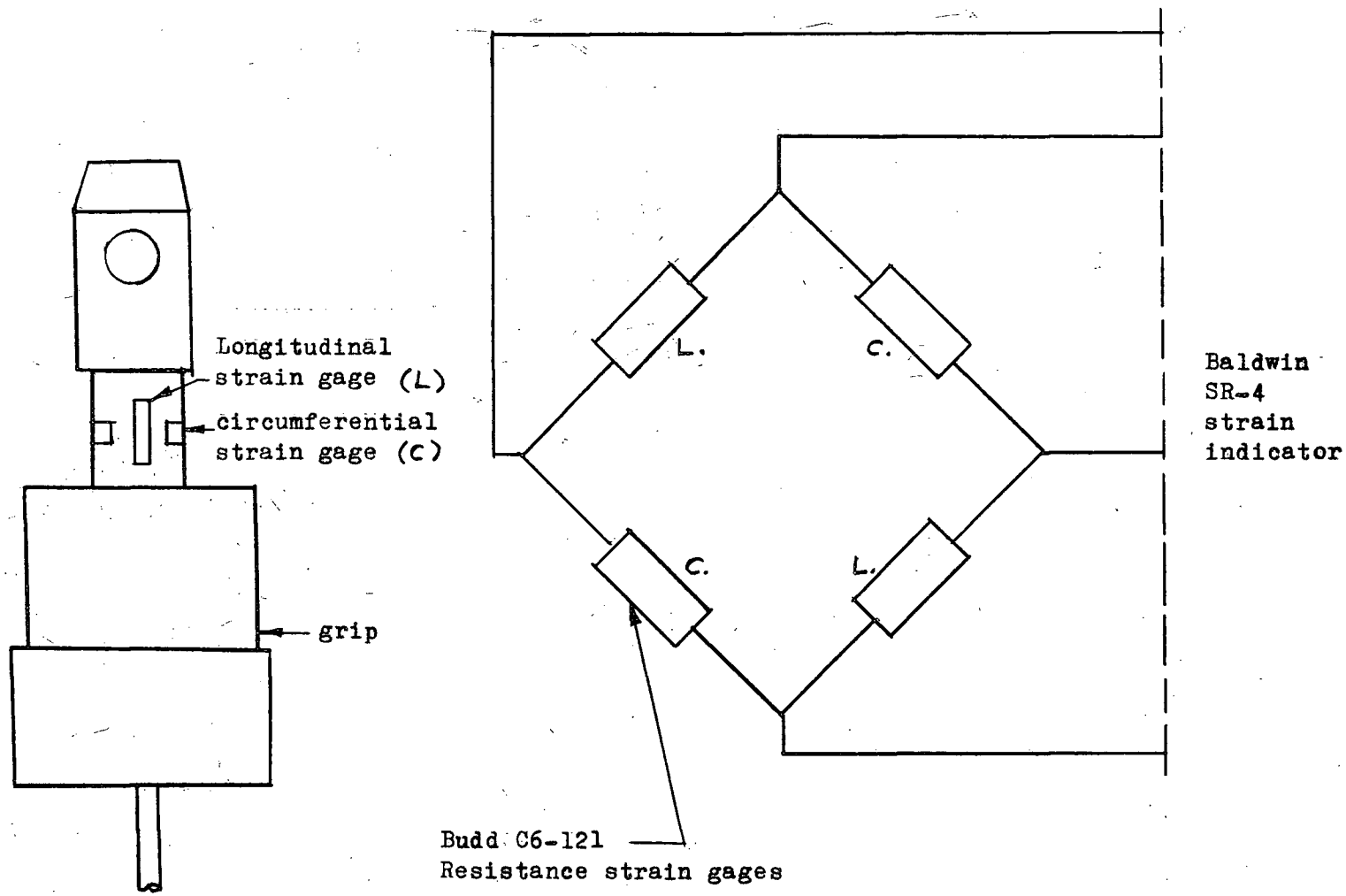

Fig. 21. Load Cell

Cathode Ray Oscilloscope Triggering Circuit

The C.R.O. triggering circuit is designed to provide single synchronized horizontal sweeps on the two beams of each of the oscilloscopes with the sweeps beginning at the instant of hammer-platform impact. By setting the frequency of the horizontal sweep to a suitable value, it is possible to display on the C.R.O. screens the strain condition at specific points on the specimen beginning at the instant of impact and continuing for a predetermined number of microseconds thereafter.

The two oscilloscopes used are of the dual-beam Tektronix 502-A series. This model provides for two signals to be displayed simultaneously on each of the two instruments. The triggering inputs are designed to operate on a voltage spike and can be set to operate only on the largest voltage spike of the triggering signal. For this reason, the external triggering circuit was constructed with a resistance and capacitance in series with a 7.5 volt DC supply. The time constant of the circuit was made large (one second). Across the capacitor another circuit is connected which is closed by the contact between the hammer and platform. When this contact is made, the previously charged capacitor discharges through the triggering circuits of the two oscilloscopes. Because of the high impedence input of the C.R.O. triggering circuits, it is necessary to shunt the inputs with a low impedence to insure the complete discharge of the capacitor on the first contact of the hammer and platform, Fig. 22. If this shunt is not included, multiple traces are triggered on successive contacts of the hammer and platform.

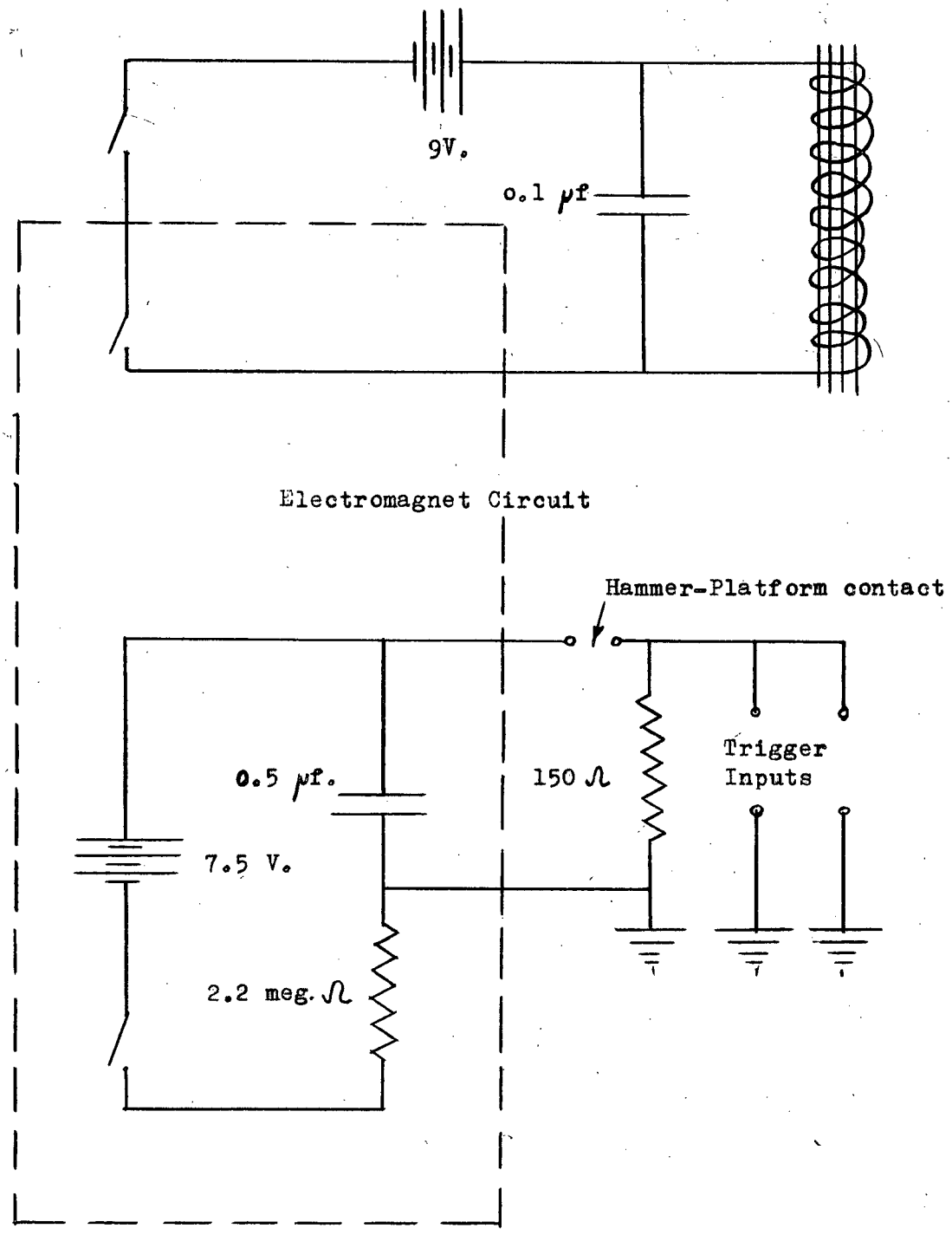

Fig. 22. Electromagnet and Triggering Circuits

The large time constant of the charging circuit is required so that during successive contacts of the hammer and platform, the capacitor cannot charge sufficiently to trigger the C.R.O.'s on discharge.

Dynamic Strain Readout Circuit

The general strain gage circuitry provides for the simultaneous dynamic readout of four of the eight dynamic gages on the two oscilloscopes and individual static readout of the eight dynamic gages and up to eight static gages on a Baldwin SR-4 strain indicator. This versatility is accomplished by connecting the eight dynamic gages to a set of four double-pole-double-throw (D.P.D.T.) switches, one gage to each end of each switch. The center terminals of these switches are then connected to the center terminals of a second set of four D.P.D.T. switches which serve to connect the gages either into the dynamic circuits or into the static circuit. Consequently, by manipulating the first set of D.P.D.T. switches, either set of four dynamic gages can be connected into the dynamic circuit at one time. Since the static circuit provides for individual gage readout, all eight dynamic gages and the static gages can be read out.

The dynamic circuit consists of eight active strain gages, two sets of four D.P.D.T. switches, four compensating or dummy strain gages (mounted in the central control unit), four Ellis BAM-1 (bridge amplifier and meter) units and two Tektronix 502-A dual-beam oscilloscopes.

The eight active strain gages (Budd Metalfilm C9-121 series) are connected to the central control unit and the first set of D.P.D.T. switches by means of four, four-lead, shielded cables which are grounded to the control box. (These cables are from 12 to 30 feet in length depending upon what part of the specimen they are servicing). The center terminals of the first set of D.P.D.T. switches are connected to the center terminals of the second set of D.P.D.T. switches. One side of each of these switches is then connected to a terminal block where the four dummy gages are also connected. To the terminal block, four, four-lead, shielded cables are connected, each one being connected to an active gage with two leads, and to a dummy gage with the other two leads. The four cables which are grounded to the central control box, are connected in half bridges to the four BAM-1 units, Fig. 23. A later addition to the dynamic readout circuit was to connect small resistances (2-5 ohm) in series with the compensating gages. This served to greatly extend the strain range over which the BAM-1 units could be zeroed.

The four BAM-1 outputs are connected by means of standard phone jacks, one each to the upper and lower DC inputs of each of the two oscilloscopes.

The central control unit, to which all shielding is grounded and to which the triggering circuit is grounded, is connected to the common ground terminals of the two oscilloscopes, providing a common ground potential for all components of the system.

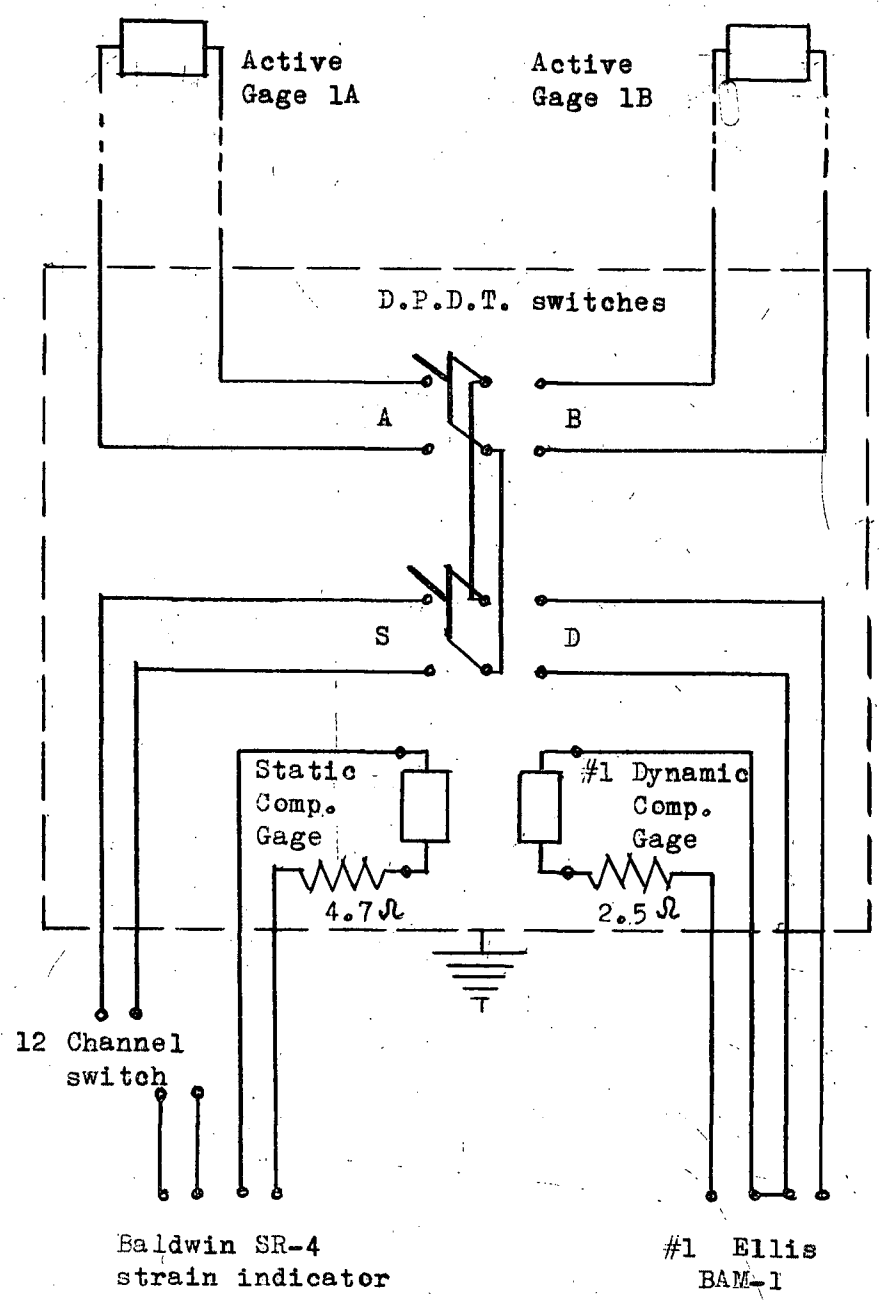

Fig. 23. Readout Circuits for Strain Gages 1A and 1B

Static Strain Readout Circuit

The static strain readout circuit consists of eight static strain gages, eight dynamic strain gages, one compensating strain gage, one twelve-channel polyphase switching unit, and one Baldwin SR-4 strain indicator.

The eight dynamic gages are connected through the two sets of D.P.D.T. switches, the static readout being taken from the opposite side of the second set of switches to the dynamic readout. The four sets of terminals are then connected to four separate channels of the polyphase switch.

The static gages are connected by means of shielded leads to terminal blocks in the central control unit (the shielding being grounded to the common ground). The terminal blocks are then connected to the polyphase switch, one gage being connected to each channel of the switch. The switch output is connected to the active gage terminals of the Baldwin SR-4 strain indicator. By switching to any channel of the twelve channel switch, any one of twelve strain gages can be connected to the SR-4 indicator. The remaining four dynamic gages can be switched into the SR-4 indicator by throwing the first set of D.P.D.T. switches and turning the polyphase switch to the four channels involved. The compensating gage is connected directly from its permanent location in the central control unit to the compensating gage terminals on the Baldwin SR-4 strain indicator, and consequently takes the place of up to sixteen separate compensating strain gages, Fig. 23.

A later addition to the static readout circuit was the connection of a high-stability 4.7 ohm resistance in series with the compensating strain gage. This addition extended the static strain scale of the Baldwin SR-4 strain indicator by about 23,000 micro-inches per inch giving a possible positive strain reading of up to 50,000 micro-inches per inch.

Recording System

Due to the high propagation velocity of strain pulses in metals (10,000 fps to 20,000 fps) and the undesirability of reproducing reflected waves on the C.R.O. screens, the full sweep time of the oscilloscopes is in the order of one millisecond. Because of this rapid display of the strain vs time plots on the C.R.O. screens, it is necessary to photograph the displays for future analysis. Photographs are taken using a Dumont 35 mm camera with oscilloscope adapter and a Yashica Model C 35 mm camera with a Konica #1 close-up lens mounted on a suitable oscilloscope adapter.

Satisfactory reproduction of the oscilloscope displays is obtained using Kodak Tri-X (ASA 400) black-and-white film with lens settings of f 2.8. Time exposures are used, obtained by manually opening and closing the shutters before and after impact, giving an effective exposure time of approximately one second.

CALIBRATION

Before the testing was begun, the load cell, the horizontal sweeps of the two Tektronix 502-A dual-beam oscilloscopes, and the specimen material were calibrated.

The load cell was calibrated in an Instron testing machine, the readout of the cell being taken on an SR-4 strain indicator. The load (as read on the Instron) was increased in 250 pound increments from 0 to 4,000 pounds, the reading of the SR-4 indicator being recorded for each increment. A plot was then made of SR-4 reading increment vs load increment. The inverse slope of the curve gives the factor by which the SR-4 strain indicator increment must be multiplied to give the actual load on the cell. The load is then easily converted to stress since the cross-sectional area of the specimen is known. The calibration curve is found in Fig. 24.

The horizontal sweeps of the two oscilloscopes were calibrated using a Hewlett-Packard function generator. The sweep frequency of the oscilloscopes was set to the value used during testing (.2 m.sec/cm) and a signal of known frequency was fed in from the function generator. The traces were photographed and from the photographs, the accuracy of the sweep frequency was checked.

The specimen material was calibrated by determining cross-sectional area (for stress calculation) and by obtaining stress-strain diagrams. To obtain the stress-strain diagrams, short lengths of rod were cut from the end of some of the specimens. These samples were

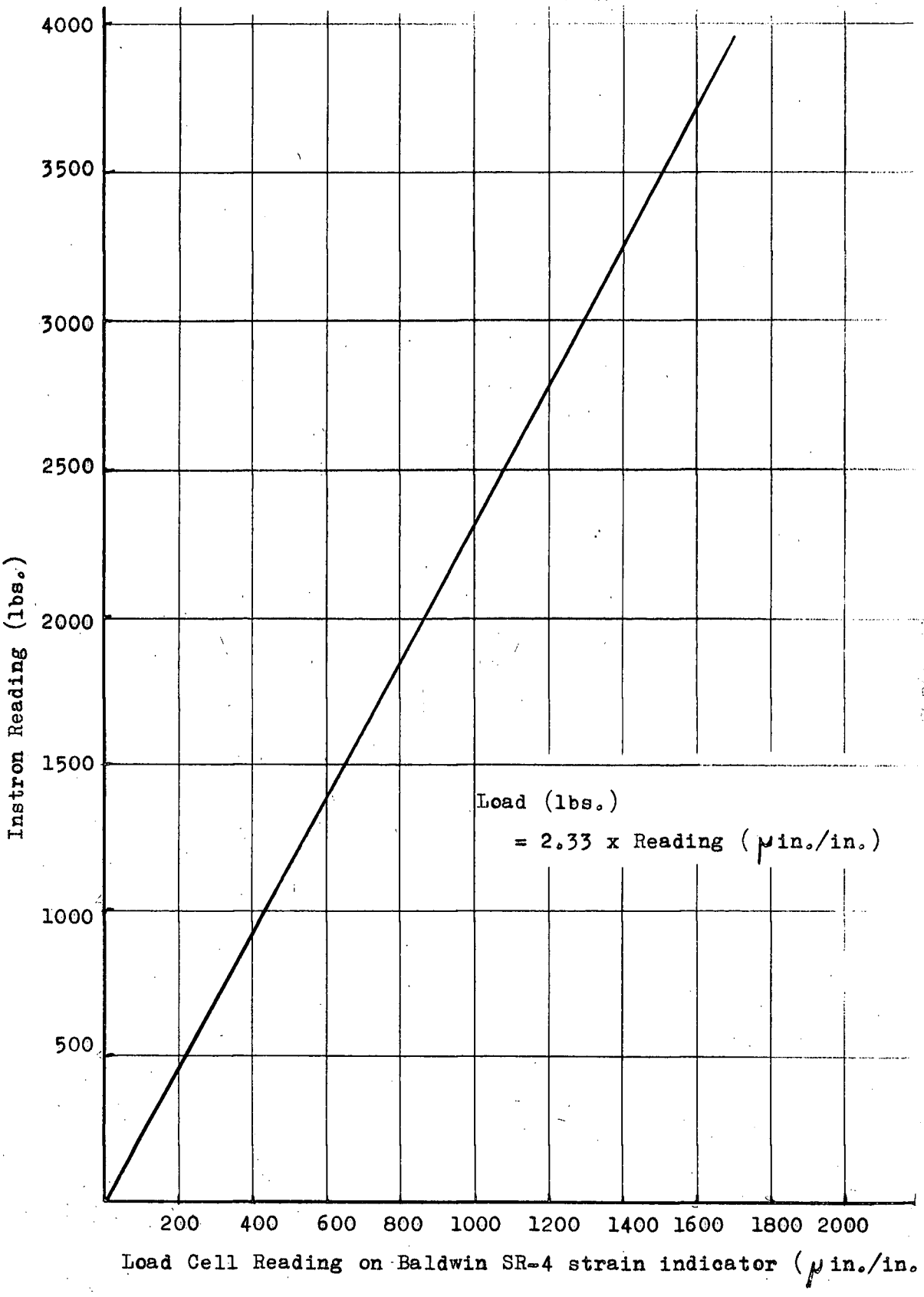

Fig. 24. Load Cell Calibration Curve

then tested in tension in an Instron testing machine, which gave a graphical record of engineering stress vs strain, Fig. 25.

Specimen Preparation

A great amount of difficulty was encountered in getting the strain gages (Budd Metalfilm Types C9-121 and C6-121) to remain bonded to the specimens as the prestress was increased into the plastic region. It was found that Eastman 910 contact cement failed under dynamic loading at as low as 5,000 μ in/in strain, while Budd B-3 two-component room-temperature curing epoxy failed at less than 15,000 μ in/in. (These figures were the best results of a series of tests using different gage mounting techniques).

The solution finally adopted was to use GA-5 two-component temperature-curing epoxy as the bonding agent. The curing temperature required by the epoxy necessitated construction of a 20 foot long electric oven to accommodate the specimens for curing.

The most successful technique employed in mounting the gages was as follows:

(a) The metal was prepared by cleaning and cross-hatching with fine emery paper. The metal was then cleaned with metal conditioner after which meutralizer was applied and wiped off.

(b) The gage was prepared by carefully roughening the gage back with pumice powder, then cleaning thoroughly with metal conditioner.

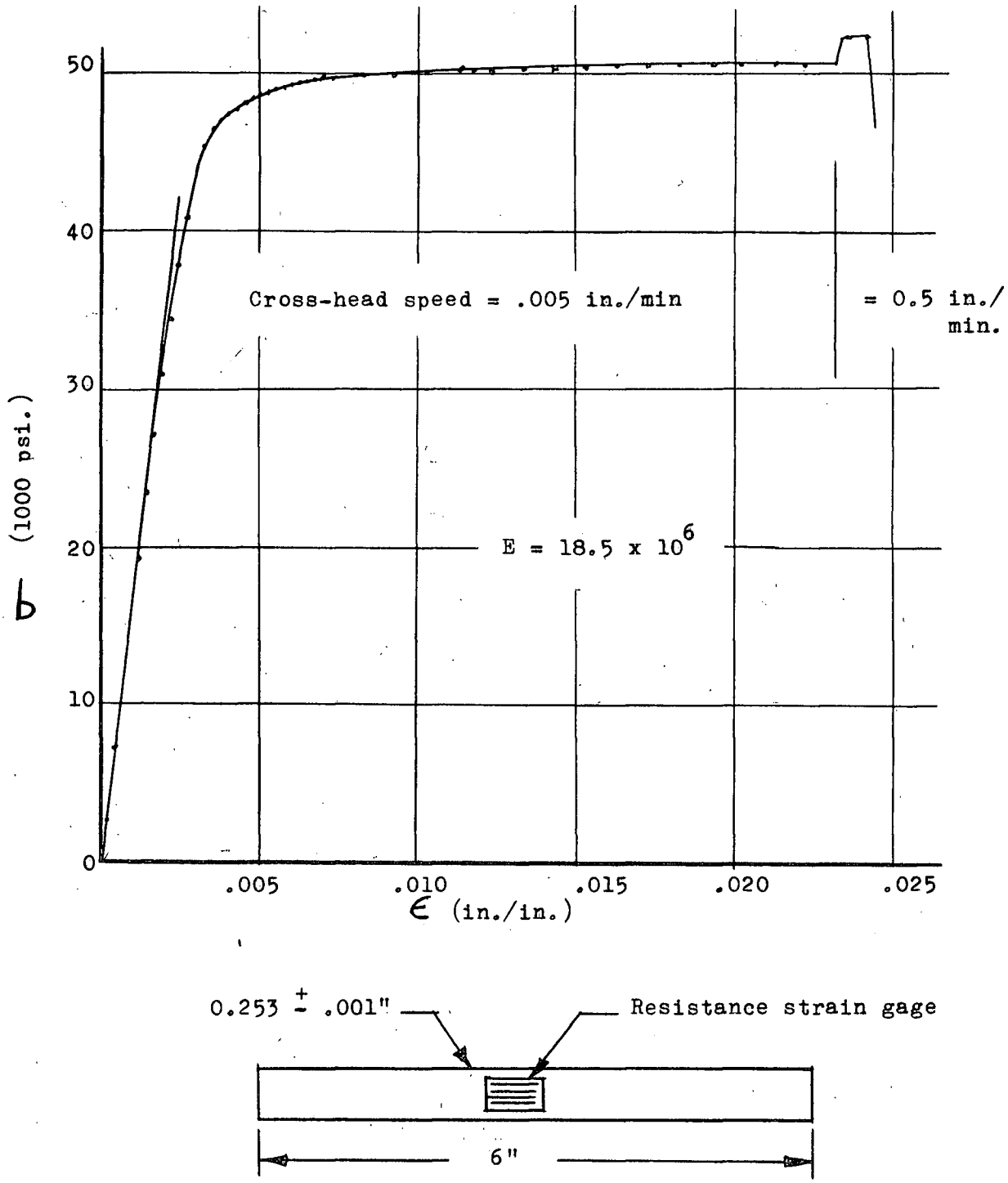

Fig. 25. Quasi-Static Stress-Strain Curve and Specimen Shape

(c) After the GA-5 was applied and the gage taped down, it was found to be best to apply pressure by wrapping with rubber tape. (Pressure pads were frequently found to cause epoxy starvation of the gages resulting in a poor bond.

(d) The epoxy was cured by heating the specimen from room temperature to 220°F, cycling the temperature between 180°F and 220°F for two hours and cooling slowly to room temperature.

(e) The bond quality was determined by checking the gage to ground resistance. If the resistance was greater than 2 meg.ohms, the bond was satisfactory.

(f) The gages were wired up using standard techniques.

TEST PROCEDURE

Preliminary to running a series of tests on a specimen, the electronic equipment had to be calibrated and checked, and the mechanical equipment and the cameras had to be set.

After the specimen was erected in the test apparatus the platform located, and the grips locked, the strain gages were wired into the electronic circuit. After each gage was connected, the respective channel was checked out to insure that the gage was working and that it was connected into the correct channel. The checking out was done on the SR-4 indicator. The BAM-1's and oscilloscopes were then turned on and allowed a thirty minute warmup time.

During the warmup time, the specimen was given a light load, to keep it taut, and the striking hammer pivot was adjusted so that the hammer would be level when resting on the impact receiving screws. The lateral and radial positions of the hammer were also adjusted along with the vertical placement of the impact receiving screws. The hammer was then level, centered on the platform, and exerting equal force on the two impact receiving screws. The hammer drop height and hammer weight were also adjusted and set.

Before the test could be started, the BAM-1's and C.R.O.'s had to be calibrated in terms of μin/in strain per cm. deflection on the C.R.O. screens. Calibration was done most simply by reading out the dynamic gages on the SR-4 for light loading, switching into the dynamic circuit, zeroing the BAM-1's and zeroing the C.R.O. traces.

Then a load was applied to the specimen, the static strains read out on the SR-4, static strain calculated by subtracting the two sets of readings, channels switched into the dynamic circuit, required deflection calculated from static strains, and deflection set on the C.R.O. traces by adjusting the BAM-1 gains. The calibration was then checked and re-checked. Once calibration is complete, the gain controls on the BAM-1 units cannot be touched.

The cameras were loaded with Tri-X film and set with apertures at f 2.8 and shutter speeds on time exposure. The Yashica 35 mm camera was focused by holding a ground glass plate against the film plane and adjusting the focusing ring until a sharp image was projected. The DuMont camera has a fixed focus.

The triggering level was set to give single sweeps on hammer-platform contact. The beam intensity was set to about 50 per cent, the screen intensity to about 10 per cent, and the sweep frequency set to the desired value (0.1 or 0.2 m.sec/cm).

The testing could then begin. First, the zero load SR-4 indicator readings were recorded. The specimen was then loaded to the first prestress value (calculated from the load cell reading). Static readings were taken on the SR-4 indicator, and the dynamic channels switched into the dynamic circuit. The BAM-1's were zeroed and jacked into the oscilloscppes. The magnet was energized, hammer raised, shutters cocked open, magnet de-energized, hammer dropped, and shutters closed. The films were then advanced and the dynamic gages switched back onto the static circuit. Static strain readings were again taken on the SR-4 indicator. The differences between

the two sets of SR-4 readings give the permanent strains due to impact. This procedure was then repeated at different prestress values until the series of tests was completed.

APPENDIX B

SAMPLE CALCULATIONS

CALCULATION OF ELASTIC SHAPE

Elastic Velocity $\quad c_o = \left(\frac{E}{\rho}\right)^{\frac{1}{2}}$

$E = 18.5 \times 10^6$ psi.

$\rho = 0.322$ lb./in.^{3}

$= 0.10$ lb./sec.^{2}/ft.in.^{3}

$c_o = 12{,}420$ fps.

Elastic Shape - for 3 hammer-mass values

Data $\quad \rho = 0.322$ lb./in.^{3}

$E = 18.5 \times 10^6$ psi.

$V_h = 11.66$ fps

$W_p = 0.765$ lb.

$W_h = 1.265$ lb.

1.977 lb.

2.867 lb.

now $\quad \epsilon = \epsilon_o \exp\left[-2t\sqrt{E\rho}/m\right]$

where m = mass of impact obj./unit area of rod cross-sections.

$$m = \frac{W_h + W_p}{.049 \times 32.2} = 0.634\ W \text{ lb.sec.}^2\text{/ft.}$$

$$\epsilon_o = \frac{V_h}{c_o} \times \frac{W_h}{W_h + W_p} \times (1 + e)$$

Assume e = 0.1

$$\epsilon_{01} = \frac{11.66}{12,420} \times \frac{1.265}{2.030} \times 1.1 = 644 \text{ in./in.}$$

$$\epsilon_{02} = \frac{11.66}{12,420} \times \frac{1.977}{2.742} \times 1.1 = 744 \text{ in./in.}$$

$$\epsilon_{03} = \frac{11.66}{12,420} \times \frac{2.867}{3.632} \times 1.1 = 815 \text{ in./in.}$$

$$\epsilon = \epsilon_0 \exp\left[-2t\sqrt{E\rho}/.634\,W\right] = \epsilon_0 e^{-4690\frac{t}{W}}$$

now $e^{-.133} = .875 = \frac{1}{8}$ decay

$e^{-.29} = .750 = \frac{1}{4}$ decay

$e^{-.47} = .625 = \frac{3}{8}$ decay

$e^{-.70} = .50 = \frac{1}{2}$ decay

$e^{-.99} = .375 = \frac{5}{8}$ decay

$e^{-1.38} = .25 = \frac{3}{4}$ decay

Solving for t

Case #1, $W_h = 1.265$ case #2, $W_h = 1.977$ case #3, $W_h = 2.867$

t(μ sec)	ε (μ in./in.)	t(μ sec)	ε (μ in./in.)	t(μ sec)	ε (μ in./in.)
0	644	0	744	0	815
58.6	563	77.7	650	103	713
125	483	169	558	224	611
204	402	275	465	363	509
303	322	409	372	541	407
432	242	584	279	772	305
598	161	807	186	1065	204

Theoretical curves (as derived above) are plotted over the experimental curves in Fig. 5.

CALCULATION OF DYNAMIC LOADING CURVE

Loading curve from x-t plane (Fig. 38.) Specimen #2

$\sigma_{pr} = 45{,}700$ psi.

$W_h = 2.867$ lb.

$V_h = 11.66$ fps.

propagation vel. $c_n = \frac{1}{s_n} \times \frac{20}{0.4} \times \frac{10^3}{12}$ fps.

and $c_n = \left(\frac{\psi_n}{\rho} \right)^{1/2}$

$\therefore$ Deformation modulus $\psi_n = \rho\, c_n^2$

Calculation table on following page.

The dynamic loading curve ($(\sigma_{pr} + \sigma_d)$ vs. ϵ) is plotted in Fig. 41.

TABLE #1

Line	Slope	c_n (fps)	c_n^2	ψ_n	$\Delta\epsilon_n$	$\frac{\Delta\epsilon_n+\Delta\epsilon_{n+1}}{2}$	$\Delta\sigma_n$	σ_d	ϵ (μin./in)	$\sigma_{pr}+\sigma_d$ (psi.)
S_0	.33	12,620	159.5×10^6	19.13×10^6	0	25	478	478	25	46,178
S_{01}	.35	11,900	141.5×10^6	16.98×10^6	50	50	849	1327	75	47,027
S_{02}	.38	10,950	120×10^6	14.4×10^6	50	50	720	2047	125	47,747
S_{03}	.425	9,800	96×10^6	11.52×10^6	50	50	576	2623	175	48,323
S_{04}	.475	8,770	76.8×10^6	9.23×10^6	50	50	462	3085	225	48,785
S_1	.5	8,330	69.2×10^6	8.3×10^6	50	50	415	3500	275	49,200
S_{11}	.525	7,930	62.8×10^6	7.53×10^6	50	50	377	3877	325	49,577
S_{12}	.56	7,440	55.2×10^6	6.62×10^6	50	50	331	4208	375	49,908
S_{13}	.64	6,500	42.2×10^6	5.06×10^6	50	50	253	4461	425	50,161
S_{14}	.70	5,950	35.3×10^6	4.24×10^6	50	50	212	4673	475	50,373
S_2	.76	5,480	30×10^6	3.6×10^6	50	150	540	5213	625	50,913
S_3	1.0	4,170	17.35×10^6	2.08×10^6	250	250	520	5733	875	51,433
S_4	1.23	3,385	11.45×10^6	1.375×10^6	250	250	344	6077	1125	51,777
S_5	1.40	2,970	8.85×10^6	1.062×10^6	250	125	133	6210	1250	51,910

PARTICLE VELOCITY CALCULATION

Values from Table #1

$$V = \int_0^{\epsilon} \left(\frac{\psi_n}{\rho}\right)^{\frac{1}{2}} d\epsilon \quad = \sum_{n=0}^{i} C_n \frac{\Delta\epsilon_n + \Delta\epsilon_{n+1}}{2}$$

Calculated at position 5 inches from impact

$$V = \Big[25 \times 12{,}620 + 50\ (11{,}900 + 9{,}800 + 8{,}770 + 8{,}330 + 7{,}930 + 7{,}440 + 6{,}500 + 5{,}950) + 150 \times 5{,}480 + 250\ (4{,}170 + 3{,}385) + 125 \times 2970\Big] \times 10^{-6}$$

$$= 6.36 \text{ fps.}$$

Calculated at position 57 inches from impact

$V = 4.1$ fps.

APPENDIX C

SUPPLEMENTARY FIGURES

Figs. 26. - 41.

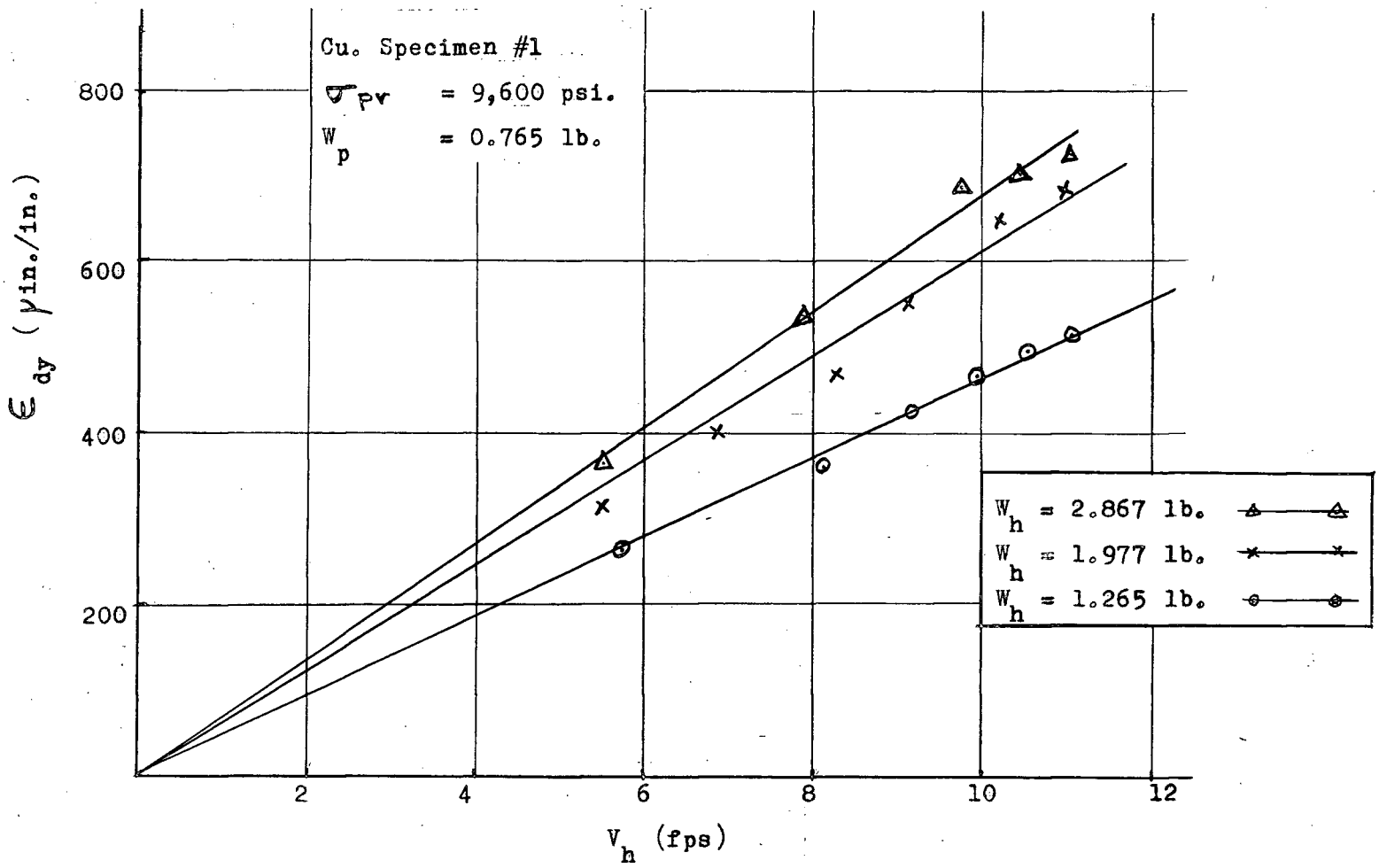

Fig. 26. Dynamic Strain Wave Amplitude vs Hammer Velocity for Three Hammer Weights.

Cu. Specimen #1

c_o = 12,420 fps.

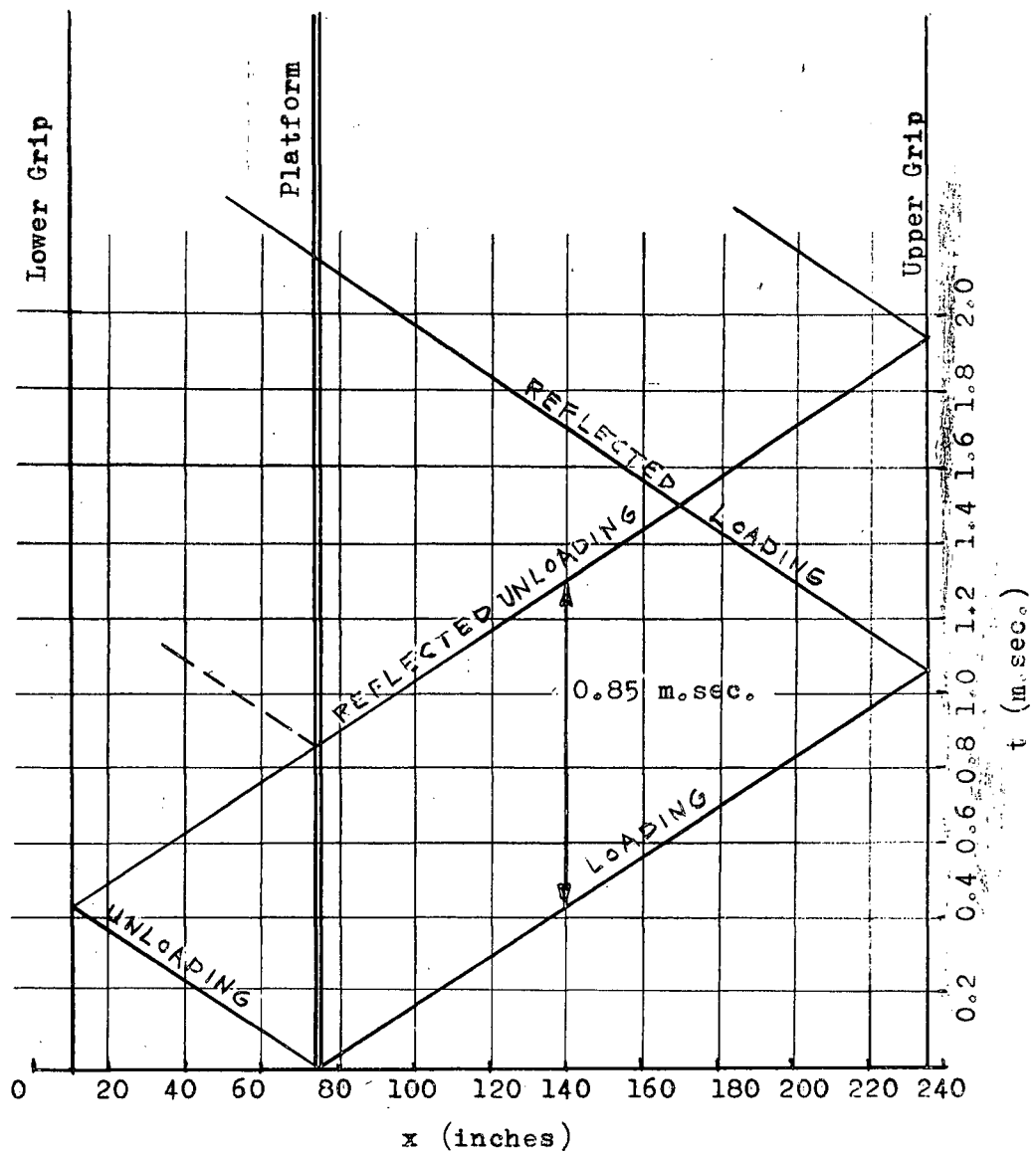

Fig. 27. Plot of Incipient Increment of Strain Wave in x-t Plane Showing Reflections from Fixed Ends.

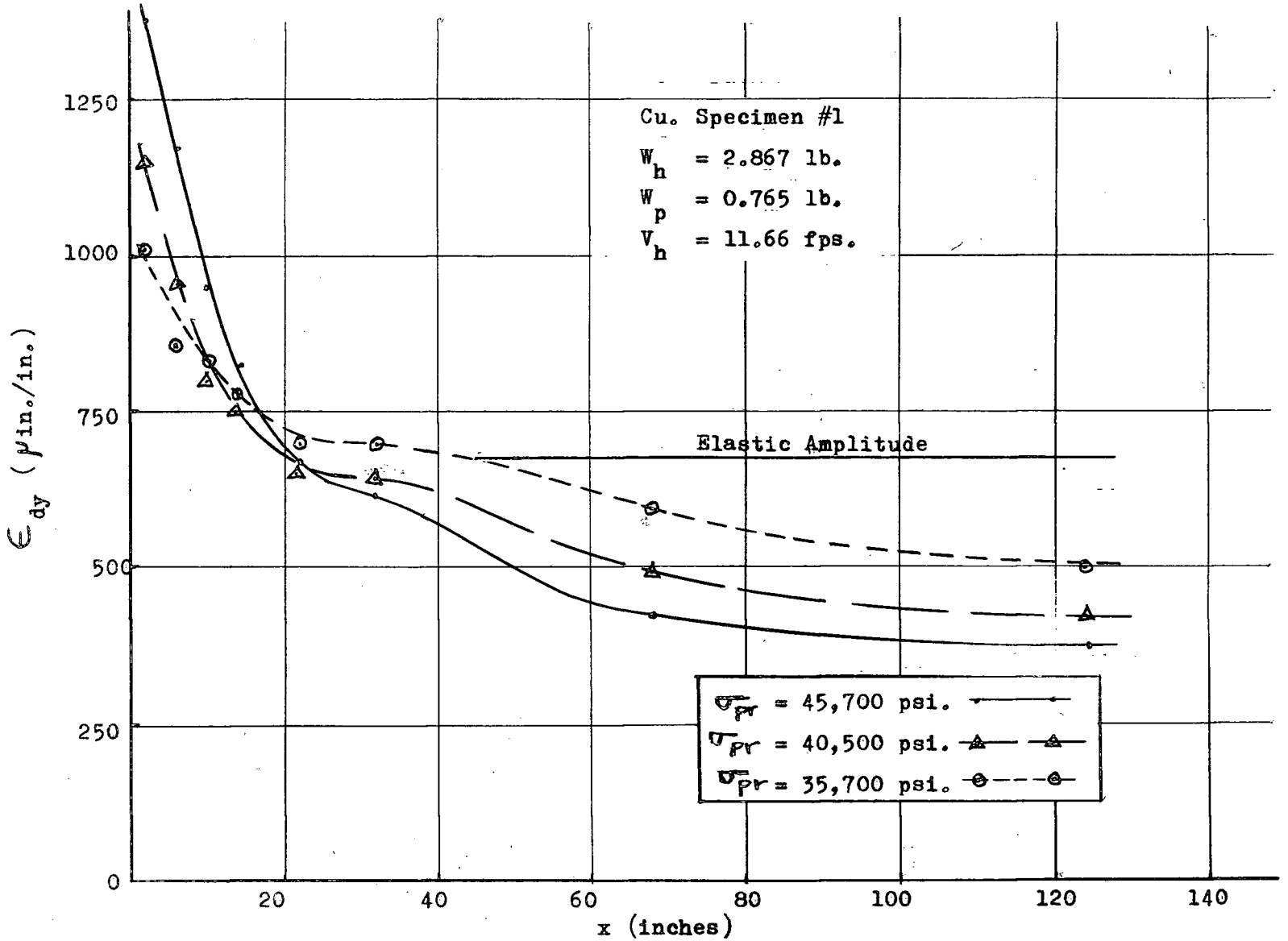

Fig. 28. Dynamic Strain vs Distance from Impact for Three Prestress Values.

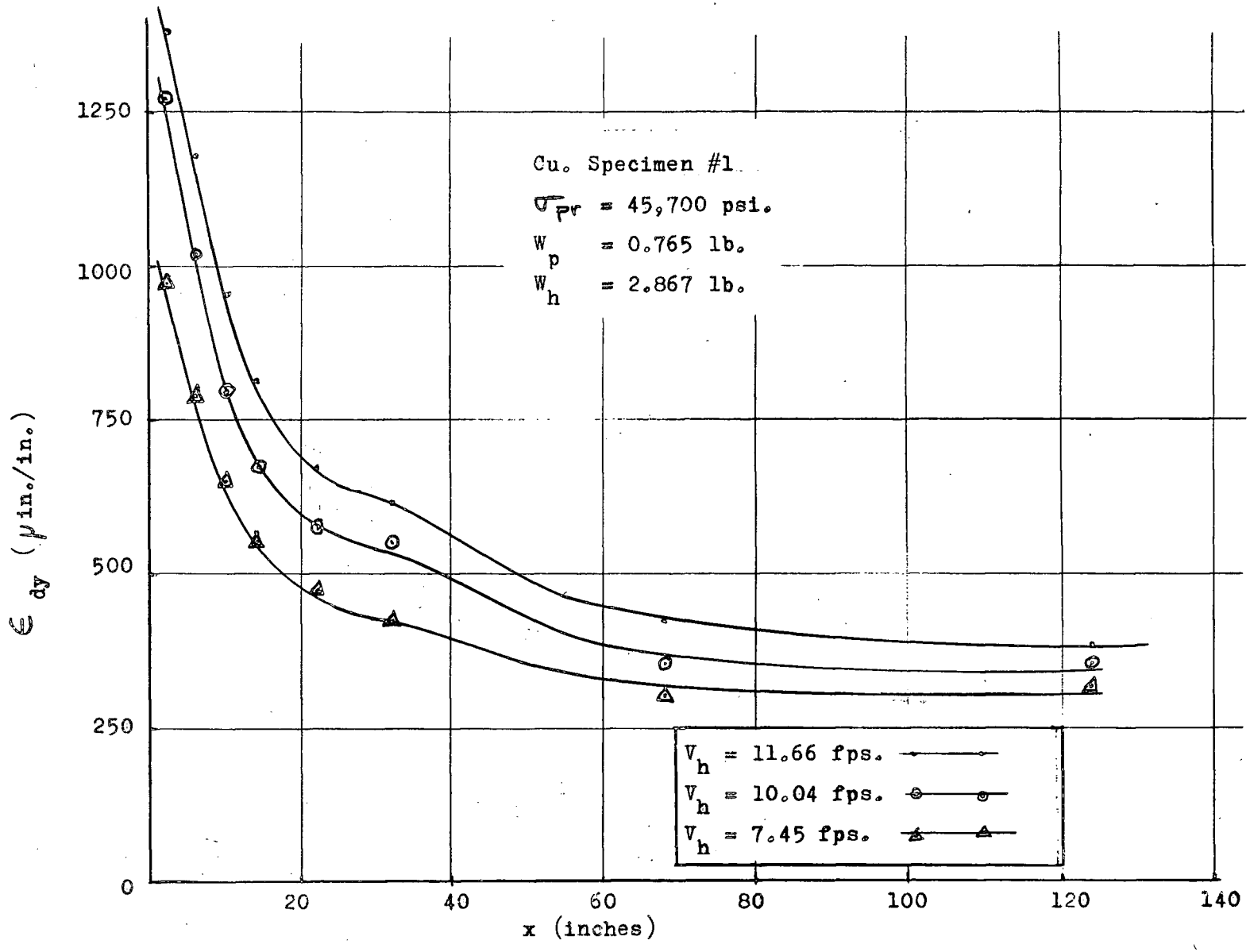

Fig. 29. Dynamic Strain vs Distance from Impact for Three Hammer Velocities.

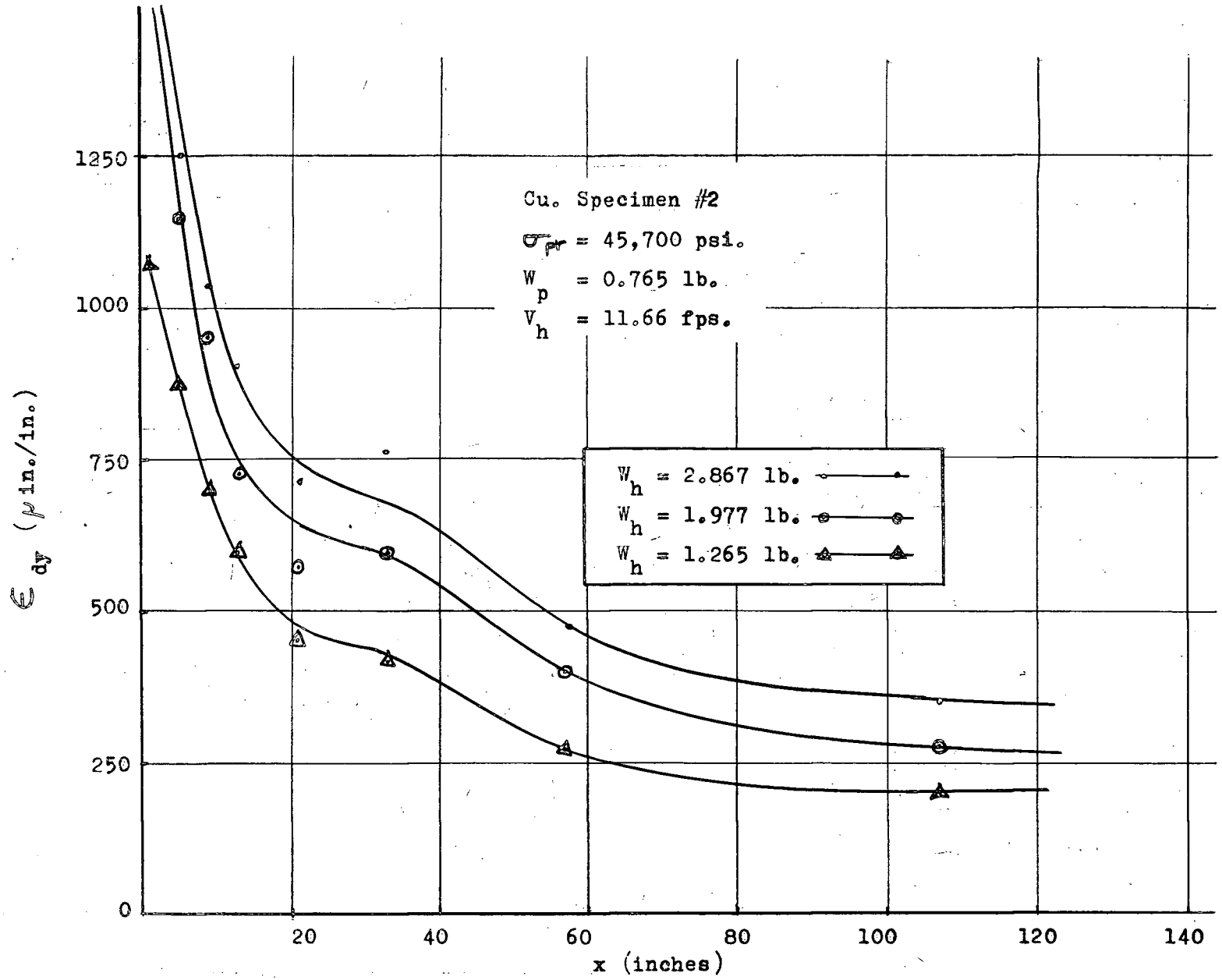

Fig. 30. Dynamic Strain vs Distance from Impact for Three Hammer Weights.

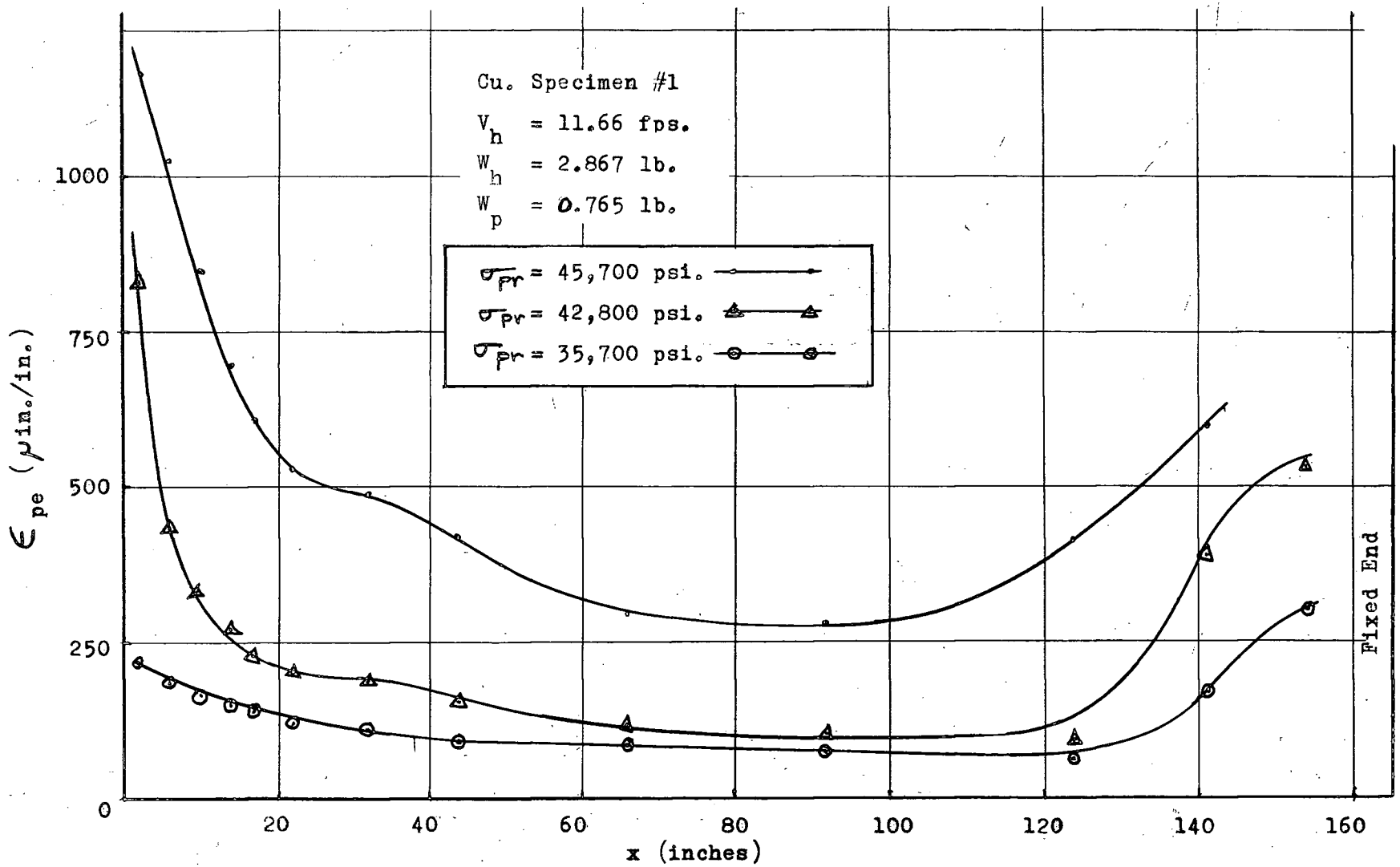

Fig. 31. Permanent Strain vs Distance from Impact for Three Prestress Values.

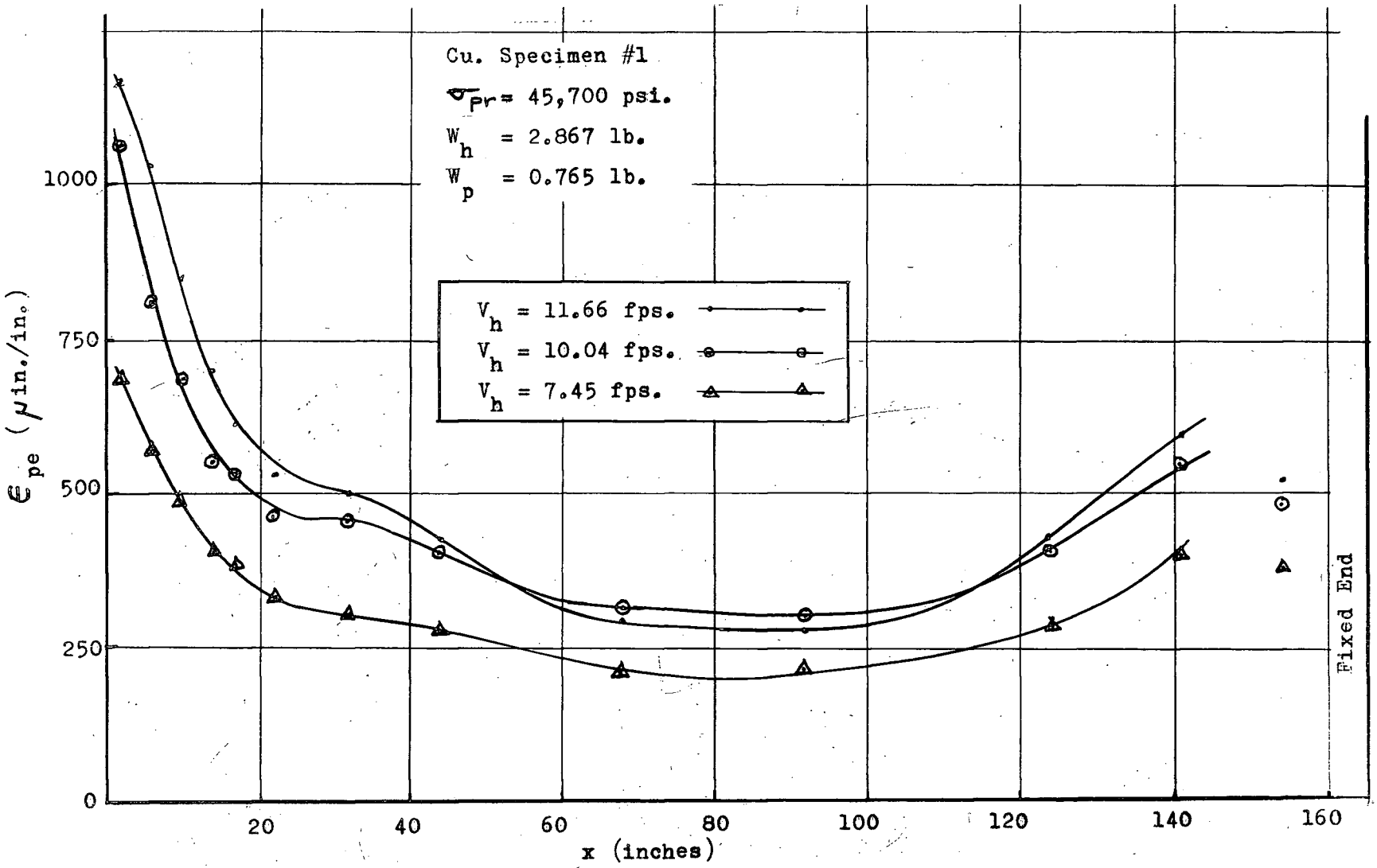

Fig. 32. Permanent Strain vs Distance from Impact for Three Hammer Velocities.

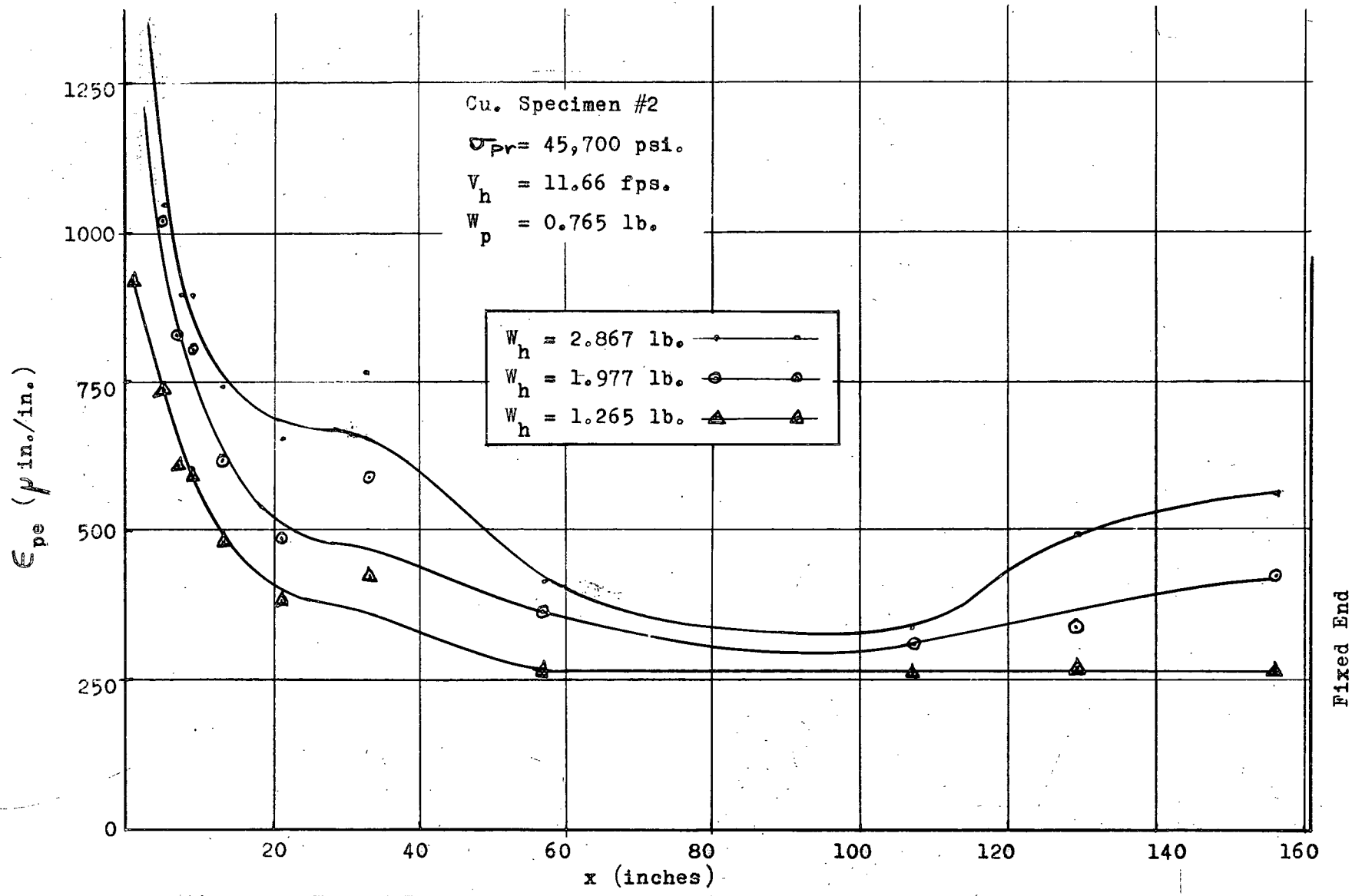

Fig. 33. Permanent Strain vs Distance from Impact from Three Hammer Weights.

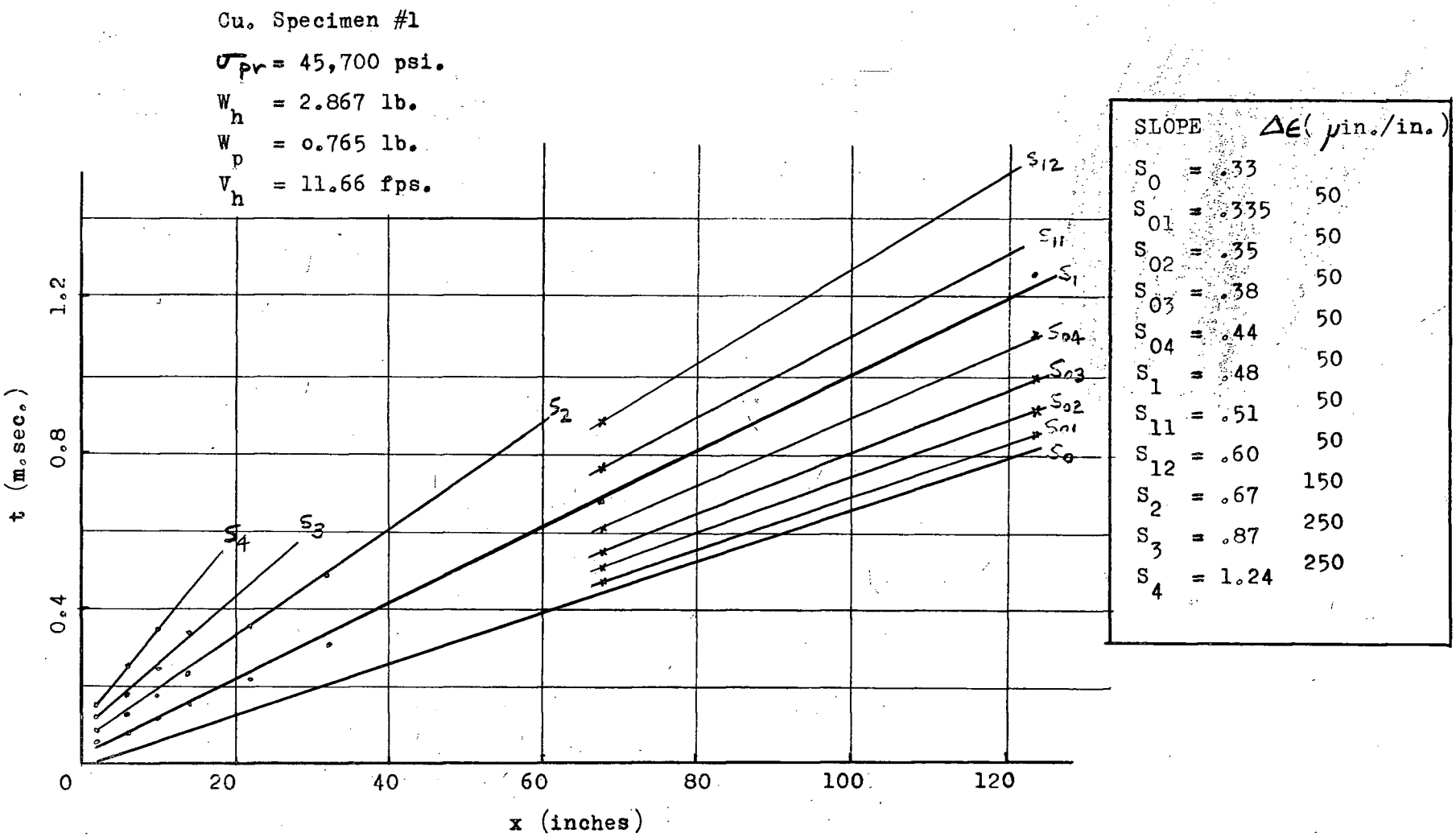

Fig. 34. Constant Strain Curves in x-t Plane for Cu. Specimen #1, V_h = 11.66 fps.

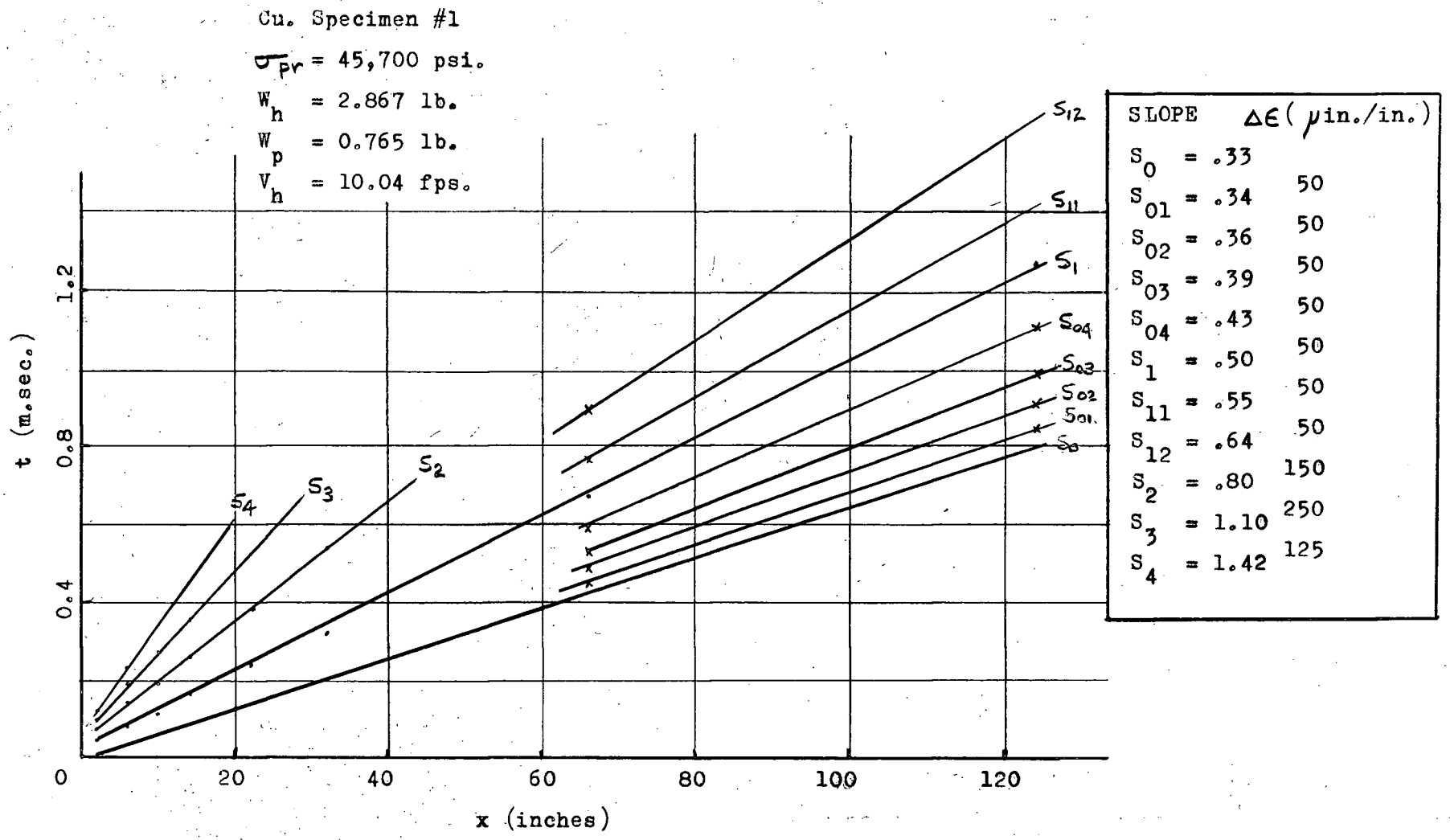

Fig. 35. Constant Strain Curves in x-t Plane for Cu. Specimen #1, V_h = 10.04 fps.

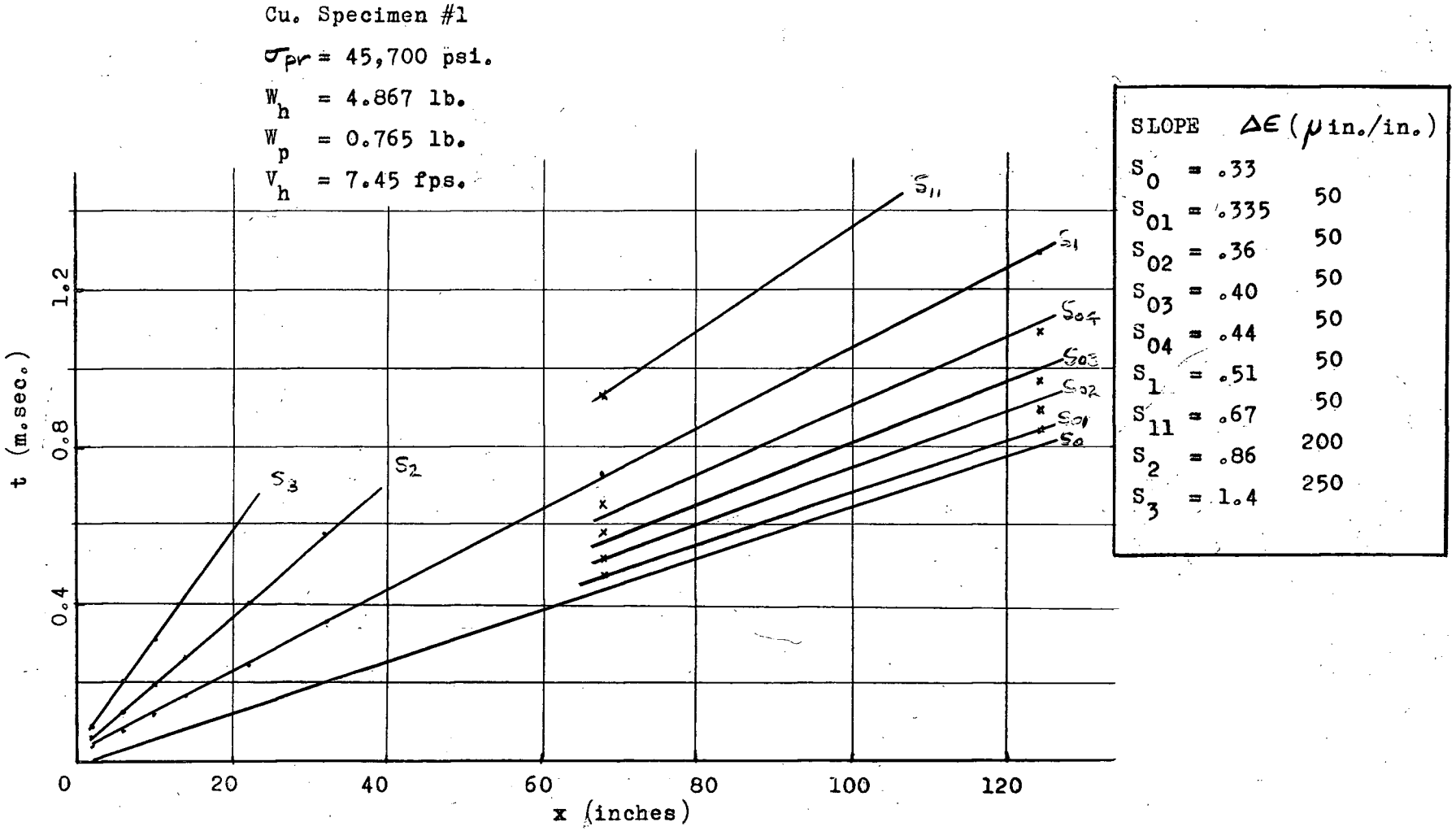

Fig. 36. Constant Strain Curves in x-t Plane for Cu. Specimen #1, V_h = 7.45 fps.

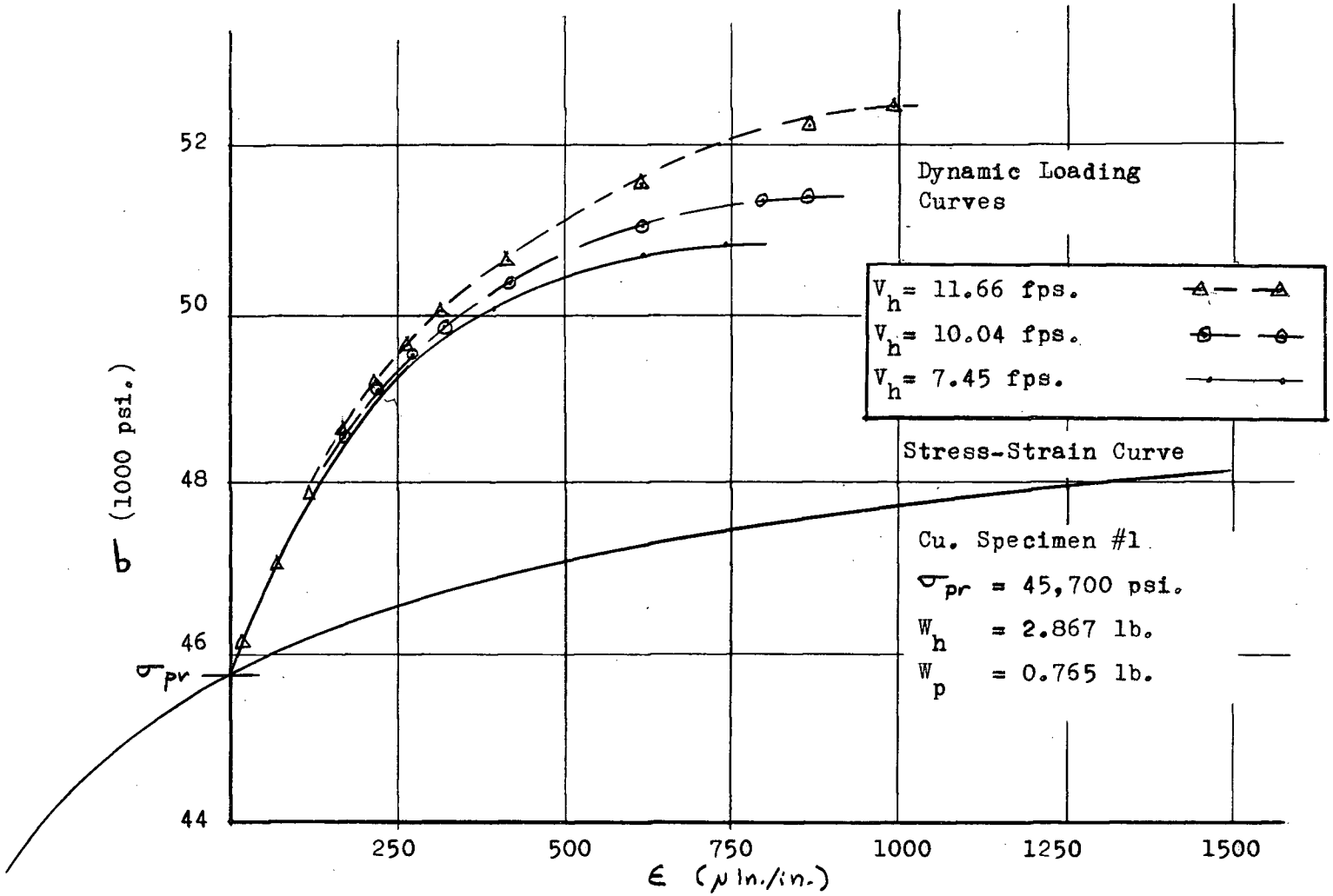

Fig. 37. Dynamic Loading Curves for Three Hammer Velocities on Quasi-Static Stress-Strain Curve.

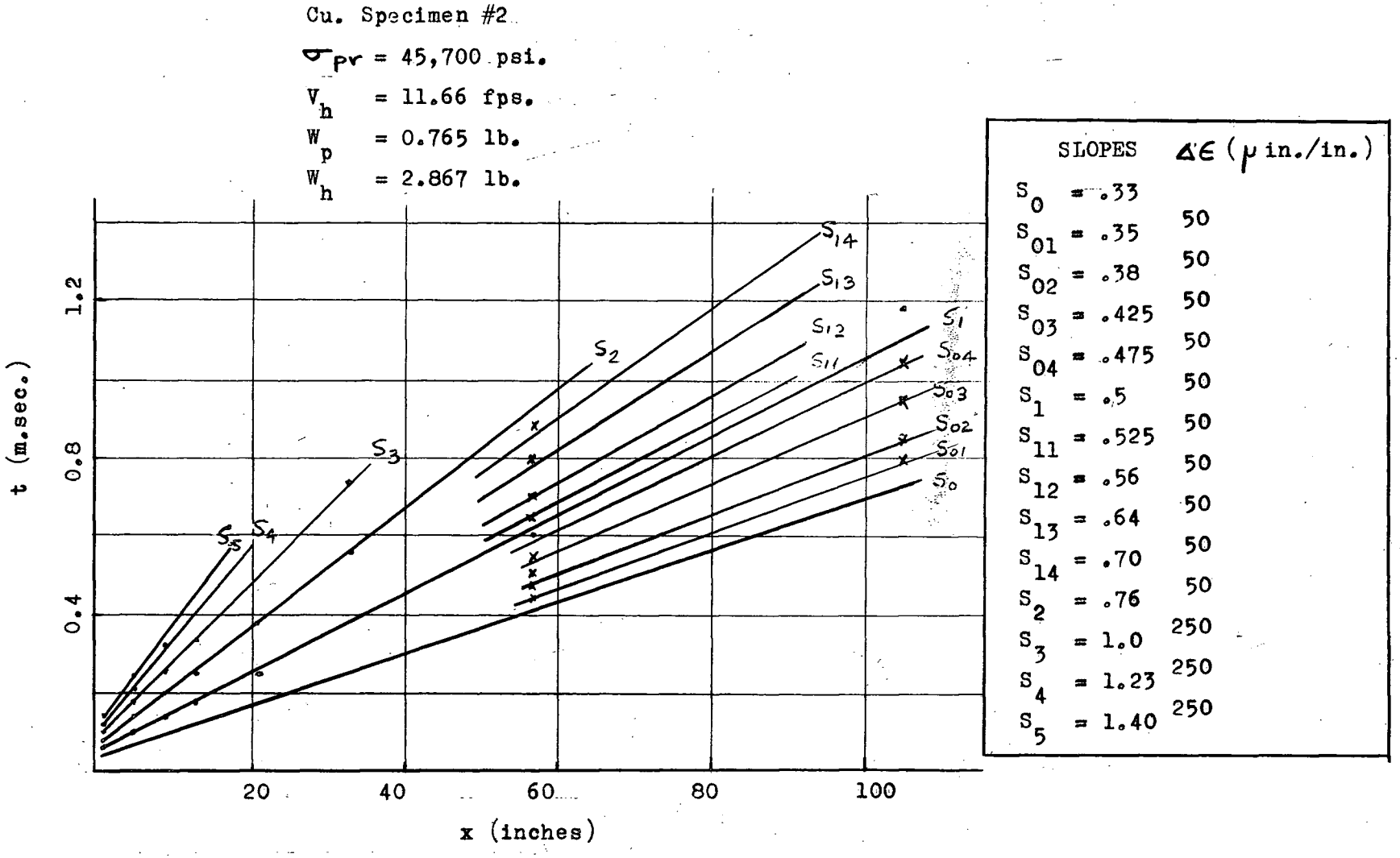

Fig. 38. Constant Strain Curves in x-t Plane for Cu. Specimen #2, W_h = 2.867 lb.

Cu. Specimen #2

σ_{pr} = 45,700 psi.

V_h = 11.66 fps.

W_p = 0.765 lb.

W_h = 1.977 lb.

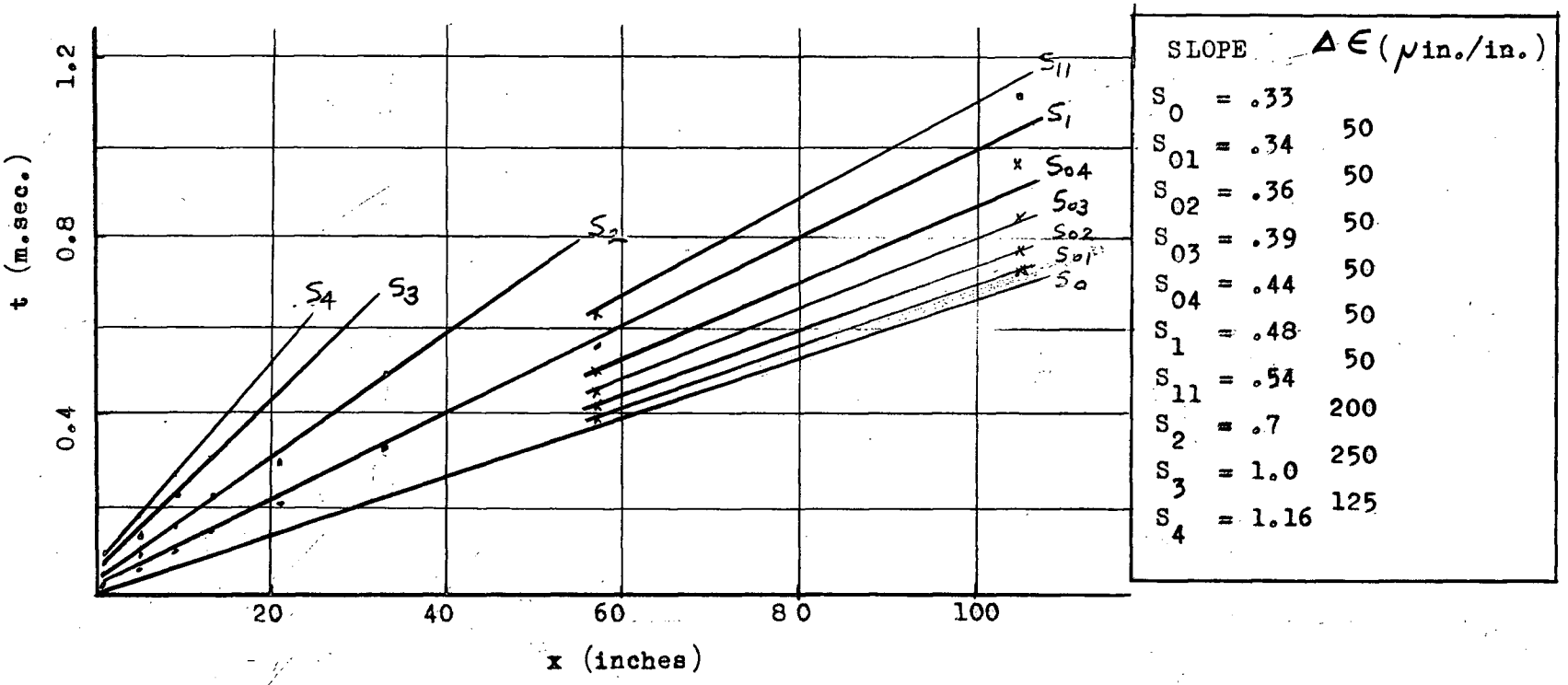

Fig. 39. Constant Strain Curves in x-t Plane for Cu. Specimen #2, W_h = 1.977 lb.

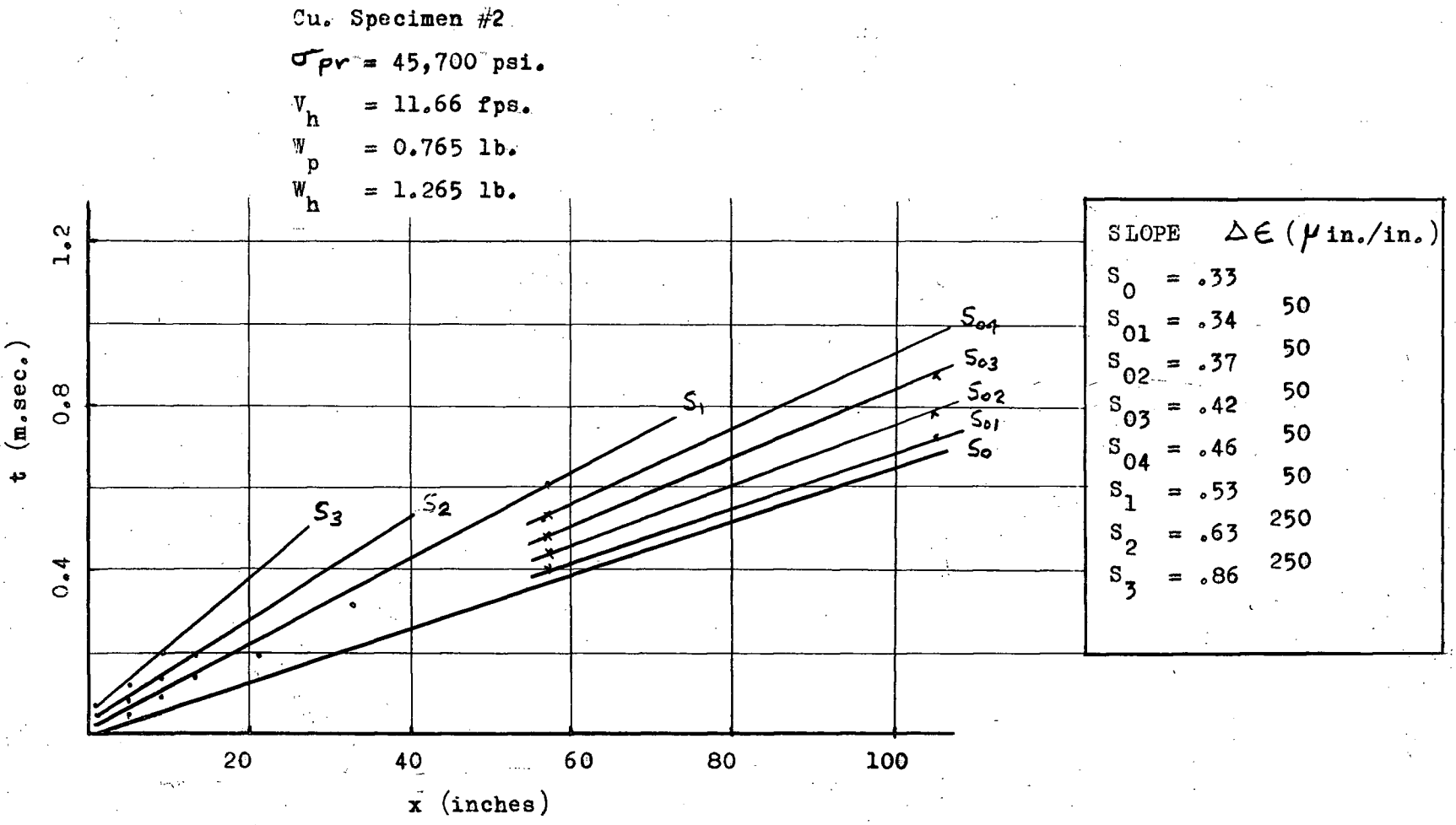

Fig. 40. Constant Strain Curves in x-t Plane for Cu. Specimen #2, W_h = 1.265 lb.

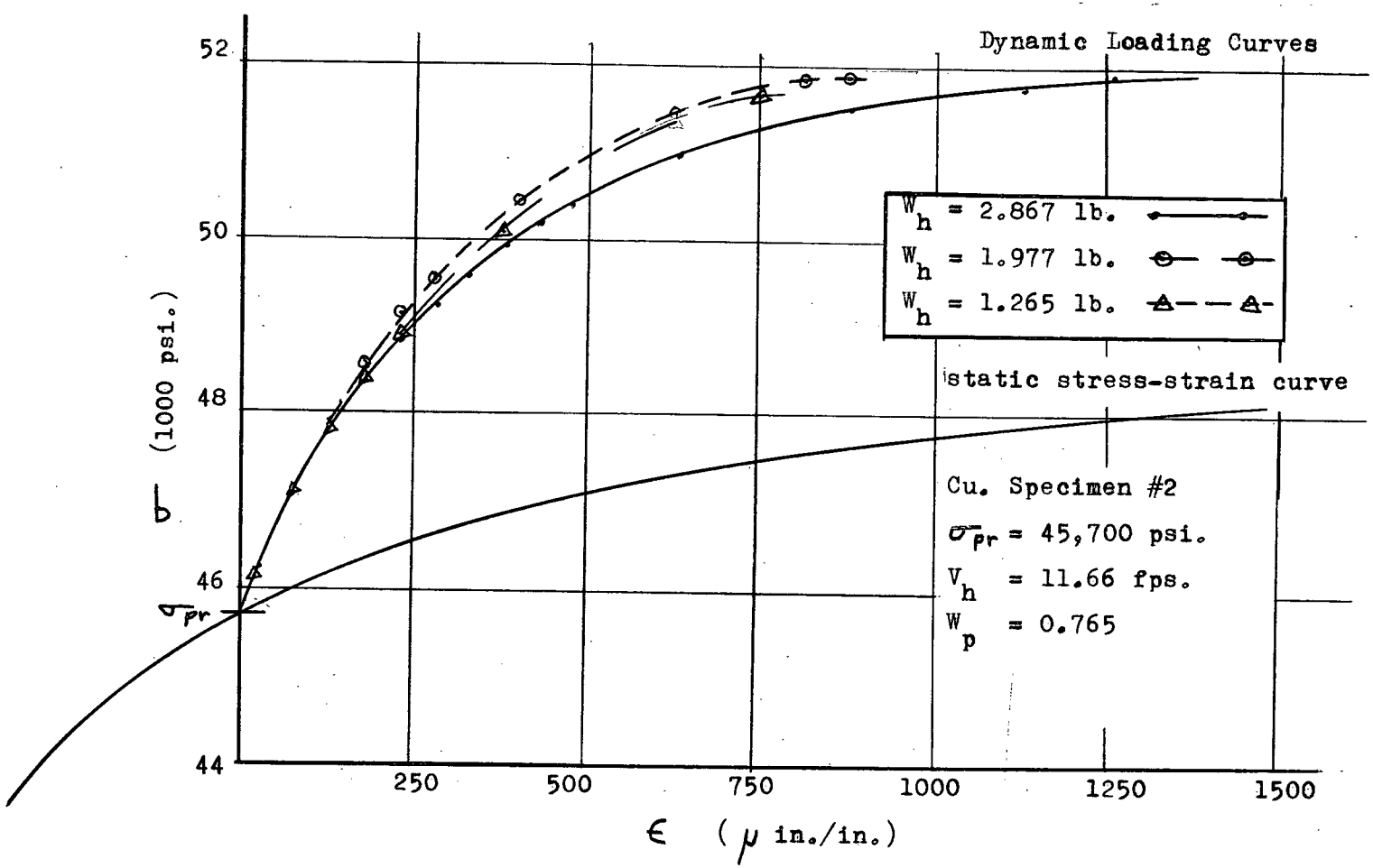

Fig. 41. Dynamic Loading Curves for Three Hammer Weights on Quasi-Static Stress-Strain Curve.

BIBLIOGRAPHY

1. Timoshenko and Goodier, "Theory of Elasticity" (2nd edition), McGraw Hill, 1951, pp. 438-448.

2. H. Kolsky, "Stress Waves in Solids", Oxford Clarendon Press, 1953.

3. H. Kolsky, "Experimental Wave Propagation in Solids" from "Proceedings of First Symposium on Naval Structural Mechanics", Pergamon Press, 1960.

4. Norman Davids, (editor) "International Symposium on Stress Wave Propagation in Materials", Interscience Publishers, Inc., New York, 1960.

5. Penny and Lissner, "Strain Gage Primer", (2nd edition) McGraw Hill.

6. Mills Dean, (editor) "Semiconductor and Conventional Strain Gages", Academic Press, New York-London, 1962.

7. M. Hetenyi, (editor), "Handbook of Experimental Stress Analysis", Wiley, 1950.

8. T. von Kármán and P. Duwez, "The Propagation of Plastic Deformations in Solids", Journal of Applied Physics, Volume 21, October 1950, pp. 987-994.

9. E.J. Sternglass and D.A. Stuart, "An Experimental Study of the Propagation of Transient Longitudinal Deformations in Elastoplastic Media", Journal of Applied Mechanics, Vol. 20, September, 1953, pp. 427-434.

10. M.P. White and Le Van Griffis, "The Permanent Strain in a Uniform Bar due to Longitudinal Impact", Journal of Applied Mechanics, Vol. 14, December 1947, pp. A-337 - A-343.

11. L.E. Malvern, "The Propagation of Longitudinal Waves of Plastic Deformation in a Bar of Material Exhibiting a Strain-Rate Effect", Journal of Applied Mechanics, Volume 73, June 1951, pp. 203-207.

12. H.N. Abramson, H.J. Plass, and E.A. Ripperger, "Stress Wave Propagation in Rods and Beams", Advances in Applied Mechanics, Volume 5, 1958, pp. 139-151.

13. B.E.K. Alter and C.W. Curtis, "Effect of Strain-Rate on the Propagation of a Plastic Strain Pulse along a Lead Bar", Journal of Applied Physics, Volume 27, 1956, pp. 1079-1085.

14. D.S. Clark and D.S. Wood, "The Time Delay for the Initiation of Plastic Deformation at Rapidly Applied Constant Stress", Proceedings of the American Society for Testing Materials, 1949. Volume 49, 1949, pp. 717-735.

15. C. Riparbelli, "On the Time Lag of Plastic Deformation", Reprint from Procedures of the First Midwestern Conference on Solid Mechanics, April 1953, pp. 148-157.

16. L.M. Barker, C.D. Lundergan and Walter Herrmann, "Dynamic Response of Aluminum", Journal of Applied Physics, Volume 35, Number 4, April 1964, pp. 1203-1212.

17. J. Lubliner, "A Generalized Theory of Strain-Rate-Dependent Plastic Wave Propagation in Bars", Journal of the Mechanics and Physics of Solids, Volume 12, 1964, pp. 59-65.

18. J.F. Bell and A. Stein, "The Incremental Loading Wave of the Pre-Stressed Plastic Field", Journal de Mecanique, Volume 1, Number 4, December, 1962, pp. 397-411.

19. P.E. Duwez and D.S. Clark, "An Experimental Study of the Propagation of Plastic Deformations Under Conditions of Longitudinal Impact", Proceedings of the American Society forTesting Materials, Volume 47, 1947, pp. 502-532.